CONTROL OF A VARIABLE-SHAFTSPEED ELECTROMECHANICAL ENERGY-CONVERSION SYSTEM

by

HARVEY ROY SIMKOVITS

Submitted in partial fulfillment of the
Requirements for the Degree of
Bachelor of Science
at the
MASSACHUSETTS INSTITUTE OF TECHNOLOGY
June, 1976

Signature of Author.....
Department of Electrical Engineering and Computer Science
May 7, 1976

Certified by.....
Thesis Supervisor

Accepted by.....
Chairman, Departmental Committee on Thesis

CONTROL OF A VARIABLE SHAFTSPEED ELECTROMECHANICAL ENERGY CONVERSION SYSTEM

by

Harvey Roy Simkovits

Submitted to the Department of Electrical Engineering and Computer Science on May 7, 1976 in the partial fulfillment for the requirements for the degree of Bachelor of Science

ABSTRACT

The extraction of maximum power from the wind, in a windmill power system, requires adjusting windmill shaft load as a function of wind velocity. A method to maximize wind power extraction, when the load consists of battery storage cells coupled to the windmill through an electromechanical converter, is introduced.

However, the development of a windmill simulator, also presented, demonstrates the effects of power losses in a windmill power system. These issues and their effects on windmill control criteria are discussed.

Thesis Supervisor: John G.Kassakian
Title: Assistant Professor of Electrical Engineering

ACHNOWLEDGEMENTS

The author wishes to express his gratitude to Professor John. G. Kassakian for his continued enthusiasm and guidance in the research.

Also thanks go to Messrs. Trevor Creary and Dave Otten for their help and ideas.

Lastly, I wish to express a deep thanks to my parents, especially my father, for their continued interest in my education.

TABLE OF CONTENTS

Table of Contents (continued) Page

LIST OF FIGURES

List of Figures (continued)

List of Figures (continued) Page

LIST OF TABLES

INTRODUCTION

The variable nature of the wind may not allow a windmill system to instantaneously supply the power demands of a load. Thus some form of energy storage becomes necessary to filter out the effects of variable wind-derived power.

The development of the Stored Energy Processor[3] (SEP) may be one solution to the energy storage problem. The SEP, firstly, can be supplied power from a variable source and stores that power in battery banks. Secondly, the SEP switch these batteries in series combinations to produce a variable-voltage, variable-frequency output adaptable to many load applications. Because of these characteristics the SEP has also been referred to as the AC Battery.

The power supplied to the SEP must be in the form of electricity. Yet a windmill is a mechanical source of power. Thus coupling the two systems requires an electromechanical converter. It is the purpose of this thesis to propose a technique to perform this electromechanical conversion. It is also desired that a control scheme be implemented that will transfer maximum power from the wind to the electrical system.

The testing and evaluation of the steady-state and dynamic behaviors of the proposed control system requires an actual windmill to provide the desired power input characteristics. Since it is difficult to bring a windmill

into a laboratory environment, then some means of windmill simulation is required. Thus it is also the purpose of this thesis to introduce a method of windmill simulation.

CHAPTER I

SYSTEM DESCRIPTION AND MODELING

A simplified block diagram of the proposed windmill power system is shown in Fig.1. The steady-state operation of the overall system is determined by the nature of both the input (windmill) and output (SEP) subsystems. Note that the electromechanical converter performs the coupling between the two subsystems and thus is a part of both.

To achieve maximum power transfer, from the wind to the batteries, it is necessary to understand, and thus model, the characteristics of both the input and output subsystems of the overall power system.

1.1 Input Subsystem (windmill characteristics)

The total power available in the wind is proportional to the kenetic energy of the wind and is given by

$$\text{Wind Power} = \tfrac{1}{2}\rho A v_w^3 \qquad (1)$$

where p is the density of air, A is the area swept by the blades of the windmill and v_w is the velocity of the wind. All units are in mks.

Typical power-speed characteristics for a windmill are shown in Fig.2. The axes are normalized power (power ratio) and normalized shaftspeed (velocity ratio).

The power ratio, c_p, is the ratio of windmill shaft-power, or wind-power extraction, to the total wind-power,

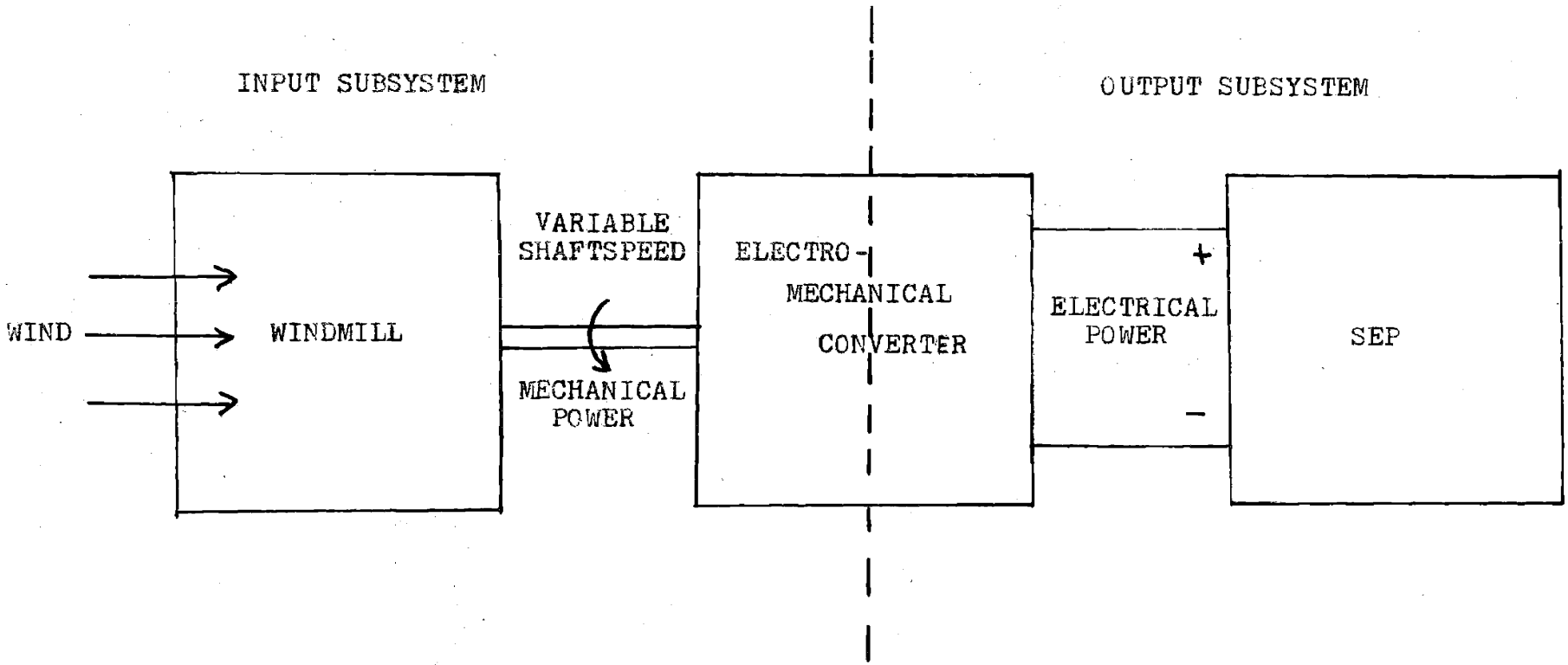

Fig.1 : Simplified Windmill Power System

Eq.1. Simple windmill theory shows a fundamental restriction on c_p. This restriction limits the wind-power extraction by a windmill to 60% of the available wind-power.

Tip speed is defined as the product of windmill shaft-speed, w_s, and windmill radius, i.e. blade length, R. The velocity ratio is the ratio of windmill tip speed to wind velocity, $w_s R/v_w$.

The family of curves in Fig.2 are for a typical windmill with blade pitch, θ, the varied parameter. Fig.2 also shows how θ is measured.

Using c_p, windmill shaft-power can be related to available wind-power.

$$\begin{aligned} \text{Shaft-Power} &= c_p \cdot \text{Wind-Power} \\ &= c_p\left[\frac{w_s R}{v_w}, \theta\right] \cdot \tfrac{1}{2}\rho A v_w^3 \\ &= c_p\left[\frac{w_s R}{v_w}, \theta\right] \cdot \tfrac{1}{2}\rho A \left(\frac{w_s R}{v_w}\right)^{-3} R^3 w_s^3 \end{aligned} \qquad (2)$$

For a given windmill of radius R and pitch θ, if the velocity ratio is maintained constant then Eq.2 shows that the shaft-power is proportional to the cube of the shaftspeed. Using Eq.2 and the c_p curve, in Fig.2, with optimum pitch, θ_1, the windmill characteristic can be replotted on a power-speed curve for different values of wind velocity. Fig.3 shows this plot for three values of wind velocity, v_{w1}, $1.5v_{w1}$, and $2v_{w1}$. Notice that the shaftspeeds where maximum power is extracted from the wind

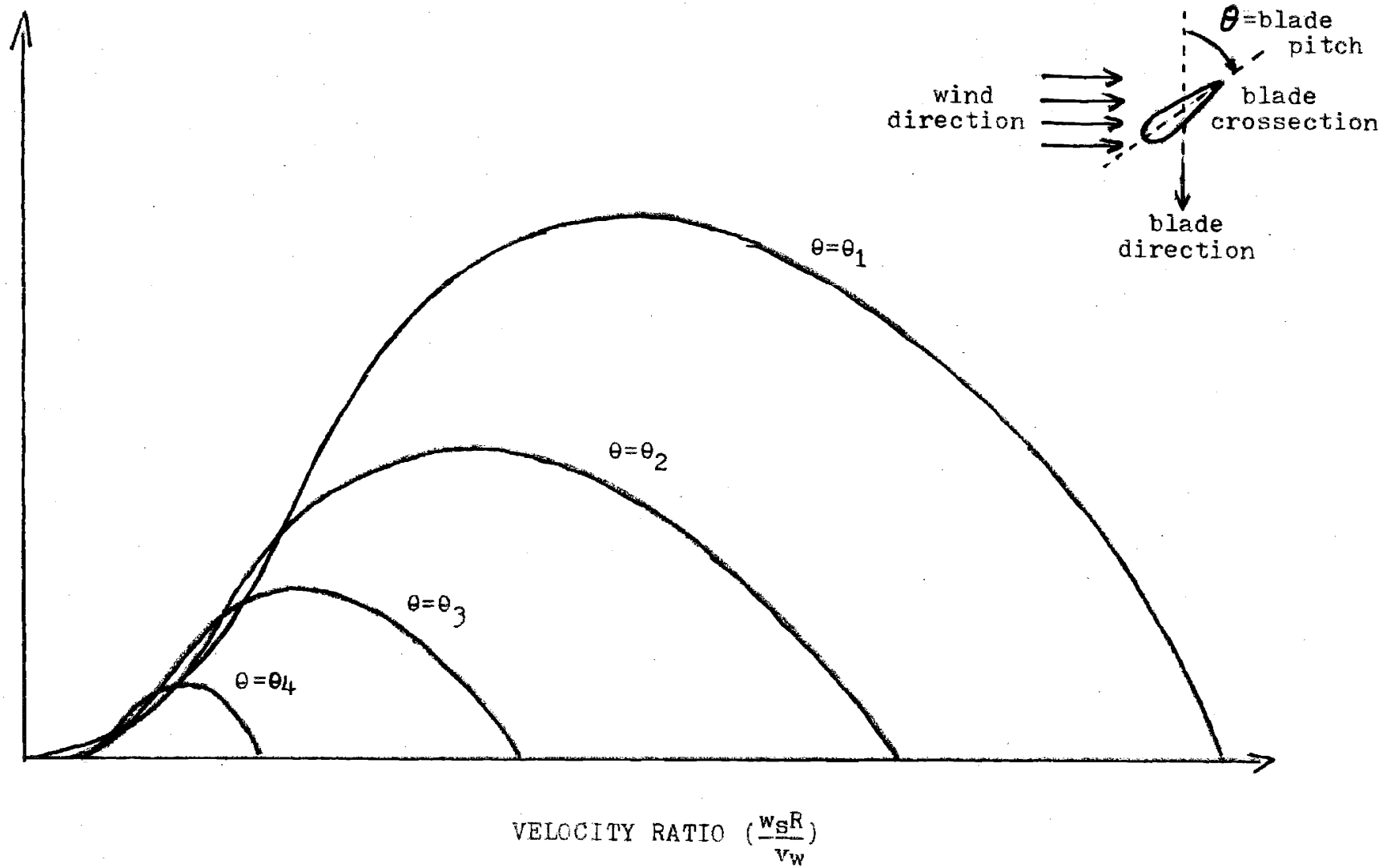

Fig 2 : Windmill Characteristics

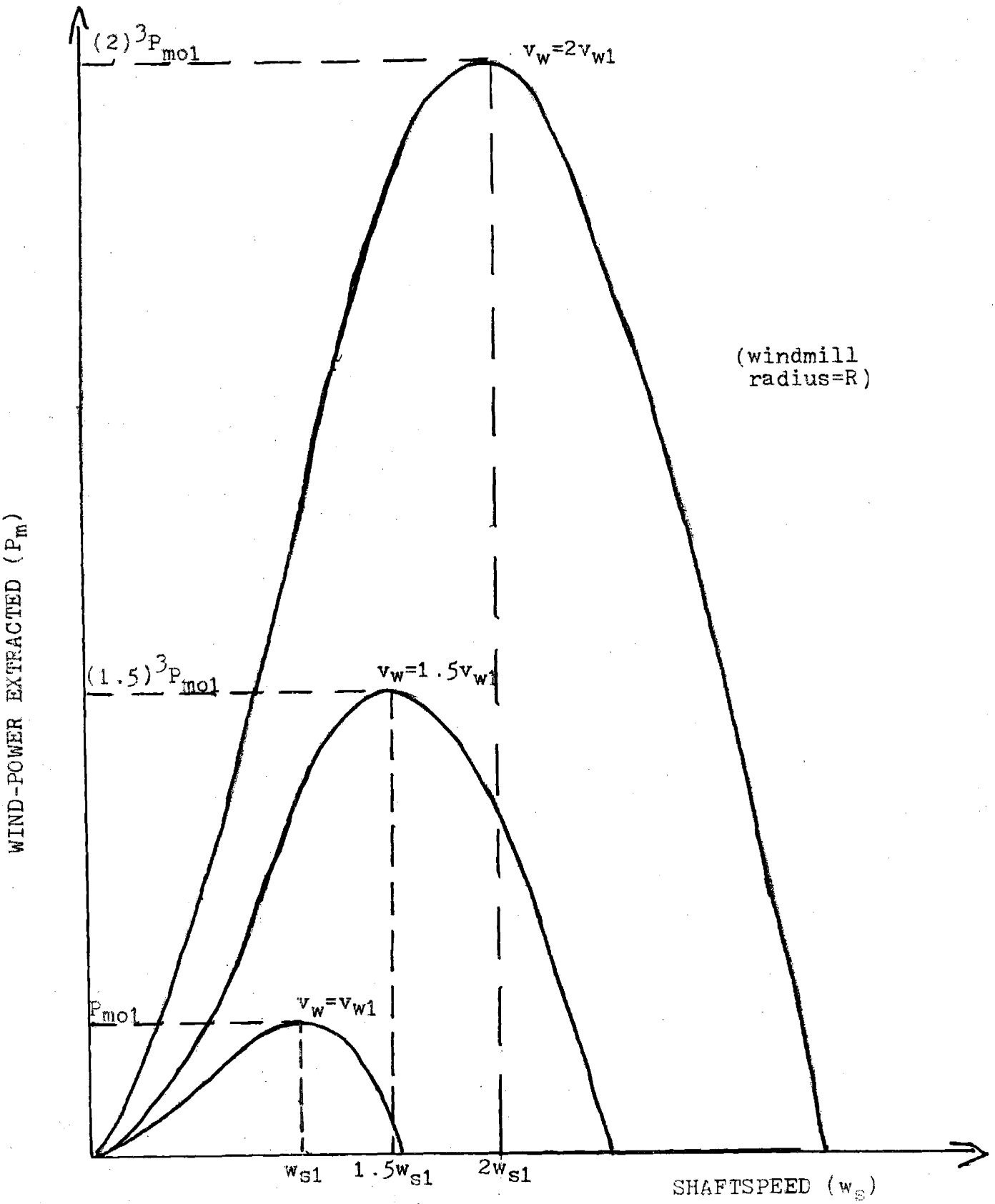

Fig.3 : Wind-Power Extraction as Functions of Wind Velocity and Shaftspeed

are, respectively, w_{s1}, $1.5w_{s1}$, and $2w_{s1}$. Thus corresponding to the peak of the power-speed curves is the particular value of the velocity ratio, $w_{s1}R/v_{w1}$. If the velocity ratio can be held at this value, by controlling shaft load as a function of wind velocity, then steady-state windmill operation occurs at the peak of the power-speed curve. In this way maximum power can be extracted from the wind.

1.2 Output Subsystem (SEP characteristics and constraints)

The battery banks to be charged consist of four 42-volt battery sections. This nominal voltage was picked so that, when discharging, these batteries can be switched in series combinations to produce a 168V-peak or 120V-rms, 60-hz stepped sine wave. The SEP system has other voltage and frequency capabilities but the above requirement is mandatory for any home application. The harmonic content of this waveform is approximately 8% and is acceptable for most power applications.

Under the designed SEP system these batteries can be charged only in 42V sections, and multiples thereof, up to 168V. Also the peak charging current is restricted to 18 amperes. These constraints are set by the design and limitations of the power switching electronics.

A battery cell may be modeled as a voltage behind an internal resistance, Fig.4. The internal battery voltage varies as a function of the state of charge of the cell. A typical profile of a battery discharging and

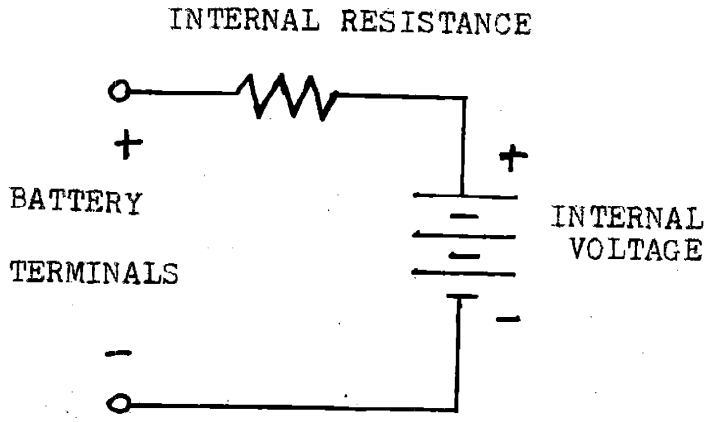

Fig.4 : Battery Circuit Model

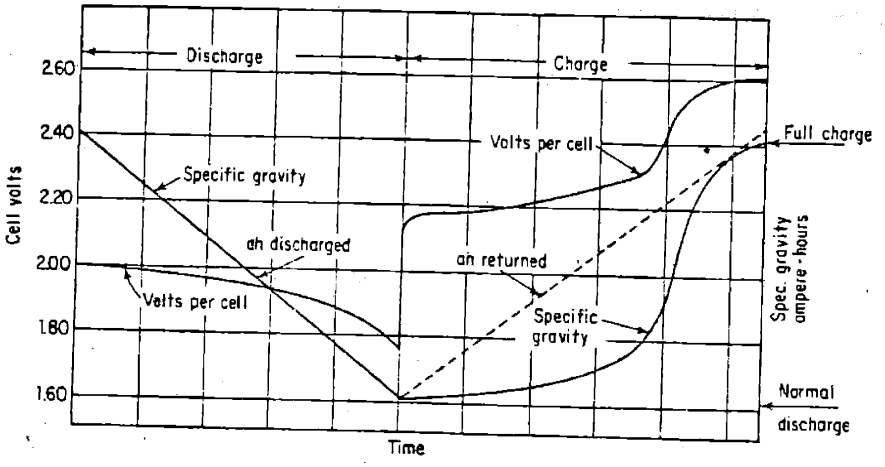

('specific gravity' refers to specific gravity of battery acid)
('a-h' ≡ amperes-hours, refers to quantity of charge removed or added to cell)

Fig.5 : Discharging and Charging Profile for a 2V Lead-Acid Cell

charging is shown in Fig.5 for a unit 2V lead-acid cell. Note that the battery terminal voltage varies from 1.8 to 2.6 volts as the cell is discharged and charged.

The internal resistance of a battery cell is dependent on several factors. These factors include the capacity of the cell, its state of charge, the current flowing through the cell, and whether this current is flowing into or out of the cell.

Further description of the SEP battery section and detailed measurements of its internal resistance and open-circuit voltage can be found in Appendix A

1.3 Output Subsystem (battery charging system)

The proposed electromechanical power converter is a single-phase synchronous altenator with a full-wave rectified output. A synchronous machine is used, instead of a dc machine, because it is a simplier and more efficient mechanical device. Full-wave rectification of the altenator output has two advantages over half-wave rectification. Firstly it allows charge to be supplied from the machine twice every electrical cycle, instead of once as in a half-wave rectification system. this leads to a higher average current, for the same peak current, in the charging system.

Secondly, in a half-wave rectification system, a dc current component flows in the power, or armature, circuit of the machine. This current puts a dc bias on the flux level in the machine. Conversely, in a full-wave rectification system, current is allowed to flow in both directions of the machine's armature winding. The subsequent lower flux levels in the machine increase generator efficiency.

The generator and charging circuit may be modeled as seen in Fig. 6. E_f is the open-circuit terminal-voltage of the generator and L_s the inductance seen behind the armature terminals of the generator. V_b and R_b are, respectively, the open-circuit terminal-voltage and internal resistance of the batteries being charged. The full-wave bridge, as discussed previously, is used to rectify the alternating voltage produced by the generator. The effect of the series inductance, L, is to alter the output-current waveform such that a lower peak and higher average current is attained.

Voltage applied to the field terminals of the generator produces a magnetic flux density in the air-gap of the machine. The forced rotation of the machine's rotor causes magnetic flux lines to be cut by the generator's armature winding. This induces a voltage in the armature winding that is proportional to field excitation and shaftspeed, i.e.

$$E_f = K\emptyset w_e \sin(w_e t)$$

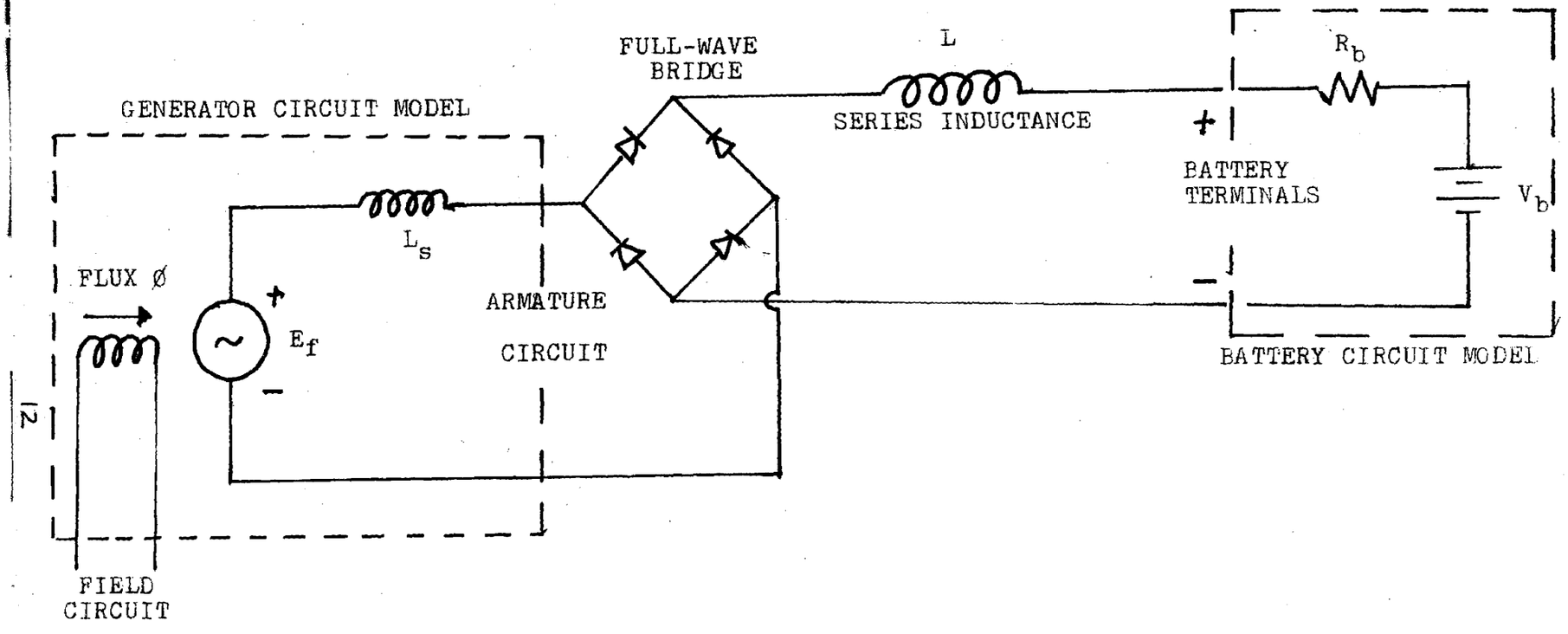

Fig.6 : Generator, Charging Circuit and Battery Model

where $\emptyset$ is the flux level in the machine and K is a constant dependent on the characteristics of the machine and the units of measure used. w_e is the electrical frequency of the armature voltage and is directly proportional to rotor shaftspeed, w_s.

CHAPTER II

OUTPUT SUBSYSTEM ANALYSIS

This chapter is concerned with determining the power output of the electromechanical converter, or generator, as a function of the parameters in the charging system, Fig.6. However, the analysis of this circuit model is difficult. To simplify the analysis it is assumed that the effects of the internal battery resistance, R_b, and generator armature inductance, L_s, are small. Thus, as a first approximation, these circuit elements will be ignored. Their effects, however, will be discussed in a later section.

2.1 Simplified Charging System Analysis

The simplified battery charging circuit and appropriate waveforms are shown in Fig.7.

When the diodes are conducting, one pair at a time, then the current can be considered to consist of two components; one due to the source and one due to the battery emf. The analytical form of the rectified generator voltage, Fig.7a, is different in the two time periods, $0<w_e t<\pi$ and $\pi<w_e t<2\pi$. Thus the circuit must be analysed separately for both regions of time.

If α is the angle measured from $E_f=0$ to when $E_f=V_b$, and γ is the angle for which a pair of diodes are conducting then the source component of current, i_s, is given by

$$K\phi w_e \sin(w_e t) = L\frac{di_s(t)}{dt} = w_e L\frac{di_s(t)}{d(w_e t)}$$

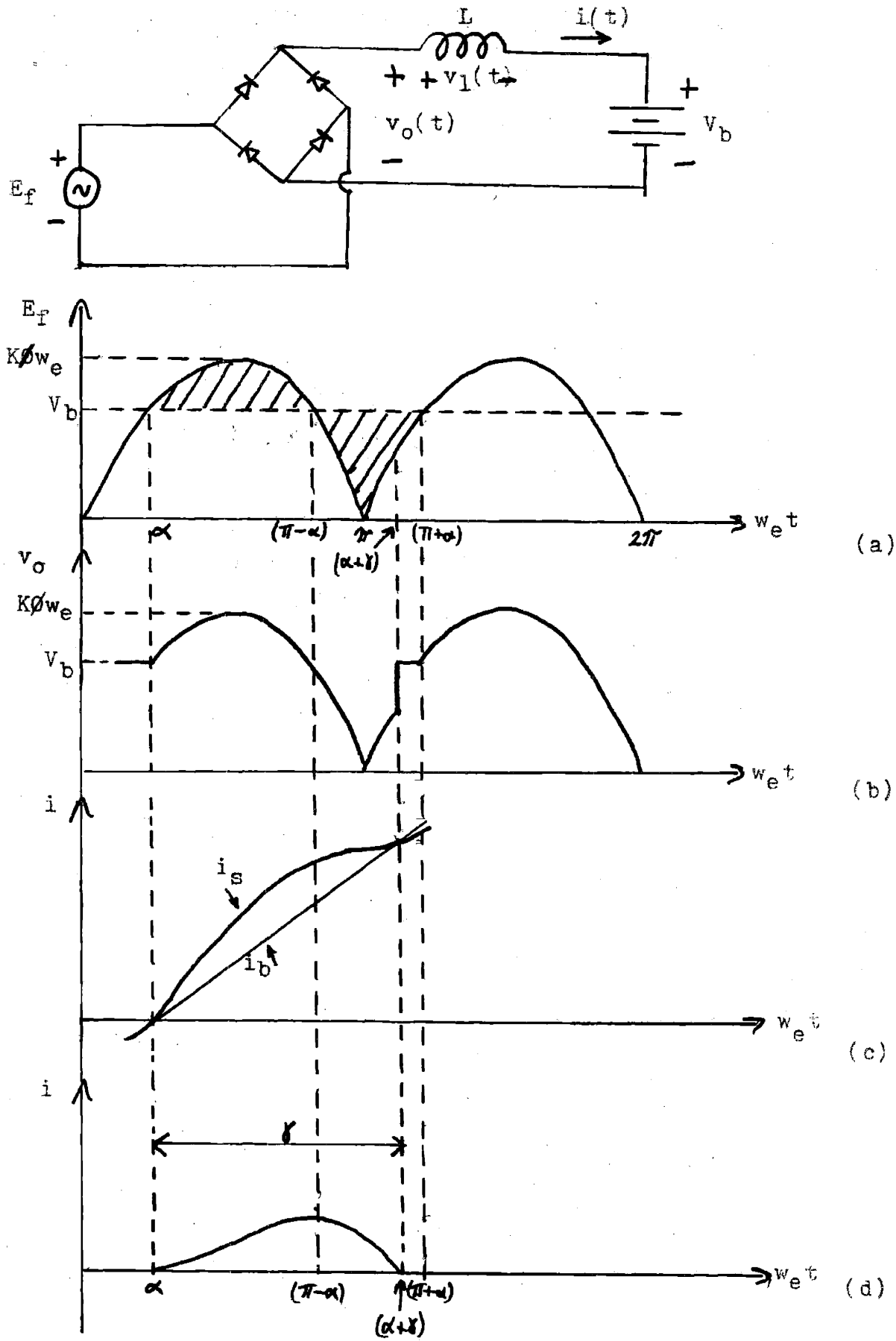

Fig.7 : Battery Charging Circuit and Waveforms

$$i_s(t) = \frac{K\phi}{L}\int_{\alpha}^{w_e t} \sin(w_e t)\, d(w_e t) = \frac{K\phi}{L}\left(\cos\alpha - \cos w_e t\right) \quad ; \alpha < w_e t < \pi$$

The battery component of current, i_b, is given by

$$-V_b = L\frac{di_b(t)}{dt} = w_e L \frac{di_b(t)}{d(w_e t)}$$

$$i_b(t) = \frac{-V_b}{w_e L}\int_{\alpha}^{w_e t} d(w_e t) = \frac{-V_b}{w_e L}\left(w_e t - \alpha\right)$$

The total current, i(t), is thus

$$i(t) = i_s(t) + i_b(t) = \frac{K\phi}{L}\left(\cos\alpha - \cos w_e t\right) - \frac{V_b}{w_e L}\left(w_e t - \alpha\right) \quad ; \alpha < w_e t < \pi \qquad (3)$$

Maximum current occurs when the derrivative $\frac{di(t)}{dt} = 0$ or $w_e t = \pi - \alpha$. Substituting this value of $w_e t$ into Eq.3 gives the peak current

$$i(w_e t = \pi - \alpha) \equiv i_{PEAK} = \frac{2K\phi}{L}\cos\alpha - \frac{V_b}{w_e L}(\pi - 2\alpha)$$

$$= \frac{K\phi}{L}\left[2\cos\alpha - (\pi - 2\alpha)\sin\alpha\right] \qquad (4)$$

where $V_b/K\phi w_e = \sin\alpha$ has been used. This latter relationship can be seen from Fig.7a, where, at $w_e t = \alpha$, $K\phi w_e \sin\alpha = V_b$.

From Eq.3 the value of i(t) can also be found for $w_e t = \pi$,

$$i(w_e t = \pi) = \frac{K\phi}{L}(1 + \cos\alpha) - \frac{V_b}{w_e L}(\pi - \alpha) \qquad (5)$$

Eq.5 provides the initial condition for i(t) when $\pi \leq w_e t \leq \pi + \alpha$. In this region of time the source component of current is given by

$$K\phi\, w_e \sin(w_e t - \pi) = w_e L \frac{d i_s(t)}{d(w_e t)}$$

$$i_s(t) = \frac{K\phi}{L}\int_{\pi}^{w_e t} \sin(w_e t - \pi)\, d(w_e t)$$

$$= \frac{K\phi}{L}\left[1 - \cos(w_e t + \pi) + C_1\right] \quad ; \pi < w_e t < \pi + \alpha$$

where C_1 is a constant of integration and depends on the initial conditions of the current, at $w_e t = \pi$. For $\pi < w_e t < \pi + \alpha$ the battery component of current is given by

$$-V_b = w_e L \frac{d i_b(t)}{d(w_e t)}$$

$$i_b(t) = \frac{-V_b}{w_e L}\int_{\pi}^{w_e t} d(w_e t) = \frac{-V_b}{w_e L}(w_e t - \pi) + C_2 \quad ; \pi < w_e t < \pi + \alpha$$

where C_2 is again a constant of integration.

The total current is again the sum of source and battery components.

$$i(t) = i_s(t) + i_b(t) = \frac{K\phi}{L}\left[1 - \cos(w_e t + \pi)\right] - \frac{V_b}{w_e L}(w_e t - \pi) + C' \quad ; \pi < w_e t < \pi + \alpha$$

where C_1 and C_2 have been combined into the constant C'. From the initial conditions given by Eq.5, C' can be determined. The result is

$$C' = \frac{K\phi}{L}(1 + \cos\alpha) - \frac{V_b}{w_e L}(\pi - \alpha)$$

Thus

$$i(t) = \frac{K\phi}{L}\left(2 + \cos\alpha + \cos w_e t\right) - \frac{V_b}{w_e L}(w_e t - \alpha) \quad ; \pi < w_e t < \pi + \alpha \qquad (6)$$

Fig.7c shows the source and battery components of

current. Their sum is shown in Fig.7d.

2.2 Charging Circuit Constraints

Fig.7 shows that the charging current falls to zero when the shaded areas are equal. This is because the average voltage across inductor must be zero over an electrical cycle. Thus

$$\int_{\alpha}^{\alpha+\pi} v_L(t)\, d(\omega_e t) = 0$$

$$\int_{\alpha}^{\alpha+\pi} v_0(t)\, d(\omega_e t) - \int_{\alpha}^{\alpha+\pi} V_b\, d(\omega_e t) = 0$$

$$\frac{1}{\pi}\int_{\alpha}^{\alpha+\pi} v_0(t)\, d(\omega_e t) = V_b \qquad (7)$$

The left side of Eq.7 is the average value of $v_0(t)$, (see Fig.7). This quantity, as stated by Eq.7, must equal the battery voltage.

If the amplitude of E_f is increased then the average value of $v_0(t)$ will eventually become larger than V_b. The average voltage across the inductor is now finite and positive. This means that the inductor current will now monotonically increase. In a practical circuit this ramping current is limited only by internal battery resistance and stray resistance in the wire connections.

To prevent the charging current from exhibiting this instability the average value of E_f must be held less than the battery voltage. The average value of a full-wave rectified sine-wave is $2/\pi$ times the peak value of the sine-wave. Thus for stable charging current

$$\frac{2}{\pi} E_{f_{PEAK}} < V_b$$

or $$\frac{2K\phi w_e}{\pi} \leq V_b$$

$$\frac{V_b}{K\phi w_e} \geq \frac{2}{\pi}$$

$$\sin\alpha \geq \frac{2}{\pi} \qquad (8)$$

If Eq.8 is satisfied then the current will fall to zero, as seen from Fig.7, when $w_e t = \alpha + \gamma$. Replacing this quantity into Eq.3 & 6 gives two equations that relate the conductance angle γ to the angle α.

$$\tan\alpha = \frac{1-\cos\gamma}{\gamma-\sin\gamma} \qquad ;\alpha \leq \alpha+\gamma \leq \pi \qquad (9)$$

$$2+(1+\cos\gamma)\cos\alpha-(\sin\gamma+\gamma)\sin\alpha = 0$$

$$; \pi \leq \alpha+\gamma \leq \alpha+\pi \qquad (10)$$

Eq.7 & 8 may be solved numerically to find γ as a function of α. The result is plotted in Fig.8 Note, again, the unallowable values for α. The figure also shows that γ is limited to the maximum conductance angle of π radians or a full cycle of the rectified source-voltage waveform.

The limitations of the battery switching electronics of the SEP system cannot allow for a charging current greater than 18 amperes (see section 1.2). Thus, from Eq.4,

$$i_{PEAK} = \frac{K\phi}{L}\left(2\cos\alpha-(\pi-2\alpha)\sin\alpha\right) \leq 18 \text{ AMP.} \qquad (11)$$

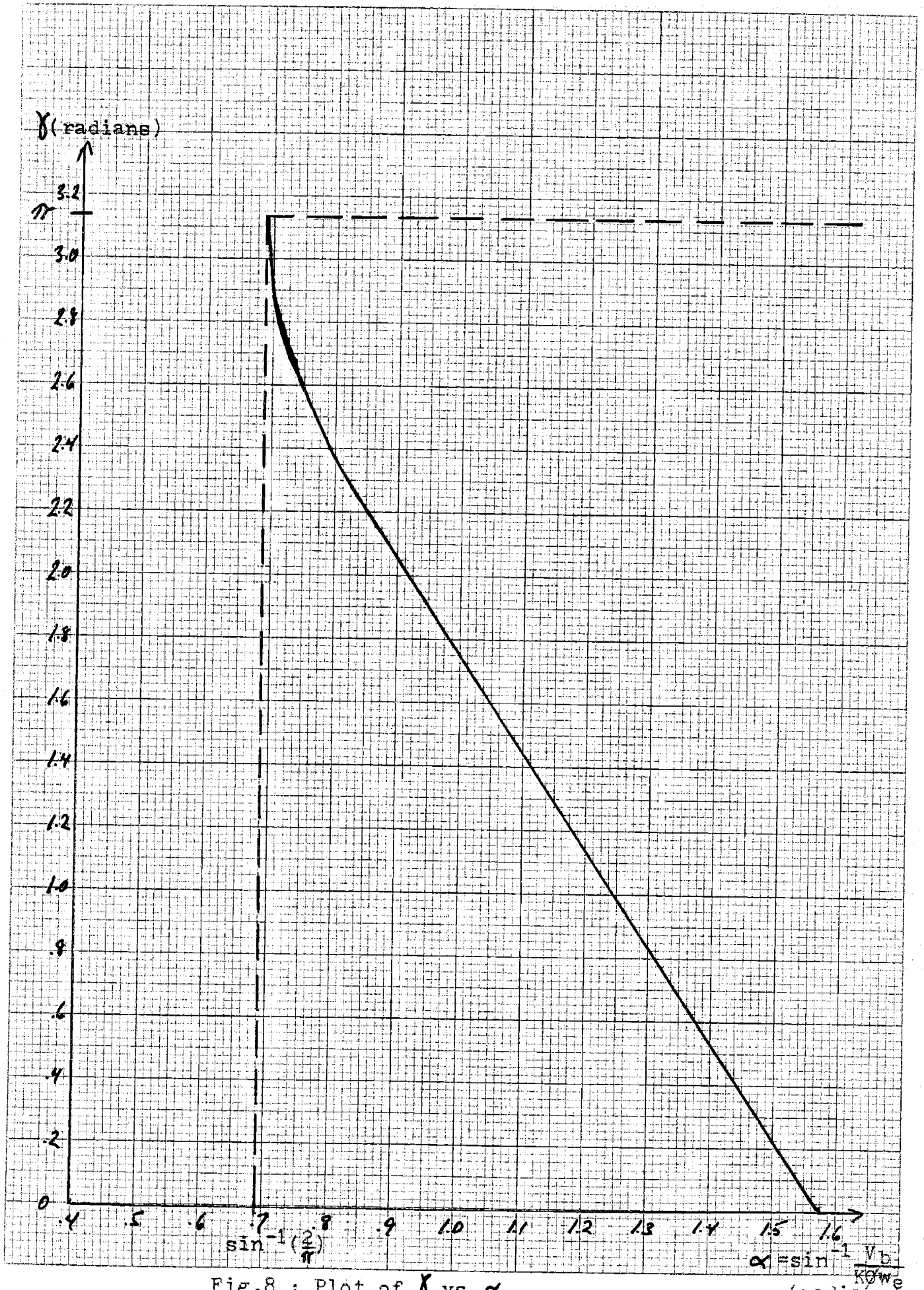

Fig.8 : Plot of γ vs. α

At the conductance limit, $\gamma = \pi$, Eq.11 must still be satisfied. From Eq.10 or Fig.8, $\sin\alpha = 2/\pi$ for $\gamma = \pi$. Substituting the corresponding value of α into Eq.11 results in

$$.42 \frac{K\phi}{L} \leq 18 \text{ AMP}$$

$$\text{or} \quad w_e L \geq 43 K\phi w_e \quad \text{HENRIES} \qquad (12)$$

The above relation between the effective impedance of the series inductor, $w_e L$, and the amplitude of the open-circuit armature voltage, $K\phi w_e$, must be satisfied if the peak charging current is to be limited to 18 amperes when the current is conducting over the full electrical cycle.

High flux levels in the machine decreases generator efficiency and the resulting heating can lead to machine deterioration. Thus the flux level, $K\phi$, is constrained to a maximum. This maximum flux level is usually chosen in terms of a maximum field current excitation. For the proposed generator* the field current will be limited to 0.7 amp. From the generator's magnitization curve* and the relation between open-circuit armature voltage and field flux*, the maximum flux level, $K\phi_m$, of the machine is

$$K\phi_m = 0.098 \text{ V-sec}^*$$

Thus, from Eq.12,

*see Appendix B

$$L \geq 43K\phi_m = 2.3 \times 10^{-3} \text{ henries}$$

This inductance is rather small. At the synchronous speed of the generator the equivalent impedance of L is $2w_e$(synchronous)L*, or approximately 12 ohms.

Considering this fact, the neglectance of the battery resistance may not have been a valid approximation. A way to test the validity of the approximation is through observations of the charging-circuit waveforms. These observations are discussed in section 4.1.

2.3 Generator Power Output

The power output of the generator may be expressed as the sum of two components. The first is the power absorbed by the batteries. This power is simply the product of the open-circuit battery voltage and the average charging current. The second component is the power lost in the internal resistance of the batteries. This power is not only given off as heat but also goes into dissociating the water in the battery cells.

For the following analysis the effects of battery resistance will again be ignored. The issues involving battery resistance will be returned to in another section.

The average current in the charging circuit is

$$i_{ave} = \frac{1}{\pi}\int_{\alpha}^{\alpha+\gamma} i(t)\,d(w_e t)$$

Using Eq. 3 & 6; for $\alpha \leq \alpha+\gamma \leq \pi$

* The factor of 2 in the impedance is because the lowest harmonic in the rectified armature voltage is $2w_e$.

$$i_{ave} = \frac{1}{\pi}\int_{\alpha}^{\alpha+\gamma}\left[\frac{K\phi}{L}(\cos\alpha-\cos w_e t)-\frac{V_b}{w_e L}(w_e t-\alpha)\right]d(w_e t)$$

$$= \frac{V_b}{\pi w_e L}\cdot f(\sin\alpha) \qquad (13)$$

where

$$f(\sin\alpha) = \frac{(\gamma-\sin\gamma)\cos\alpha+(1-\cos\gamma)\sin\alpha}{\sin\alpha} - \frac{\gamma^2}{2}$$

$$;\alpha \le \alpha+\gamma \le \pi \qquad (14)$$

and $V_b/K\phi w_e=\sin\alpha$ has been used. Also, in this case the relationship between α and γ is given by Eq.9.

For $\alpha+\pi \ge \alpha+\gamma \ge \pi$

$$i_{ave} = \frac{1}{\pi}\int_{\alpha}^{\pi}\left[\frac{K\phi}{L}(\cos\alpha-\cos w_e t)-\frac{V_b}{w_e L}(w_e t-\alpha)\right]d(w_e t)$$
$$+\frac{1}{\pi}\int_{\pi}^{\alpha+\gamma}\left[\frac{K\phi}{L}(2+\cos\alpha+\cos w_e t)-\frac{V_b}{w_e L}(w_e t-\alpha)\right]d(w_e t)$$

$$= \frac{V_b}{\pi w_e L}\cdot f(\sin\alpha)$$

where

$$f(\sin\alpha) = \frac{(\gamma+\sin\gamma)\cos\alpha+(1+\cos\gamma)\sin\alpha+2(\alpha+\gamma-\pi)}{\sin\alpha} - \frac{\gamma^2}{2}$$

$$;\alpha+\pi \ge \alpha+\gamma \ge \pi \qquad (15)$$

Again $V_b/K\phi w_e=\sin\alpha$ has been used and the relationship between α and γ is now given by Eq.10.

With the use of Eq.14 & 15 and Eq.9 & 10, $f(\sin\alpha)$ can be plotted as a function of $\sin\alpha$. The plot is shown in Fig.9.

It is of interest to calculate the maximum average-

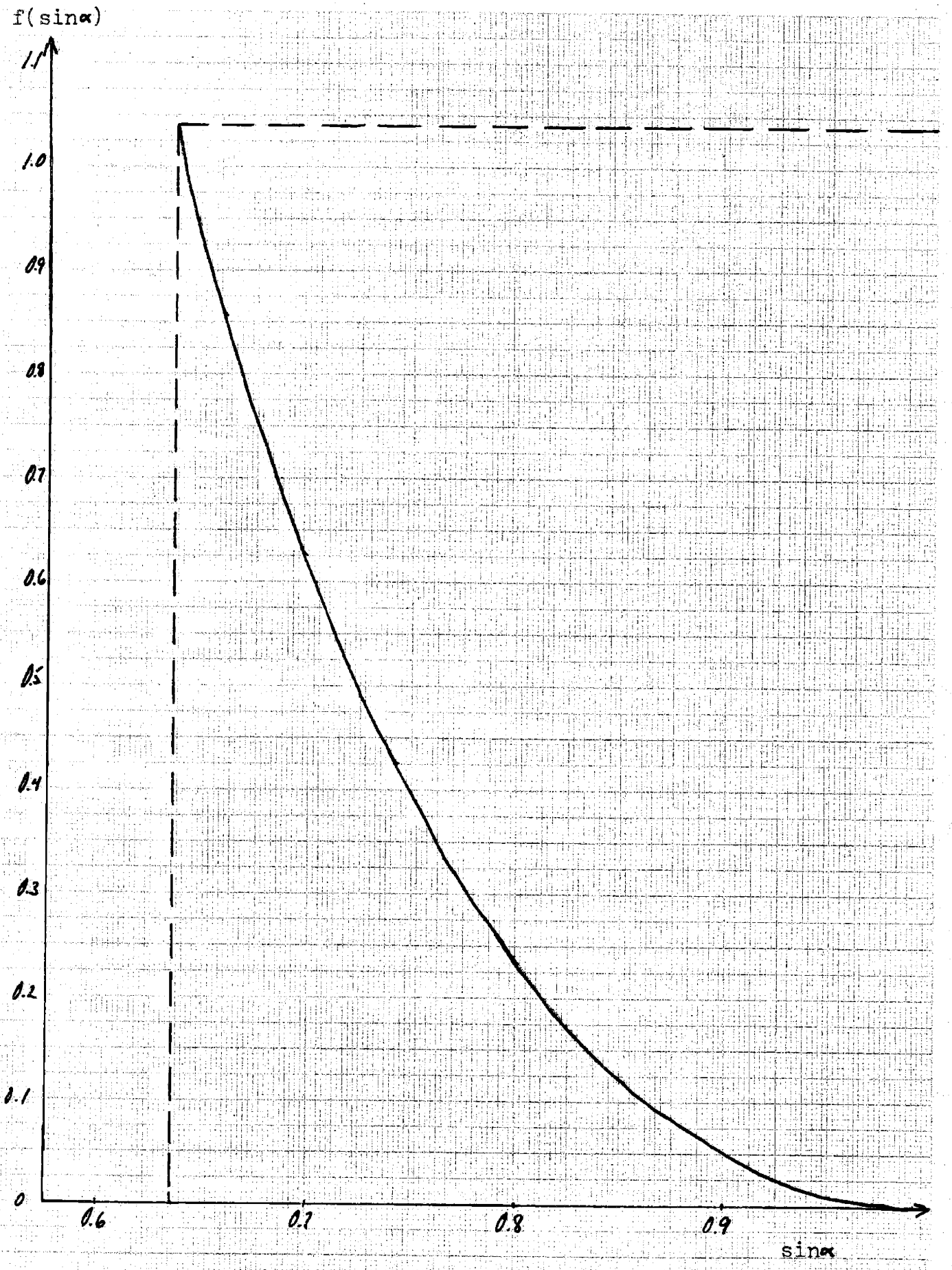

Fig.9 : Plot of f(sinα) vs. sinα

current output of the generator. When $\sin\alpha = V_b/K\phi w_e = 2/\pi$ then , from Eq.10, $\gamma = \pi$. This situation corresponds to an averge rectified generator-armature-voltage equal to the applied open-circuit battery-voltage. Here the current is finite over the whole rectified voltage cycle, except at the points of time $w_e t = n\pi (n=0,1,2...)$, where the current is zero for an instant. As was seen previously, any further increase in source-voltage leads to current instability in the charging circuit. Thus, it is for the above generator voltage that stable maximum average-current occures.

Substituting $\sin\alpha = 2/\pi$ and $\gamma = \pi$ into Eq. 13 & 15 gives the average current

$$i_{ave} = \frac{0.21K\phi}{L} \text{ amp} \qquad (16)$$

It was previous calculated (section 2.2) that a series inductance of 2.3×10^{-3} henries will limit the peak current to 18 amp when the generator flux level is at its maximum, i.e. $K\phi = K\phi_m = 0.098$V-sec. Thus the maximum average-current possible in the charging circuit, having ignored battery resistance, is

$$i_{ave}(max) = 8.9 \text{ amp}$$

The generator power output, ignoring power losses

in the battery, is again the product of the average charging current and the the open-circuit battery-voltage. Thus, using Eq.13,

$$\text{Generator Output} \equiv P_e = V_b i_{ave}$$

$$= \frac{V_b^2}{\pi w_e L} \cdot f(\sin\alpha) \qquad (17)$$

where $f(\sin\alpha)$ is given by Eq.14 or 15. However, for convenience, the power output of the generator will be represented as a function of all the circuit parameters, i.e.

$$\text{Generator Power Output} = P_e[w_e, V_b, K\Phi, L] \qquad (18)$$

where $K\Phi$ has been used as the machine flux parameter.

CHAPTER III

STEADY-STATE SYSTEM OPERATION

In chapter 2 the power output of the generator was calculated (Eq.17 or 18). However Eq.17 does not, by itself, define the electrical output of the generator. An operating point is defined for the generator where mechanical-power input and electrical-power output are identical. This is assuming total conversion, i.e. no power losses within the system. This chapter is concerned with the steady-state behavior of the electromechanical conversion system.

3.1 The Coupled System

The mechanical-power input to the conversion system is dependent on the characteristics of the mechanical system (the windmill) and its source of energy (the wind). The windmill couples the wind energy to the energy of a rotating shaft. In this form the mechanical energy is easily converted, via a rotating machine, to the desired electrical energy for storage in batteries.

For system efficiency it is also desired to maximize the energy transfer from the wind to the electrical system. Thus the problem is to operate the overall power system, windmill, generator, and battery load, at the point where maximum power transfer is achieved.

As a first approximation, the mechanical and electrical subsystems will be considered free of any power-loss

mechanisms. This assumption is a very rough one. However it leads to a much more simple discussion of the problem and gives a starting point to the analysis. The effects of loss mechanisms will be discussed in a later section.

The characteristics of a windmill were previously discussed (section 1.1). It was found that the power extracted from the wind is a function of the wind velocity, the density of the air, the characteristics of the windmill and thewindmill shaftspeed. For a given windmill if variations in air density are neglected then the power transfered from the wind to the windmill shaft can be written as, from Eq.2,

$$\text{Mechanical Shaft Power} = P_m\left[v_w, w_s\right] \qquad (19)$$

The electrical-power output of the generator was previously discussed (section 2.3) and is given by Eq.18.

From Newton's second law steady-state operation of the electromechanical conversion system occurs where Eq. 18 and 19 are identical. If P_m is not equal to P_e then the system is not in equilibrium. Provided the system is stable, the independent and/or controlled parameters would readjust themselves until equilibrum is reached.

If the generator field exitation, battery voltage and series inductance are not control parameters, i.e. are held fixed, then the only varying parameters in P_m

and P_e are wind velocity, v_w, and shaftspeed, w_s, where w_s is directly proportional to electrical frequency, w_e. Thus in equilibrium the system operates where

$$P_m[v_w, w_s] = P_e[w_s] \qquad (20)$$

Eq.20, provided that it is solvable, shows that, for a specified wind velocity, a steady-state operating shaftspeed is defined for the system. Stated previously (section 1.1) was the fact that maximum power extraction from the wind requires the operating windmill shaftspeed to be proportional to wind velocity. The actual operating shaftspeed, obtained from Eq.20, is, however, generally different than this desired shaftspeed. Thus maximum power extraction from the wind is not achieved, in this case.

The ability to adjust generator field excitation, battery voltage and charging-curcuit inductance now allows the shaftspeed to operate over a range of values given by

$$P_m[w_s, v_w] = P_e[w_s, V_b, K\emptyset, L] \qquad (21)$$

where Eq.18 & 19 have been used.

For maximum power extraction from the wind the desired operating shaftspeed is proportional to the wind velocity, i.e. $w_s = av_w$, where 'a' is a constant. Thus for a given wind velocity, V_b and/or $K\emptyset$, and/or L theoretically

can be adjusted until

$$P_m\left[v_w, w_s=av_w\right] = P_e\left[w_s=av_w, V_b, K\emptyset, L\right] \qquad (22)$$

In other words, the load on the electrical system can be altered until the desired shaftspeed is attained.

More than one combination of values for V_b, $K\emptyset$, and L may exist to solve Eq.22. However, these parameters have engineering limits to their ranges of operation. Thus any solution to Eq.22 cannot have these parameters take on values that exceed their practical limits.

3.2 Electrical and Mechanical System Constraints

It is important to know the steady-state characteristics and limitations of the proposed electrical and mechanical systems. Otherwise proper implementation of Eq.22, to maximize electromechanical power transfer, cannot be achieved.

The series inductance, L, is a parameter that cannot be easily varied in the charging circuit. Thus L was chosen, because of circuitry limitations, to limit the peak charging current.

The battery voltage, V_b, can be varied but the variation can only be partially controlled. In the SEP system, battery voltage can be applied, to the charging circuit, in four discrete steps. The nominal voltage of each step has been previously stated (section 1.2) to be

42 volts, with an approximate 10% variation due to battery state of charge. Since the battery state of charge is totally dependent on the SEP system's power input-output profile, the only possible battery voltage control is through the discrete stepping of the batteries.

The flux level, KØ, of the generator is limited by the magnetic flux saturation of the machine iron. This flux saturation results in iron-core power losses which lower generator efficiency and may lead to machine overheating.

The constant, K, is dependent on the physical size of the machine and the design of its windings.

The KØ limit is related to the voltage, speed and power ratings of the machine.

Lastly, centrifugal forces on the generator rotor set a limit on shaftspeed, w_s. This also sets a limit on the corresponding electrical frequency, w_e.

One important assumption has been made throughout the text that will be made reference to at this time. It has been assumed that a windmill can operate at the shaft-speeds required to extract maximum power from the wind. In today's technology, large-scale windmills still have a problem operating at certain shaft speeds. This problem results from resonances within the structure of the windmill. These resonances may, eventually, physically destroy the windmill.

For the purposes of this paper it has been assumed that this problem will have been solved in a few years and therefore puts no constraint on the mechanical system.

3.3 Limits on Generator Power Output (P_e)

Now that the limitations of the electrical and mechanical systems are known, the task remains to vary the control parameters, V_b and $K\phi$, until the desired shaft speed is attained. This can be done for as long as there exists a solution to Eq.22 that will satisfy the constraints on V_b, $K\phi$, and w_s. When Eq.22 can no longer be satisfied then maximum power can no longer be extracted from the wind. This situation will definitely occur for high wind velocities since the limitation on generator shaftspeed will no longer allow the desired relationship, $w_s=av_w$, to hold.

In view of the electrical and mechanical constraints, the electrical power output of the generator, P_e, can be plotted as a function of electrical frquency, w_e, and the possible operating values of V_b and $K\phi$. L is held fixed at the value calculated in section 2.2.

The greatest rate of energy transfer to the batteries was shown (section 2.2) to occur when $V_b/K\phi w_e=2/\pi$, or when the conductance angle $\gamma=\pi$. Any smaller values for $V_b/K\phi w_e$, or larger values of γ, led to charging current instability.

One can plot P_e (section 2.3, Eq.17) with $V_b/K\phi w_e=2/\pi$

and with the flux, $K\phi$, equal to its recommended maximum, $K\phi_m$=0.098V-sec (see Appendix B). This plot results in a curve that defines the steady-state limit of power-output operation for the given generator and charging system. For $V_b/K\phi w_e=2/\pi$, or $\gamma=\pi$, then from Eq.17

$$P_e = \frac{V_b^2}{\pi w_e L} f(2/\pi) \qquad (23)$$

$$\sim \frac{V_b^2}{\pi w_e L} \sim V_b \sim w_e$$

The dotted line in Fig.10 shows this steady-state operating-limit of the electrical system. All operating points of generator power-output and electrical frequency must occur below this line otherwise charging current instability or machine flux saturation will result. This power-limit line is also marked for the battery voltages that normally appear at the generator output (see Apendix A).

The curves P_{e1} to P_{e4}, in Fig.10, are plots of

$$P_{en} = \frac{(n\cdot 42V)^2}{\pi w_e L} \cdot f\left(\frac{n\cdot 42V}{K\phi_m w_e}\right) \quad ;n=1,2,3,4. \quad (24)$$

These are plots of Eq.17 with 1) the battery voltage, V_b, taking on its four possible discrete nominal values, i.e. $V_b=n\cdot 42V$;n=1,2,3,4, and 2) the flux, $K\phi$, equal to its maximum value, $K\phi_m$. The plots P'_{e3} and P''_{e3} show the ranges of P_{e3} as the voltage per battery section changes from 38V to 46V. Similar curves also exist for P_{e1}, P_{e2} and P_{e4}.

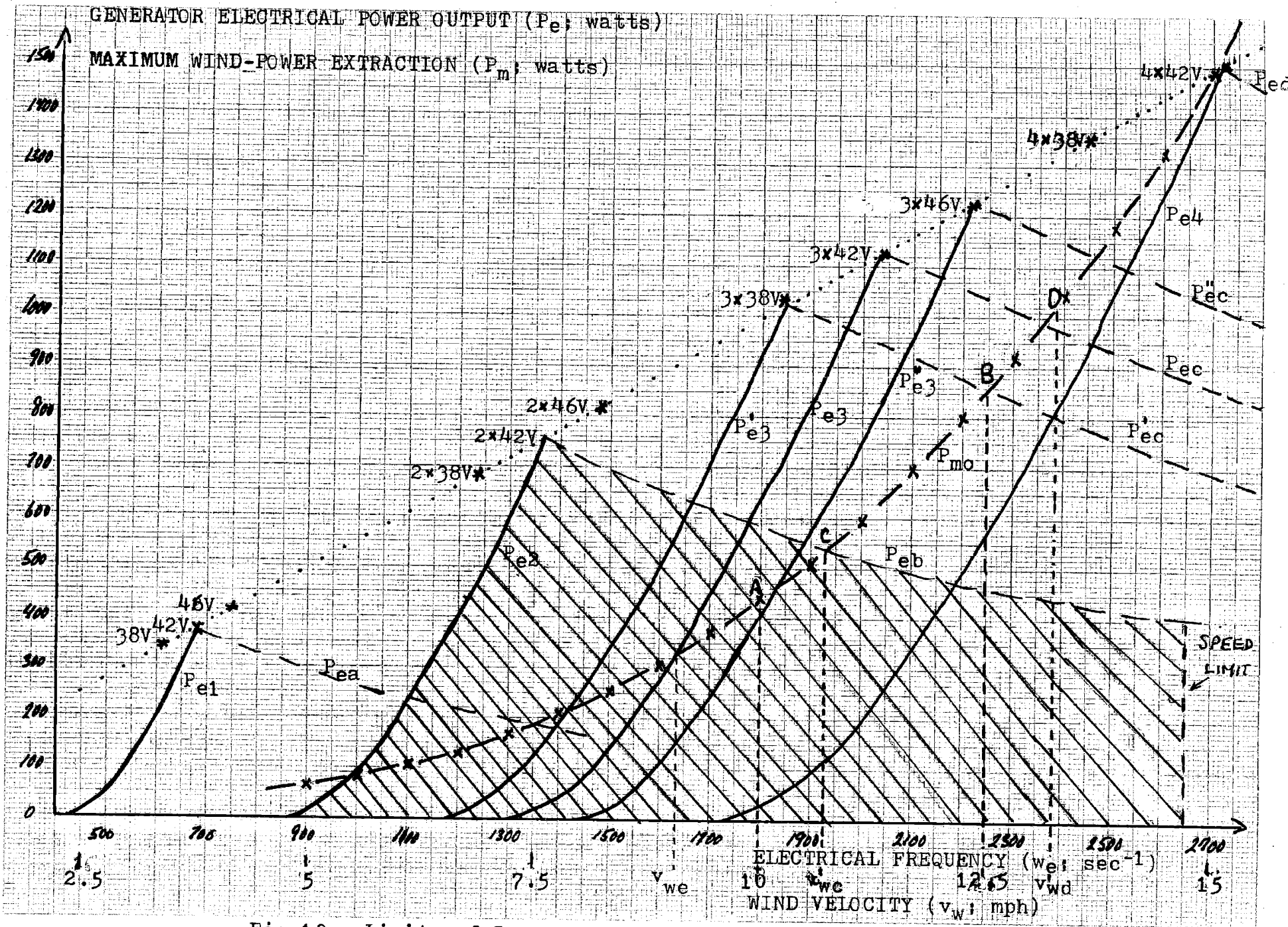

Fig.10 : Limits of Generator Operation

These curves also define operating limits for the system. If, for example, V_b=2·42V then system operation cannot occur to the left of curve P_{e2}. This is because the machine flux cannot be further increased above its already maximum value, $K\phi_m$.

Lastly curves P_{ea} to P_{ed} are plots of P_e with $V_b/K\phi w_e = 2/\pi$, or the conductance angle $\gamma = \pi$. For each curve V_b takes on one of its four possible discrete nominal values. Thus

$$P_{em} = \frac{(m \cdot 42V)^2}{\pi w_e L} \cdot f\left(\frac{m \cdot 42V}{K\phi w_e} = \frac{2}{\pi}\right) \qquad (25)$$

$$; \; m = 1(a), 2(b), 3(c), 4(d)$$

$$\sim \frac{1}{w_e} \sim K\phi$$

Note that the only other varied parameter in Eq.25, besides w_e, is $K\phi$. As $K\phi$ is varied steady-state operation occurs below a P_{em} curve because any attempt to increase the current conductance angle, γ, leads to charging-current instability. The decreasing characteristic of the P_{em} curves, with increasing frequency, is not obvious at first glance. It is because the average charging-current decreases with increasing frequency due to the increasing impedance of the inductor in the circuit.

The shaded area of Fig.10 shows an example of a power-speed operating region for the electrical system; here the battery voltage is 2·42V. Any power-speed operation

outside this region 1) results in charging current instability or 2) is beyond the limit of machine flux saturation or 3) is beyond an acceptable maximum speed for the generator, in this case taken to be at 3600 rpm, or an electrical frequency of about 2640 sec^{-1} (see Appendix B).

3.4 Coupled System Operation

Steady-state system operation, for the lossless electromechanical system, occurs when the sum of the powers into the system is zero. Fig 10, so far has shown the possible values of generator power output as a function of the electrical system parameters. To locate the system's steady-state operating points, it is now necessary to plot the power-input to the system as a function of the same parameters.

The characteristics of the power-input system (windmill) were discussed in section 1.1. There it was stated that the maximum power extractable from the wind is proportional to the cube of the wind velocity, v_w, i.e.

$$\text{Maximum Wind-Power Extraction} \equiv P_{mo} = bv_w^3 \quad (26)$$

where b is a constant of the windmill.

It was also stated in section 1.1 that the windmill shaftspeed, at which this maximum power is extracted from the wind, is proportional to the wind velocity, i.e.

$$\text{Maximum-Power Shaftspeed} \equiv w_{so} = av_w \quad (27)$$

where 'a' is also a constant of the windmill.

It is desired that system operation occure at this maximum-power shaftspeed. Using the fact that shaftspeed is related to the electrical frequency by a constant*, Eq. 26 can be plotted onto Fig.10 in the form

$$P_{mo} = bv_w^3 = \frac{b}{a^3} w_{so}^3$$

$$= \frac{b}{(7a)^3} w_{eo}^3 \qquad (28)$$

where w_{eo} is the corresponding electrical frequency of the generator-armature-voltage where maximum power is extracted from the wind. Also Eq.27 was used. The plot of Eq.28 on Fig.10 is with a=180/7 and b=0.45. The choice of 'a' and b was made under the assumption that a 15 mph wind velocity† will supply enough power to the generator to drive the generator to its maximum power output** This is also under the condition that none of the mechanical or electrical system constraints is exceeded.

Now that both the desired-input and output power-curves are plotted on the same axes, one can see how the control parameters, battery voltage and generator field-flux level, can be driven to achieve desired steady-state

*$w_e=7w_s$ for the proposed machine (see Appendix B)

**The desired peak generator output is the product of maximum battery-voltage and maximum average-charging-current. The maximum chargeable battery voltage is approximately 170V(see section 1.2). The maximum average-charging current was calculated to be about 9 amp(see section 2.3). Thus the maximum average-power output of the generator, ignoring power losses, is 170VX9amp≈1500 watts.

†These units for wind velocity are chosen for convenience.

operation. As an example consider a wind velocity of 10 mph. The shaftspeed, for which maximum wind-power extraction occurs, is thus $av_w=(180/7)\times 10\simeq 260 sec^{-1}$. The corresponding electrical frequency is $7av_w=1800\ sec^{-1}$. Maximum wind-power extraction will occur when, in Fig 10, a P_e curve intersects the P_{mo} curve at this desired electrical frequency (point A in figure). If the SEP battery voltage is 42V/section then, with two battery sections on charge, the region of system operation is the shaded area in Fig 10. Since point A is in this shaded area then maximum power extraction from the wind can be achieved. An easy way to accomplish this is by monitoring the electrical frequency, or shaftspeed, and adjusting the flux level in the machine, via field-current control, until the desired frequency is attained.

Notice when three battery sections are on charge then point A also lies in the allowed region of system operation, defined by curves P_{e3} and P_{ec}. Thus there are two ways maximum wind-power extraction can be achieved, with either two or three battery sections on charge.

For the wind velocity of 12.5 mph, point B, in Fig. 10, is the desired operating point of the system. The figure also shows that this operating point can be achieved only with three battery sections on charge. This is because point B is outside the regions of operation for any other number of battery sections on charge.

An interesting situation occurs at the wind velocity,

v_{wd}. Again consider the SEP battery voltage to be 42V/section. From Fig.10 we see that the desired maximum-power shaft-speed is $w_{ed}/7$, or an electrical frquency w_{ed}. Point D is thus the desired operating point. Yet point D is outside the operating region for any number of battery sections on charge, since point D lies above P_{ec} and to the left of P_{e4}. The situation is showed in more detail in Fig.11.

$P_m(v_{wd})$ is the power-speed characteristic of the windmill with the wind velocity at v_{wd}. From Fig.11 it can be easily seen that point D is not within a possible region of operation of the electrical system, defined by the shaded areas for 3 or 4 battery sections on charge. System operation must now occur away from the shaftspeed where maximum wind power extraction is achieved. Operation will now have to occur at a pseudomaximum-power point. With three battery sections on charge points 2 and 3, Fig.11, are the two possible pseudomaximum-power operating points for the system. Since there are two possible points of system operation the question of stability arises. The ablility to answer this question requires further analysis of the coupled electromechanical system and is not discussed here.

If four battery sections were on charge for the situation in Fig.11, then point 1 is where maximum wind-power can be extracted without exceeding the limitations of the electrical system. Whether points 1, 2 or 3 is the most desirable,

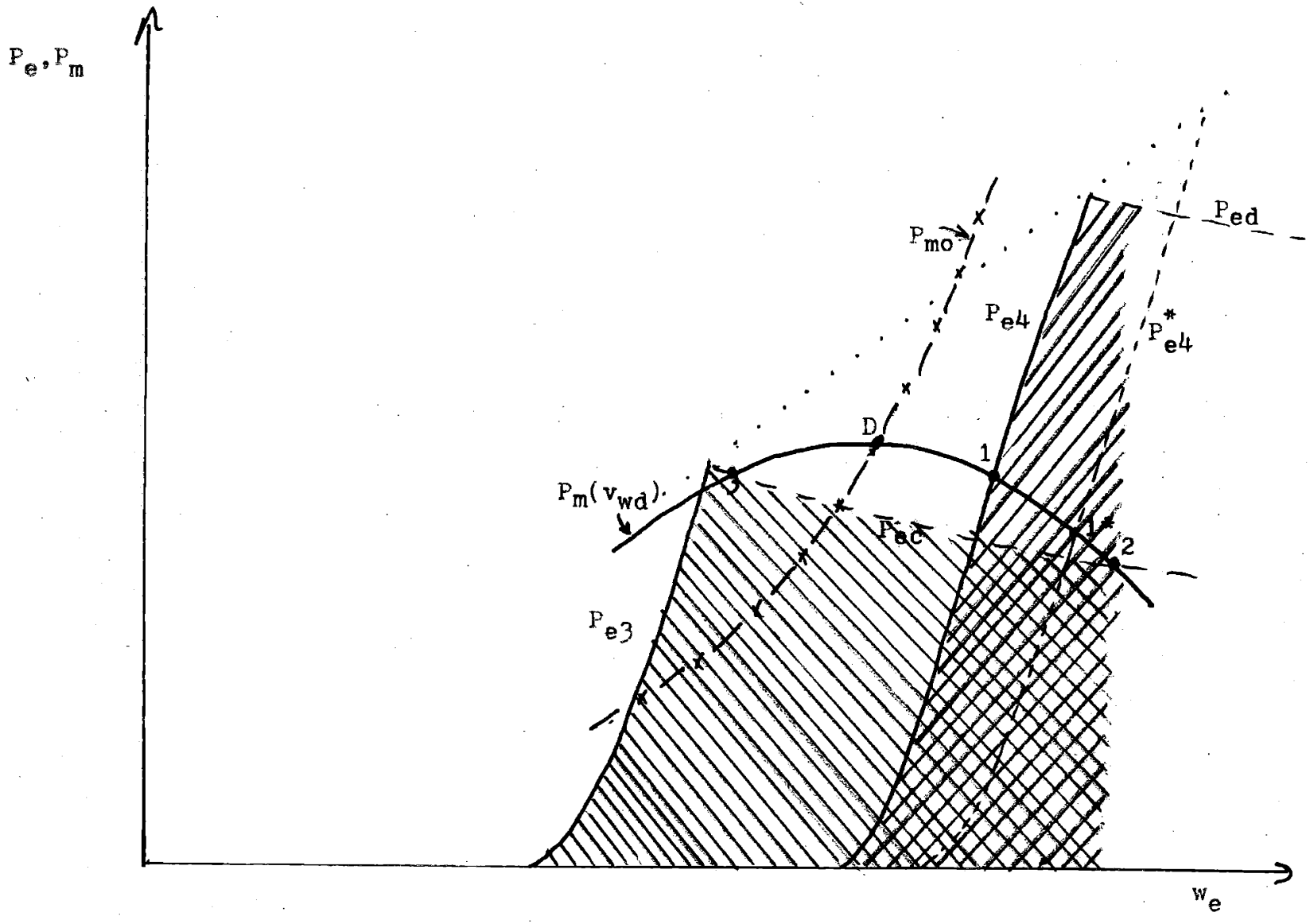

Fig.11 : More Detailed View Of System Operation

i.e. where most wind power is extracted, depends on the shape of $P_m(v_{wd})$ and on the proximity of P_{e4} with respect to P_{e3}. As drawn, Fig.11 shows that operation at point 1 offers greatest wind-power extraction. However, if P_{e4} had been actually located at P_{e4}* then point 3 becomes the most desirable operating point; power extraction at point 1* is less than power extraction at point 3.

The above discussion has shown that more than one way of varying the electrical-system control parameters, i.e. battery voltage and generator field flux, is possible to obtain maximum or pseudomaximum power extraction from the wind. The problem is to know when to switch battery sections in or out of charge. A method will now be suggested for performing these operations.

3.5 Battery Switching Criteria

Reconsider operation at point A, Fig.10, for a 10 mph wind and two 42V battery sections on charge. The shaded area defines the range of operation for the conversion system. If the wind velocity increases then a field current adjustment is necessary to keep operation at maximum wind-power extraction. If the wind velocity increases above v_{wc} then maximum power cannot be extracted from the wind. This is because operation is not allowed above curve P_{eb}. Switching another battery section into charge would redefine the region of system operation. In this way maximum wind-power extraction is again achievable

through just field-current control. This battery switching criteria can be implemented by switching another battery section into charge when continuous charging-current is sensed.

Now consider three battery sections on charge and the wind velocity decreasing from 10 mph, Fig. 10. If the wind velocity becomes lower than v_{we} then generator flux can no longer be increased, due to flux saturation in the generator, such that desired maximum-power operation can occur to the left of curve P_{e3}. Switching a battery section out of charge is now necessary to allow system operation again to occur at maximum wind-power extraction.

In summery the previous discussion suggests possible methods of controlling the operation of the electromechanical conversion system such that maximum wind-power extraction is obtained. These control methods were introduced considerein negligible battery resistance and negligible power losses in the system, The effect of power losses and battery resistance will now be discussed.

3.6 System Operation with Power Losses

Appendix D sumarizes the sources of power loss within the windmill power system. Considering these loss mechanisms, steady-state windmill operation will now occur where the power extracted from the wind is equal to the sum of the power stored on the batteries and the power consumed by losses. The object of the conversion system is no longer

the extraction of maximum power from the wind. The goal is now to maximize the power stored in the battery banks. To do this it will be necessary to model all the sources of power loss in the system. If it is possible to express all these losses as a function of windmill shaftspeed then the power being stored in the battery banks can be totally expressed as a function of the same shaftspeed and wind velocity, i.e.

$$\text{Power Stored} \equiv P_e = P_m[w_s, v_w] - P_l[w_s] \qquad (29)$$

where P_m is the power extracted from the wind and P_l is the power lost. It would now only be necessary to maximize P_e, with respect to shaftspeed, to find an expression relating wind velocity to a shaftspeed where maximum power is absorbed by the batteries. With no losses the objective was to control the windmill shaftspeed in a linear relationship to wind velocity (see section 3.1), i.e.

$$w_s = w_{so} = av_w \qquad (30)$$

At this shaftspeed maximum power was extracted from the wind. However, if losses have been totally related to the shaftspeed of the windmill, then the objective now will be to control the shaftspeed as a different function of wind velocity, i.e.

$$w_s = w^*_{so} = a[w^*_{so}]\cdot v_w \quad \text{or} \quad a[v_w]\cdot v_w \qquad (31)$$

where w^*_{so} is the shaftspeed where Eq.29 is a maximum, or

where maximum power is being absorbed by the batteries.

The task now is only to relate the losses in the system to the operating shaftspeed. This task, in itself, is difficult. The losses in the system, as discussed in Appendix D, are a function of not only the operating shaftspeed but also the flux level in the generator and the battery resistance. Steady-state system operation will again occur where the power extraction from the wind, P_m, equals the sum of the power instantaneously being stored in the batteries, P_e, and the power lost, P_l, i.e.

$$P_m[v_w, w_s] = P_e[K\emptyset, w_s, V_b, R_b] + P_l[K\emptyset, V_b, R_b]$$

$$\text{or} \quad Pe[K\emptyset, ws, V_b, R_b] = P_m[v_w, w_s] - P_l[K\emptyset, V_b, R_b] \quad (314)$$

where the internal battery resistance, R_b, and flux, $K\emptyset$, have been added as variables in the expression for power losses. R_b has also been added as a variable in the power absorbed by the batteries, P_e, since it has an effect on charging current.

Maximizing P_e, in Eq.314, with respect to shaftspeed results in a desired shaftspeed that is a function of V_b and R_b. Since V_b and R_b are partially dependent on the state of charge of the batteries, on-line measurement of these variables is necessary to maximize the power into the battery banks. However, this on-line measurement of V_b and R_b is a difficult task and the added expence may not be worthwhile.

There is, however, a compromising alternative. The mechanical losses in the windmill shaft can be totally expressed as a function of shaftspeed and have no dependence on generator flux level or battery parameters. Thus the power in the shaft can be written

$$P_{shaft}[w_s, v_w] = P_m[w_s, v_w] - P_1'[w_s] \qquad (32)$$

where P_1' represents only the mechanical losses in the shaft.

P_{shaft} can now be maximized with respect to shaftspeed. The resulting maximum shaft-power shaftspeed can be expressed in the form of Eq.31 . By making measurements on the windmill, coupled to the generator shaft, and with the generator unloaded, $P_1'[w_s]$ can be calculated. Knowing this and $P_m[v_w, w_s]$, the power extracted from the wind as a function of wind velocity and shaftspeed, $a[v_w]$ can be calculated. Knowing $a[v_w]$, we now know at what shaftspeed, as a function of wind velocity, to operate the coupled windmill-generator to maximize the power in the shaft. Due to losses, the power in the shaft will be less than ideal yet it will be the maximum achievable by the system.

The effects of power losses may also change the battery switching criteria presented in the previous section for a no-loss system. One important effect is that of the internal battery resistance, R_b. Measurements

on the charging circuitry* showed that this resistance had the effect of limiting charging current when the average rectified generator voltage became larger than the battery voltage. Previously the suggested scheme was to switch in an additional battery section for charging when the charging current became continuous. Now, however, we may wish the system to wait until the peak charging current reaches the electronic limitations of the SEP charging circuitry before another battery section is swithed in for charge. Because when this section is switched in, the flux level in the generator must be increased. This increases the peak generator terminal-voltage to a value greater than the increased battery voltage such that power can again be fed into the batteries. The higher flux level, however, produces increased core losses in the generator thus decreasing the net power into the batteries. Yet waiting until peak charging current reaches the current limitations of the of the SEP circuitry, before switching in another battery for charge, will keep generator flux levels lower, thus decreasing core losses. On the other hand, the resulting increased charging current produces greater I^2R losses in the internal battery resistance and thus also decreases system efficiency. A sophisticated control system would be necessary to estimate machine and battery losses and decide on how many batteries to charge based on which configuration produces the least power losses.

*see section 4.1

As a final point, the issue of system stability is important, especially in terms of battery switching. It is still not well understood how the system would dynamically react when a battery section is instantaneously added to or removed from charge. These considerations have to be further studied.

CHAPTER IV

POWER SYSTEM OBSREVATIONS AND MEASUREMENTS

4.1 Charging Circuit Observations

Obsrevations were made on the charging circuitry to see the effects of battery resistance, R_b and synchronous inductance, L_s†. Fig. 13 shows the voltage $v_o(t)$ and current $i(t)$ (defined in Fig. 7)*. The battery voltage is approximately 80V and the peak rectified generator voltage is approximately 95V. The high frequency ripples in the voltage waveform is due to the nonuniform distribution of the windings in the generator. Notice that these waveforms are what one expects when battery resistance and machine inductance are ignored. One effect of battery resistance is, however, the partial phase shifting of the current waveform. With no circuit resistance the peak of the current waveform occurs exactly where $v_o(t)$ equals the battery voltage (see section 2.1). With circuit resistance this is no longer true. Yet, in Fig.12, hardly any phase shift in the current waveform is noticable, thus battery resistance must be small compared to the impedance of the inductor.

Fig.13 shows a similar waveform as in Fig.12 but now the peak generator voltage is approximately 115V. Notice when the voltage waveform comes to zero, it does not again increase as we might expect. Instead the voltage stays at

*the value of L used was 2.3 mh, as calculated in section 2.2

† see Fig.6

zero and then steps up to the rectified voltage, before normally stepping up to the battery voltage when the current goes to zero. This effect of $v_o(t)$ remaining zero before continuing to follow the rectified voltage is due the machine inductance, L_s. At the time $v_o(t)$ goes to zero the current through the bridge want to commutate from one pair of diodes to the other such that the direction of the current is reversed in the generator. However, the inductance, L_s, does not allow the current through it to change instantaneously. It will thus take time for the current to commutate from one pair of diodes to the other pair. During this time all four diodes are conducting thus shorting the voltage $v_o(t)$.

Fig.14 shows the same waveforms again but now the average value of the rectified voltage waveform is being forced to become larger than the battery voltage. Here the current becomes continuous, never going to zero, and is limited by the battery resistance.

Fig.15 shows the same situation as in Fig.14 but the current waveform is of the generator armature circuit. Notice again that the armature circuit inductance forces the current to cross zero before one pair of dioded turns off to let the voltage, $v_o(t)$, again follow the rectified generator voltage.

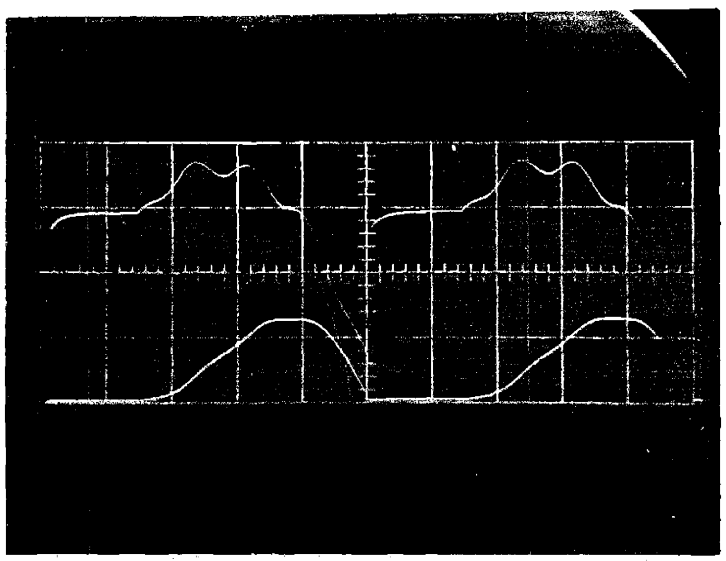

(time scale:0.5ms/div)

Fig12: Charging-Circuit Waveform

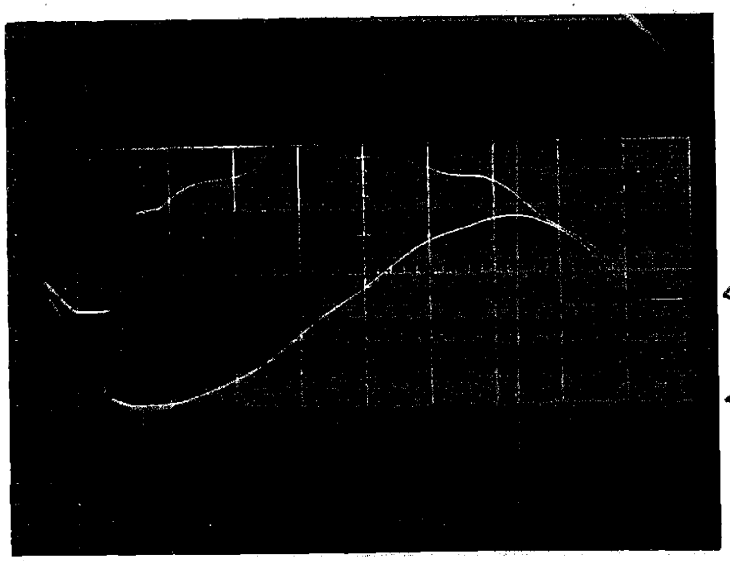

(time scale:0.2ms/div)

Fig13: Charging-Circuit Waveform

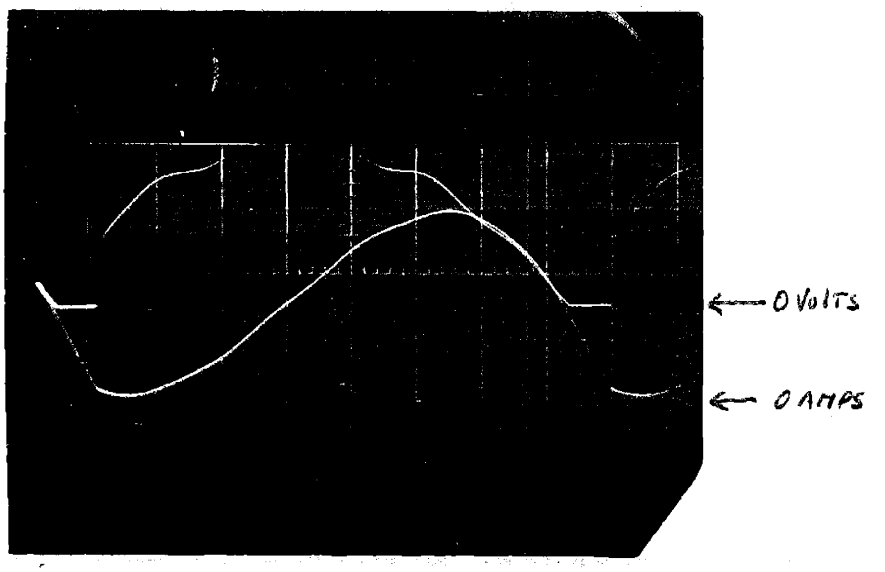

(time scale:0.2ms/div)

Fig14: Charging-Circuit Waveform

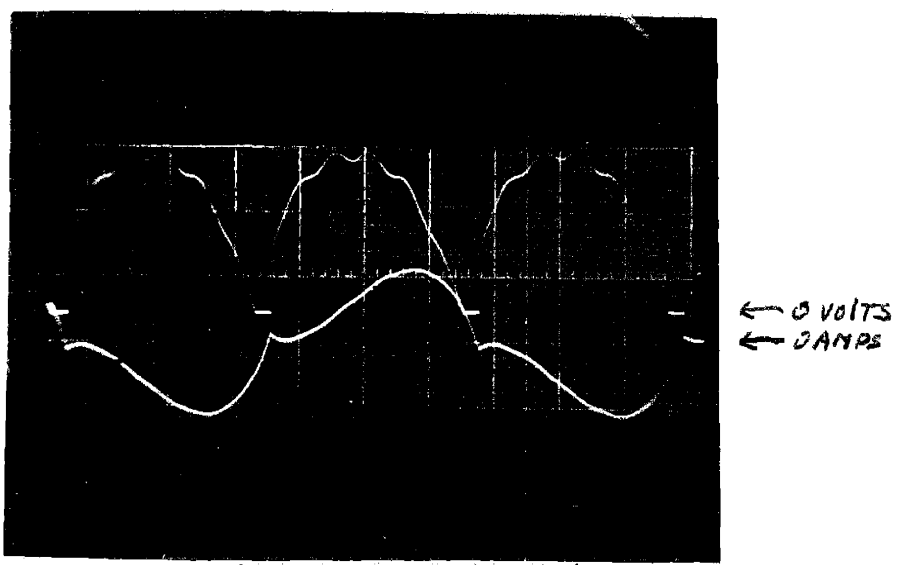

(time scale:0.5ms/div)

Fig15: Charging-Circuit Waveform

4.2 Generator Power Output Measurements

A dc motor was used to simulate the power-speed characteristics of a windmill (see Appendix C).

The plots to be presented in this section show

(1) the measured power output of the generator,

(2) the measured wind-power extraction (or power input to windmill simulator),

(3) the calculated power in the windmill (or simulator) shaft (see Appendix C),

(4) the estimated power being stored in the batteries,

(5) the ideal generator-power-output for the no-loss power system (see section 3.3 & Fig.10).

These plots were made with

(a) a constant number of battery sections on charge, and

(b) the flux level in the generator at its acceptable maximum(see Appendix B).

Thus, in making the following plots, the only varying input parameter was wind velocity.

If the system contained no sources of power loss then the power-speed curves generated in (1),(2),(3),(4) and (5), above, would all be identical. Also, under the conditions of (a) and (b) these curves would be identical to curves P_{e1} to P_{e4} in Fig.10. Since there are power losses in the system, the plots mentioned will show not only how well the actual generator power output correlates

to the ideal charging system discussed in Chapter 3, but also where the power losses occur in the system.

Fig.16 and 17 show the five plots discussed above with, respectively, two and three battery sections on charge. Also, as stated in condition (b), the generator flux level is at a maximum.

It should also be stated that these plots are not made under the condition of maximum power transfer from the wind to the electrical system. These plots only show the power-speed charactetistic of the generator output and how this characteristic relates to the power at other points in the system under the same conditions.

The data points in Fig.16 & 17 were taken by measuring the power extracted from the wind (or power into the windmill simulator) and the power output of the generator.

The power in the shaft was calculated by subtracting the estimated power losses of the windmill simulator (see Appendix C) from the power supplied to the simulator under a certain wind condition.

The power output of the generator is identical to the power entering the batteries and is the product of the battery-terminal-voltage and average charging-current.

The power stored in the batteries was calculated by subtracting the estimated losses in the battery internal resistance from the power entering the batteries. The size of the battery resistance was estimated by observing

FIG 16: SYSTEM POWER INPUT & OUTPUT AS A FUNCTION OF WIND VELOCITY

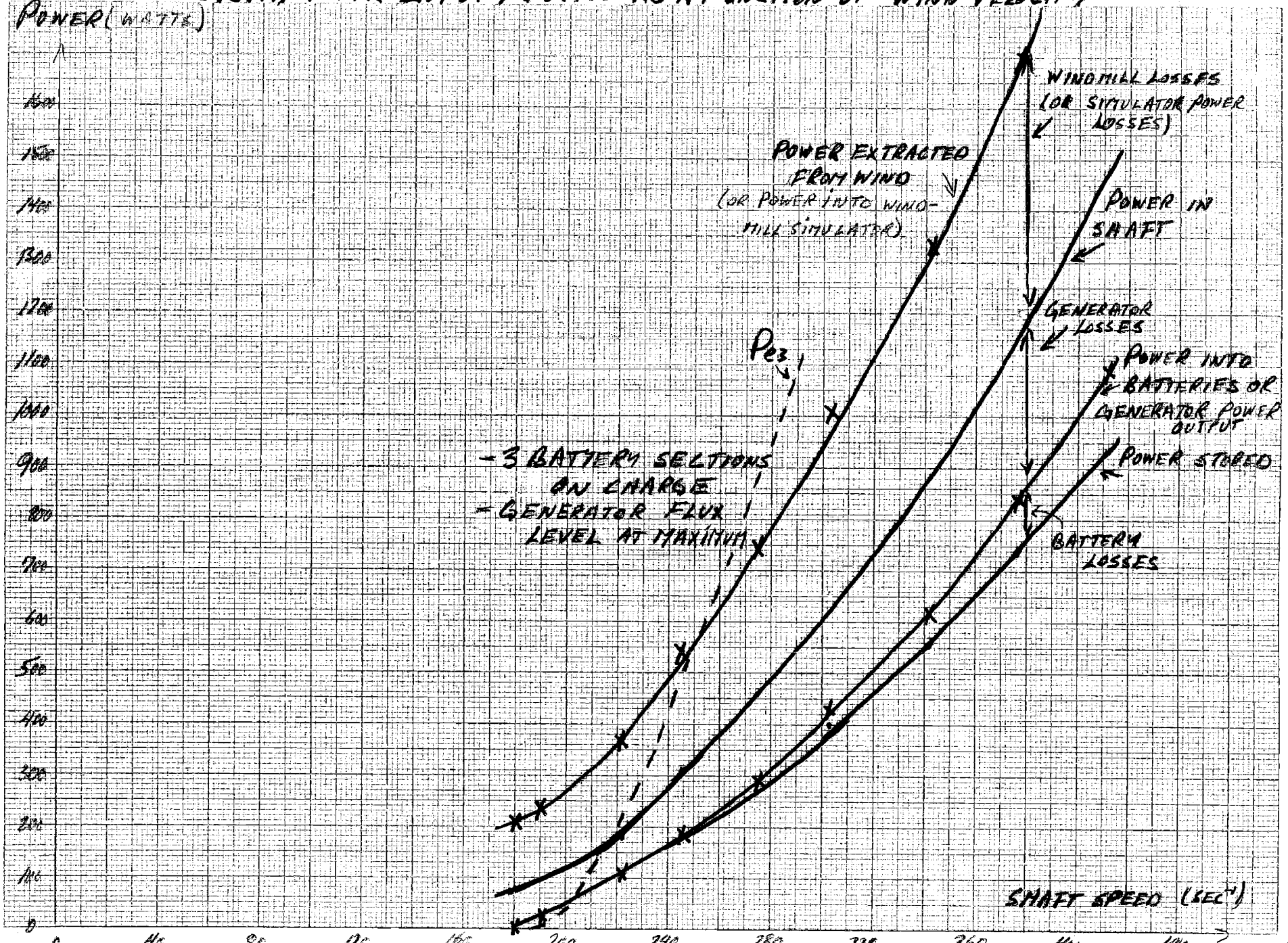

FIG: 16

FIG 17: SYSTEM POWER INPUT & OUTPUT AS A FUNCTION OF WIND VELOCITY

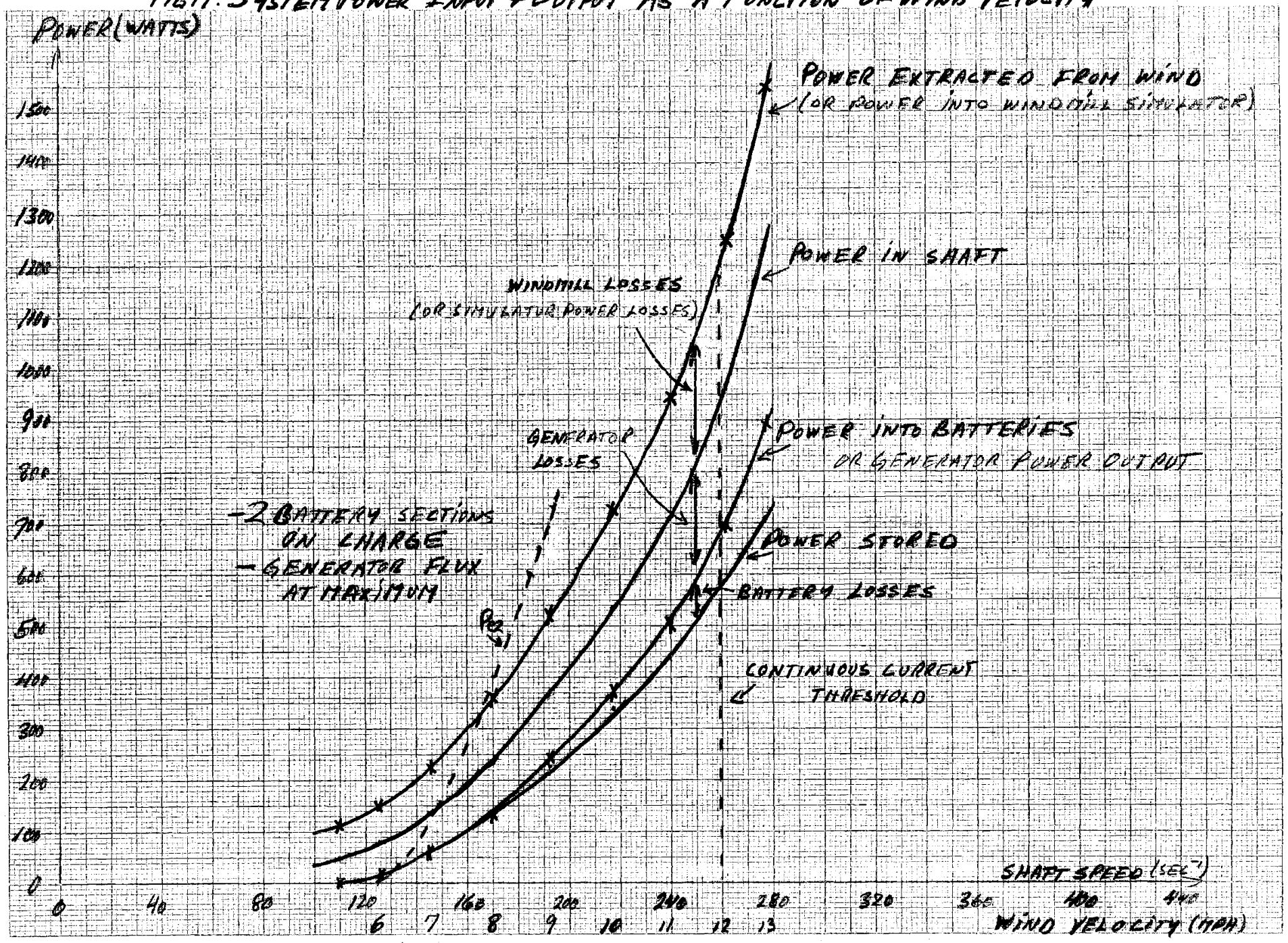

FIG. 17

the change in battery terminal voltage as a function of the average charging current.

The dashed curves, P_{e2}, P_{e3}, in the plots, are the power-speed curves one would expect to see had the system been loss-free (see Fig.10).

Note that the curves showing the power entering the batteries do not rise as sharply, with wind velocity, as does the ideal generator-output curve. One factor this may be attributed to is finite battery resistance. As wind velocity increases, battery charging current increases due to increases generator voltage. This increased charging current causes an increase in battery terminal voltage due to the finite battery resistance. Thus the generator sees an effective higher emf at its output. This higher battery emf goes to reduce the average charging current output of the generator to an extent that the power entering the batteries is less than expected. This effect can be further understood from Fig.10. Consider curve P_{e3} with the battery load of 3.42V. If battery terminal voltage increases then P_{e3} will move toward P'_{e3} thus reducing generator power output per given shaftspeed. However, this increase in effective battery voltage was not found to be a substantial reason to explain the total discrepency between P_{e3} and the measured generator output. Further analysis of the generator charging system will thus be necessary in any further study.

4.3 Further Generator Power Output Considerations

One other observation, shown in Fig.17, is of interest. The dashed vertical line in the figure represents the threshold where the charging current became continuous. Thus all power-speed operating points above this threshold have a continuous current flowing into the batteries. It was previously discussed (section 2.2) that a continous charging current meant that an average voltage was across the series inductor in the charging circuit. This would have led to a monotonically increasing charging current. However, it is seen from Fig.14, and Fig.15, that current instability does not occur in the case where the average rectified-generator-voltage is forced larger than the battery voltage. It was also stated (section 4.1) that the internal battery resistance was limiting the current in this situation. This may be true. However, further consideration must also be made in terms of system stability. A monotonically increasing charging current would load down the generator. This leads to a decrease in generator shaftspeed which, intern, decreases generator armature-voltage and thus also limits charging current. Further study is necessary to fully understand these issues of system stability.

However, the single-phase generator used in this scheme can be replaced with a three-phase generator and six-pulse rectifier. In this way the series inductor

can be removed from the charging circuit since the rectified three-phase output acts almost as a dc source to supply the batteries. The charging current will now be limited by the battery resistance. Thus this current will depend on the state of charge of the battery cells. However, the great advantage of the three-phase system over the single-phase system is that a larger average current, per given peak current, can be supplied to the batteries.Thus more power can be supplied to the batteries if the peak current is to be limited by the electronics of the system.

APPENDIX A

SEP BATTERY SECTION DESCRIPTION AND INTERNAL RESISTANCE MEASUREMENTS

The SEP 42V battery sections consist of four lead-acid batteries. The voltage and capacity rating of each battery is listed in Table A1.

Battery Voltage	Capacity*
1·24V cell	17 a-h**
1·12V cell	25 a-h
2·6V cells***	40 a-h

Table A1: Make-up of SEP Battery Section

Measurements were made of the internal resistance of a 42V section. The variations in this resistance were noted as a function of battery state of charge and charging current. The measurements were taken as a source voltage was instantaneously impressed on the battery section. Thus no change in battery open-circuit voltage or internal resistance was allowed to occur as a function of time.

The results are summarized in Table A2. The resistance measurements are approximate, ±10 to 20%, the worse case being for the smaller resistance values.

*taken at an 8 hour rate

**amperes-hours

***the added 6V is used in the SEP output waveform to keep

Table A2 : Internal Resistance Measurement of 42V SEP Battery Section

Battery Section Capacity	Open-Circuit Voltage	Charging Current	Internal Resistance
Fully Charged	45V±1V	Less than 20% variation in resistance measurement over 2 to 10 amp charging current range	0.7ohm
3 amps out for 1 hour	43V "		0.3ohm
3 amps out for 2 hours	42V "		0.3ohm
3 amps out for 3 hours	41V "		0.3ohm
3 amps out for 4 hours	39V "		0.5ohm
3 amps out for 5 hours	30V-35V	2amps	2.75ohm
		5amps	1.75ohm
		10amps	1.25ohm

In the last set of readings, Table A2, the variation in open-circuit voltage was due to the quick rise in that voltage as the batteries were charged such that the readings could be made. Also note that the open-circuit battery voltage remained in the range of 42V±10% for nearly the whole capacity range.

---

the output voltage nomimal (approximately 42V/battery section) when the state of charge of the batteries is low.

APPENDIX B

GENERATOR CHARACTERISTICS

The synchronous generator used as the electromechanical converter was a Long Island Altenator. Its ratings and specifications are listed in Table B.

Table B : Generator Ratings and Specifications

Rated Shaftspeed	3450 rpm
Rated Armature-Voltage	115V rms
Armature-Voltage Frequency (at rated speed)	400 hz
Rated Armature-Current	17.4 amp
Rated Power Output	2 kw
Field Resistance (at 25°C)	(a) 300 ohm (b) 150 ohm
Armature Resistance (at 25°C)	0.25 ohm

Notice that there are two field windings on the machine, each with a different resistance.

Fig.B shows shows the magnitization curve for the generator. To obtain the curve, the open-circuit armature-voltage was measured at the rated speed of the machine. The relationship between this voltage and the machine shaftspeed is

$$\underset{(OCAV)}{\text{Open-Circuit Armature-Voltage}} = k\phi w_s \text{ V-rms}$$

where w_s is the shaftspeed, ϕ is the flux produced by the field current excitation, and k is a constant

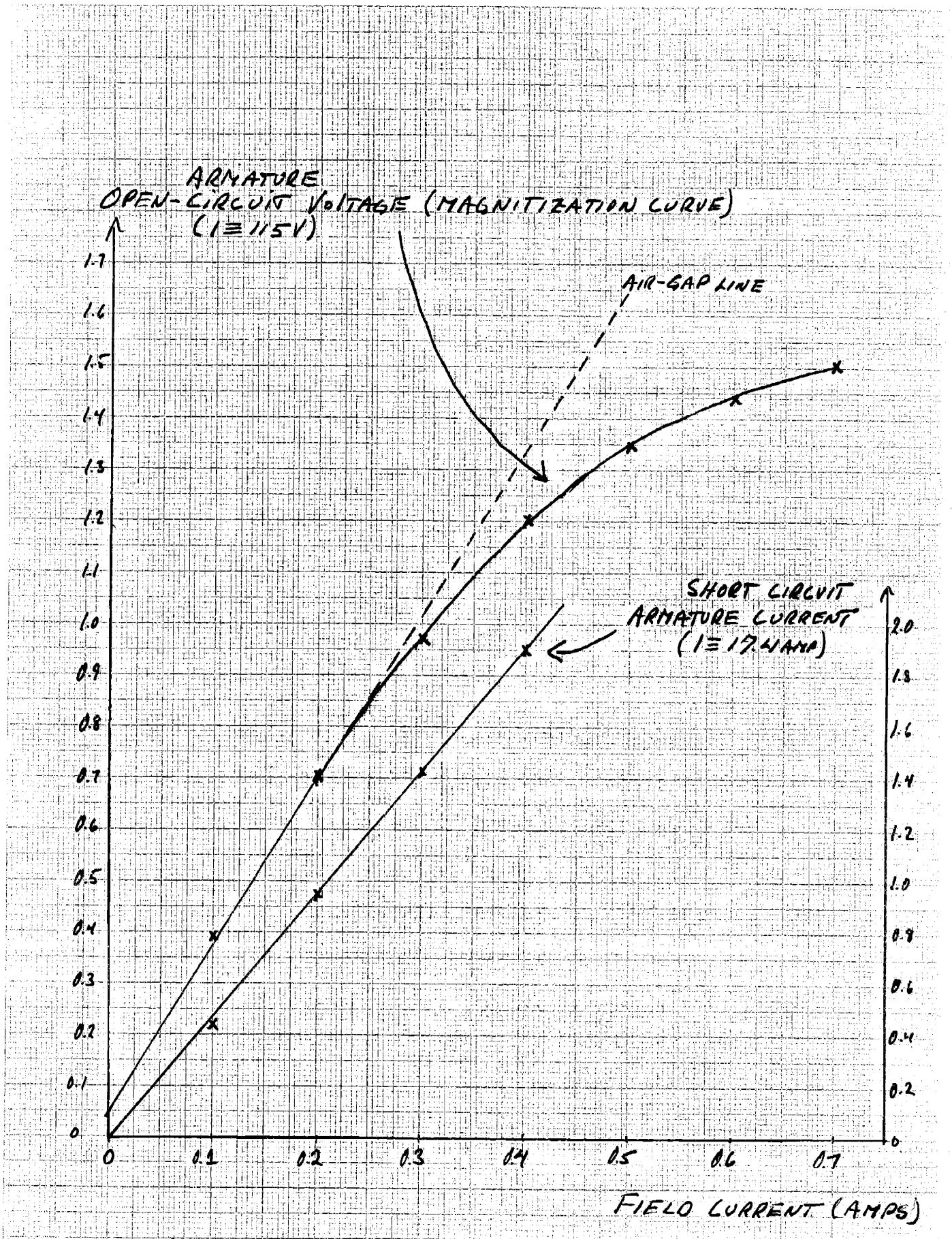

FIG. B: GENERATOR OPEN-CIRCUIT VOLTAGE & SHORT-CIRCUIT CURRENT AS A FUNCTION OF FIELD CURRENT (MEASURED AT RATED GENERATOR SPEED)

dependent upon the size of the machine and the design of its windings. All units are in mks.

Hysterisis effects caised a variation in open-circuit voltage of no more than 5 volts(rms) over the measured voltage range. The finite flux at zero field current (Fig.B) is due to residual magnitism in the machine iron. Fig.B also shows the short-circuit armature-current,as a function of field-current excitation, for the machine. From this curve and the open-circuit voltage curve it is possible to calculate the synchronous inductance of the machine, which comes to be about 12.5 millihenries.

If k' is defined as $\sqrt{2}\cdot k$ then $k'\emptyset w_s$ is the peak open-circuit armature-voltage. The armature-voltage waveform can now be described as

$$OCAV = k'\emptyset w_s \cdot \sin(w_e t) \qquad (B.1)$$

where w_e is the electrical frequency of the armature-voltage waveform. By converting rated shaftspeed and armature-voltage frequency(at rated speed), from Table B, into mks units, i.e. radians per second, the relationship between the two frequencies comes to be

$$w_e = 7w_s \qquad (B.2)$$

Thus the machine is a $2\cdot 7=14$ pole device.

Substituting Eq. B.2 into B.1 results in

$$OCAV = \frac{k'\emptyset w_e}{7} \cdot \sin(w_e t)$$

$$= K\emptyset w_e \cdot \sin(w_e t) \equiv E_f \qquad (B.3)$$

where $K=k'/7$ and E_f is the symbol used, in the main text, for the open-circuit armature-voltage.

The open-circuit armature-voltage is limited by the maximum allowable speed of the machine and the flux saturation of the machine iron. The former can be taken as the rated speed of the machine. The latter is restricted by machine core-power-losses which can lead to machine overheating and deterioration. Because of this the field current of the machine will be restricted to less than 0.7 amps. Thus the maximum value for the flux variable, $K\phi$, will be, from Fig.B and Eq. B.3, and with field current=0.7amp,

$$K\phi(\text{maximum}) \cong K\phi_m = \frac{\text{Peak OGAV(synchronous speed)}}{w_e(\text{synchronous})}$$

$$= \frac{\sqrt{2}\cdot(1.5\cdot 115\text{V})}{2\pi\cdot 400\text{hz}}$$

$$= 0.098\text{V-sec}$$

APPENDIX - C

WINDMILL SIMULATION

The purpose of the work described in this appendix is to simulate, with a dc machine, the power-speed characteristics of a typical windmill. The dc machine is chosen because of its wide range of operating speeds. An analysis will be presented followed by system implementation and system testing and evaluation.

C.1 Simulation Objectives

The properties of a windmill were discussed in section 1.1. There it was stated that the maximum power extractable from the wind is proportional to the cube of the wind velocity, v_w, i.e.

$$\text{Maximum Wind-Power Extraction} \equiv P_{mo} = bv_w^3 \qquad (C.1)$$

where b is a constant of the windmill.

It was also stated in section 1.1 that the windmill shaftspeed, at which this maximum power is extracted from the wind, is proportional to the wind velocity, i.e.

$$\text{Maximum-Power Shaftspeed} \equiv w_{so} = av_w \qquad (C.2)$$

where 'a' is also a constant of the windmill.

In section 3.4 it was shown that in a lossy system the best that can be easily done is the maximization of the

power in the windmill shaft. To achieve this the windmill shaftspeed must be controlled as in Eq.31, i.e

$$w_s = w^*_{so} = a\left[v_w\right] v_w \qquad (31)$$

The maximum power in the shaft will now be, from substituting Eq.31 into Eq. 32,

$$P_{shaft}(max) \equiv P^*_{mo} = P_m\left[w_s=w^*_{so}, v_w\right] - P_l\left[w_s=w^*_{so}\right] \qquad (C.3)$$

The power loss mechanisms of a dc machine, however, are not only of mechanical origin. In this machine losses also arise from the magnetic flux excitation in the machine. Yet the objective of the simulation is to model the dc machine in a way such that an equation similar to Eq.32 can be calculated, where P_m is now the power entering the machine and P_l is the power lost in the machine.

C.2 Steady-State Motor Operation(no-loss model)

The scematic representation of a separately excited dc motor is shown in Fig.C1. Table.C1 defines the variables.

The field current excitation produces a magnetic flux, ϕ, in the air-gap of the machine. The relation between air-gap flux and field current is shown in the dc magnitization curve, Fig.C2. It is assumed that the flux produced by the armature current has no effect on the field flux because the axes of the two fluxes are orthogonal.

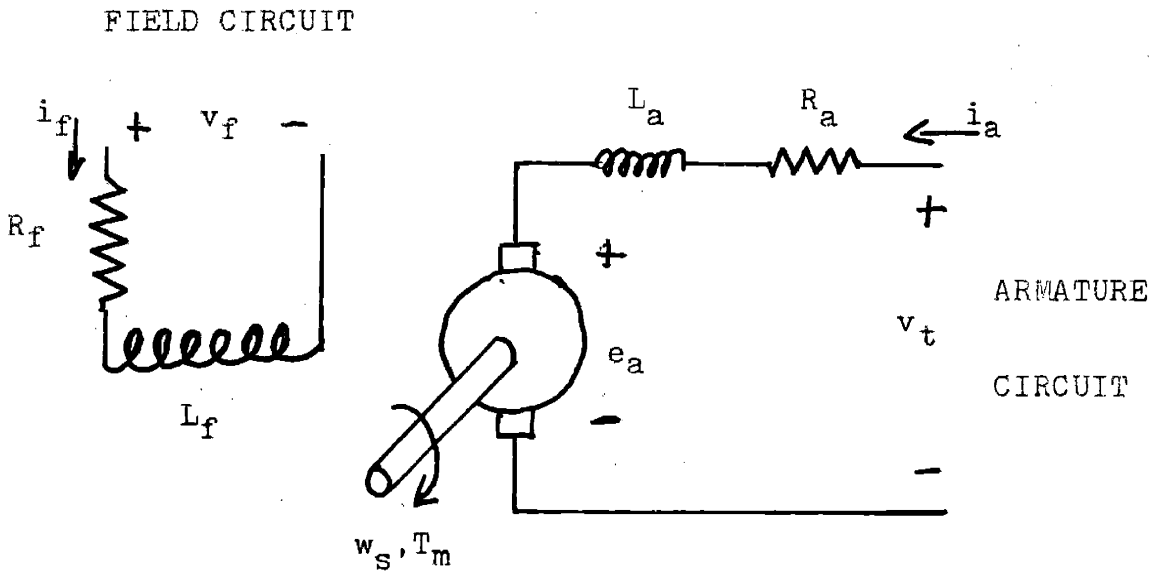

Fig.C1 DC Motor Circuit Model

Table C1 : Motor Parameters

R_f - Field Circuit Resistance

L_f - " " Inductance

R_a - Armature Circuit Resistance(winding & added circuit resistance)

L_a - " " Inductance

v_t - Armature Circuit Terminal Voltage

v_f - Field " " "

i_a - Armature Circuit Current

i_f - Field " "

w_s - Shaftspeed

T_m - Shaft Torque

e_a - Speed Voltage or Open-Circuit Armature Voltage

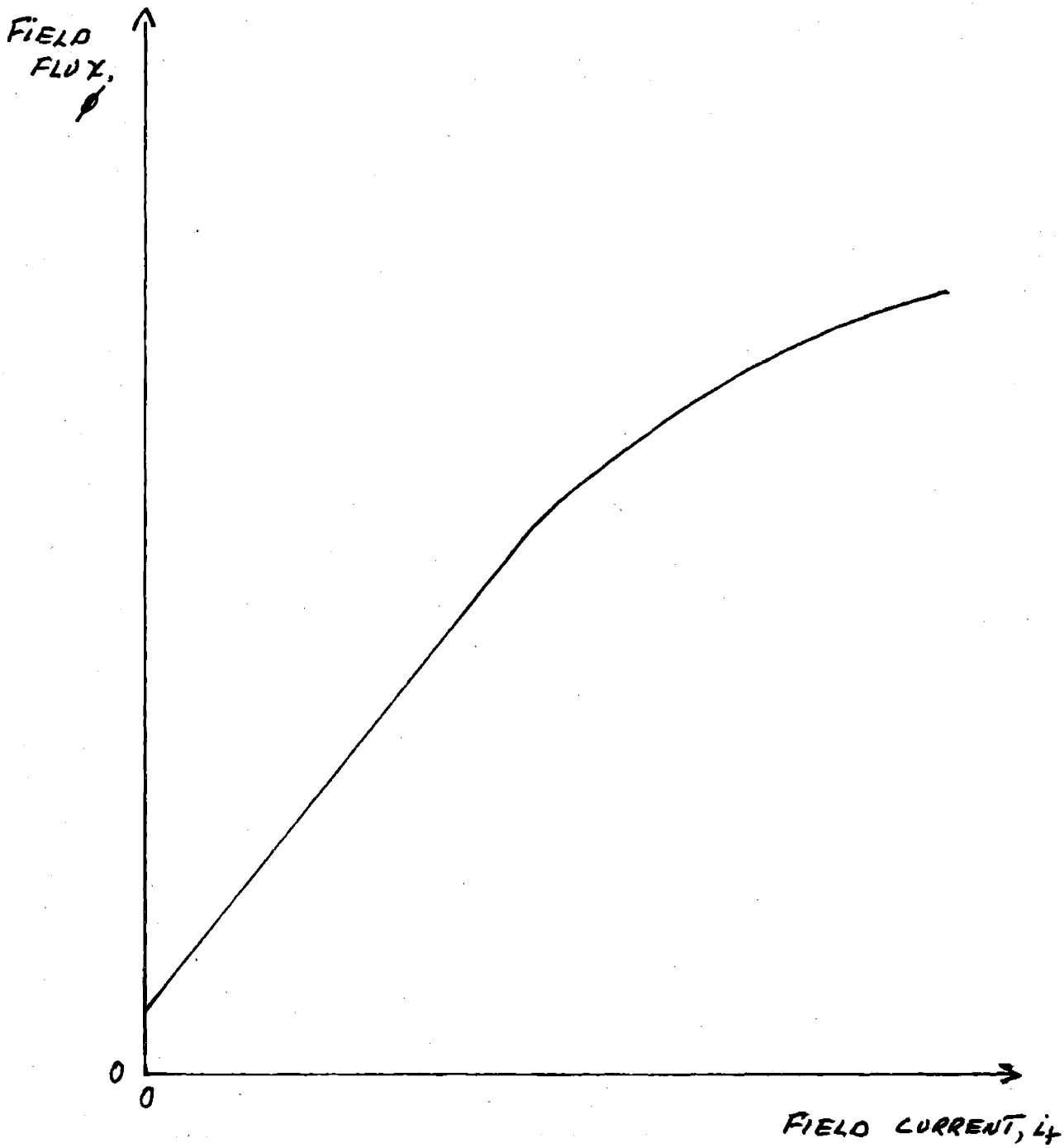

FIG. C2 : TYPICAL DC MAGNITIZATION CURVE
FOR A DC MACHINE

As seen in Fig.C2, field flux is linearly related to field current for a limited range of current. The nonlinear effect is due to the magnetic saturation of the iron within the machine. Residual magnitization of the iron accounts for the finite flux with no field current excitation.

The instantaneous torque produced by the interaction of the field and armature fluxes is given by

$$T_m = k\phi i_a \qquad (C.4)$$

where k is a constant of the machine. The back emf, or speed voltage, produced by the rotating coils cutting magnetic field lines, is given by

$$e_a = k\phi w_s \qquad (C.5)$$

where k is the same constant as in Eq.C.4.

In steady-state operation no voltage is induced across L_a. The equation for the armature circuit is then

$$v_t = R_a i_a + e_a$$

Rearranging $$i_a = \frac{v_t - e_a}{R_a}$$

and using Eq.C.5,

$$i_a = \frac{v_t - k\phi w_s}{R_a} \qquad (C.6)$$

The power in the shaft, P_m, is the product of torque and shaftspeed,

$$P_m = T_m \cdot w_s$$

or $$P_m = k\phi i_a w_s \qquad (C.7)$$

where Eq.C.4 has been used.

Substituting Eq.C.6 into Eq.C.7 gives a relation for shaft power, in a no-loss motor, as a function of the terminal variables and the shaftspeed.

$$P_m = \frac{(k\phi)^2}{R_a}\left(\frac{v_t}{k\phi} w_s - w_s^2\right) \qquad (C.8)$$

Eq.C.8 is plotted in Fig.C3. Maximum shaft power occurs at the shaftspeed, w_{so}, where the derrivative $\frac{dP_m}{dw_s} = 0$, or where

$$w_{so} = \frac{v_t}{2k\phi} \qquad (C.9)$$

Substituting Eq.C.9 into Eq.C.8 results in the maximum motor shaft power

$$P_m\left[w_s=w_{so}\right] \equiv P_{mo} = \frac{v_t^2}{4R_a} \qquad (C.10)$$

As an observation, the speed voltage, e_a, at this maximum power shaftspeed is

$$e_a = k\phi w_{so}$$
$$= \frac{v_t}{2}$$

which means that only half the power delivered by the source, v_t, makes it out the shaft. The rest of the power is dissipated in R_a.

For the dc motor to simulate the characteristics

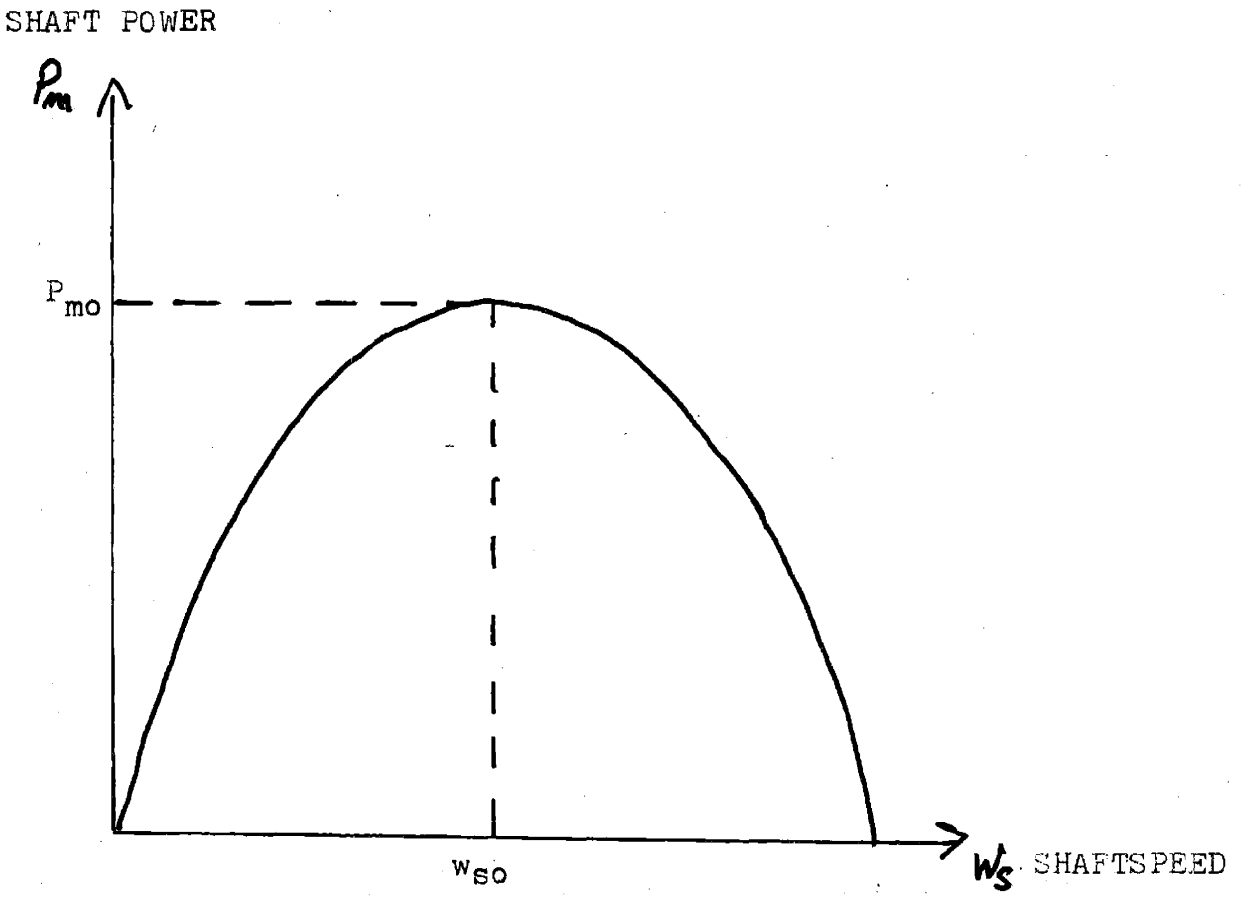

Fig.C3 : DC Motor Power-Speed Characteristic

of an ideal, no-loss, windmill, then Eq.C.1 & C.2 have to be satisfied. Relating Eq.C.9 & C.10 to Eq.C.1 & C.2 results in the motor terminal constraints:

$$\frac{v_t}{2k\phi} = av_w$$

and

$$\frac{v_t^2}{4R_a} = bv_w^3$$

or

$$v_t = 2(bR_a)^{\frac{1}{2}} v_w^{3/2} \qquad (C.11)$$

and

$$k\phi = \frac{(bR_a)^{\frac{1}{2}}}{a} v_w^{\frac{1}{2}} \qquad (C.12)$$

C.3 Motor Specifications

The motor used for the windmill simulation was a Long Island DC Motor. The motor's ratings and specifications are in Table C2.

Table C2 : DC Motor Specifications

Rated Armature Voltage	115V
Rated Armature Current	32 amp
Rated Speed	3450 rpm(360 sec^{-1})
Rated Power	4 hp(3 kw)
Field Resistance(25°C)	75 ohm
Armature Resistance(25°C)	0.1 ohm

Fig.C 4 shows the dc magnitization curve for the

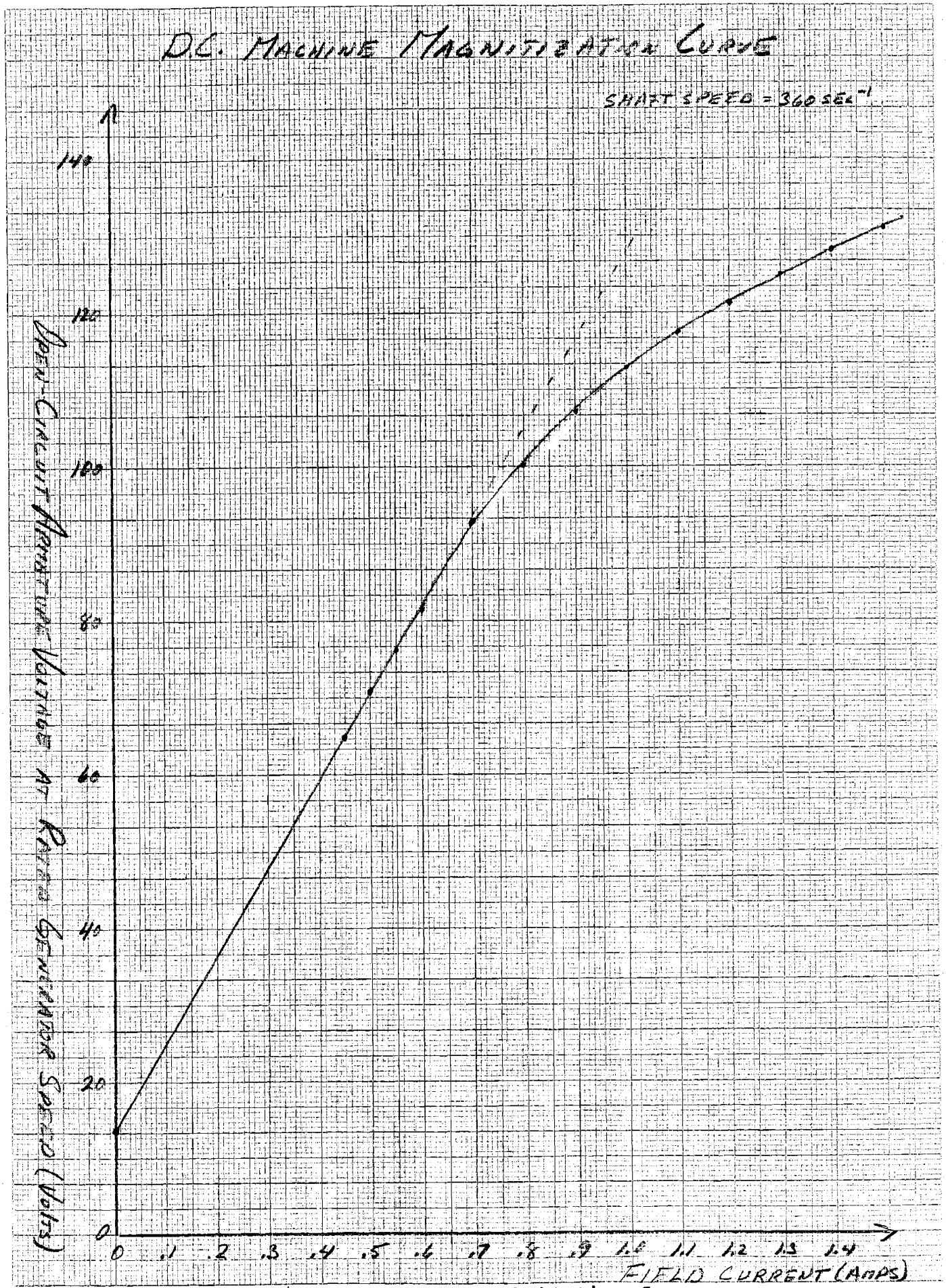

Fig.C4 : DC Motor Magnitization Curve

motor. To obtain the curve the open-circuit armature voltage was measured at the rated speed of the machine. This voltage is, from Eq.C.5,

$$e_a = k\phi w_s \qquad (C.5)$$

and thus a direct measure of the flux variable, $k\phi$. Hysterisis effects caused a variation in open-circuit voltage of no more than 3 volts over the measured range.

C.4 Desired Requirements of Motor

The battery charging circuitry of the SEP system (section 1.2), will allow a peak charging current of 18 amperes to flow into a peak battery voltage of approximately 170 volts. Analysis of the charging scheme (chapter II) shows that constraining the peak charging current to 18 amperes will constrain the average current to about 9 amps (section 2.3). Therefore the maximum power output desired of the generator is 170V·9amp or about 1500 watts (note that the power loss due to the internal battery resistance has been neglected).

The dc motor, coupled to the generator, must supply enough power not only to charge the batteries at this rate but also to cover all mechanical, magnetic and electrical power losses in the coupled system.

For efficient use of the generator, its maximum power output should be delivered at rated generator speed. Measurements on the generator (Appendix D) show that if 1500 watts is to be delivered to the batteries, at

rated generator speed and with generator flux level at a maximum*, then 1800 watts of power must be supplied from the shaft. Hysterisis and eddy current power losses in the generator iron, copper losses in the generator armature windings, and stray losses in the machine account for the 300 watts power loss. Windage and bearing losses in the generator will be lumped in with the dc motor's mechanical losses. Since 1800 watts of net shaft power is desired, then it is necessary to lump together all shaft power losses, those produced in the motor and coupled generator.

C.5 Motor Power Losses

If the power losses in the dc machine are signified as P_l then the shaft power can be represented as

$$\text{Shaft Power} \equiv P_m^* = (\text{Power into Motor}) - (\text{Power Lost})$$
$$= P_m - P_l \qquad (C.13),$$

where P_m is given by Eq.C.8.

C.5.1 Loss Clasification and Modeling

The two major components of power losses in a dc machine are:

1) Mechanical Losses - These consist of brush and bearing friction, windage and the power required to circulate air through the machine. These losses are measured by noting the power input to the machine as a

*the generator flux level must be at its maximum to provide enough armature terminal voltage with which to charge the batteries.

function of shaftspeed,with the machine unloaded and unexcited. These losses vary linearly as well as with the square of shaftspeed.

2) Open-Circuit Core Losses - These consist of eddy current and hysterisis power losses arising from changing flux densities in the iron of the machine. These losses are measured by noting the power input to the machine as a function of field current excitation. The measurements are made at a particular value of shaft-speed and friction and windage losses,occuring at this speed, must be deducted from the results.

Eddy current loss is dependent on the squares of flux density and shaftspeed. This loss can be represented as

$$P_{le} = k_e \phi^2 w_s^2$$

where k_e is a function of core lamination thickness, volume of iron in the machine, and the resistivity of the iron.

Hysterisis loss can be empirically expressed as

$$P_{lh} = k_h w_s \phi^n$$

where k_h is dependent on the characteristics and the volume of the iron. The constant, n, also dependent on the characteristics of the iron and ranges from 1.5 to 2.5 with the value 2 often used for the purposes of estimation.

Other power loss mechanisms in a dc machine include:

3) Stray Losses which arise from nonuniform current distributions in the copper windings, and core loss produced by the distortion of the magnetic flux when the machine is running a load. For a dc machine these losses are usually taken as 1% of power output.

4) Copper Losses, or I^2R losses, which are present in the armature windings of the machine. These power losses are small due to the small value of armature resistance.

I^2R loss also exists in the field winding of the machine. But if the field current is driven from a separate source then these losses have no bearing on the armature-power-input to shaft-power-output characteristic of the machine.

C.5.2 Loss Measurement

Loss measurements were made by noting the dc machine's power input under the described conditions.

Fig.C5 shows no-load torque-speed characteristics for the coupled dc motor and generator. Measurements were made with the two machines coupled so as to lump together all mechanical losses. The measurements were also made at two different field flux excitations.

Note that the amount of torque necessary to overcome mechanical losses is approximately linearly related to shaftspeed. Thus mechanical power losses, the product of shaftspeed and no-load torque, have both a linear and

Fig.C5 :

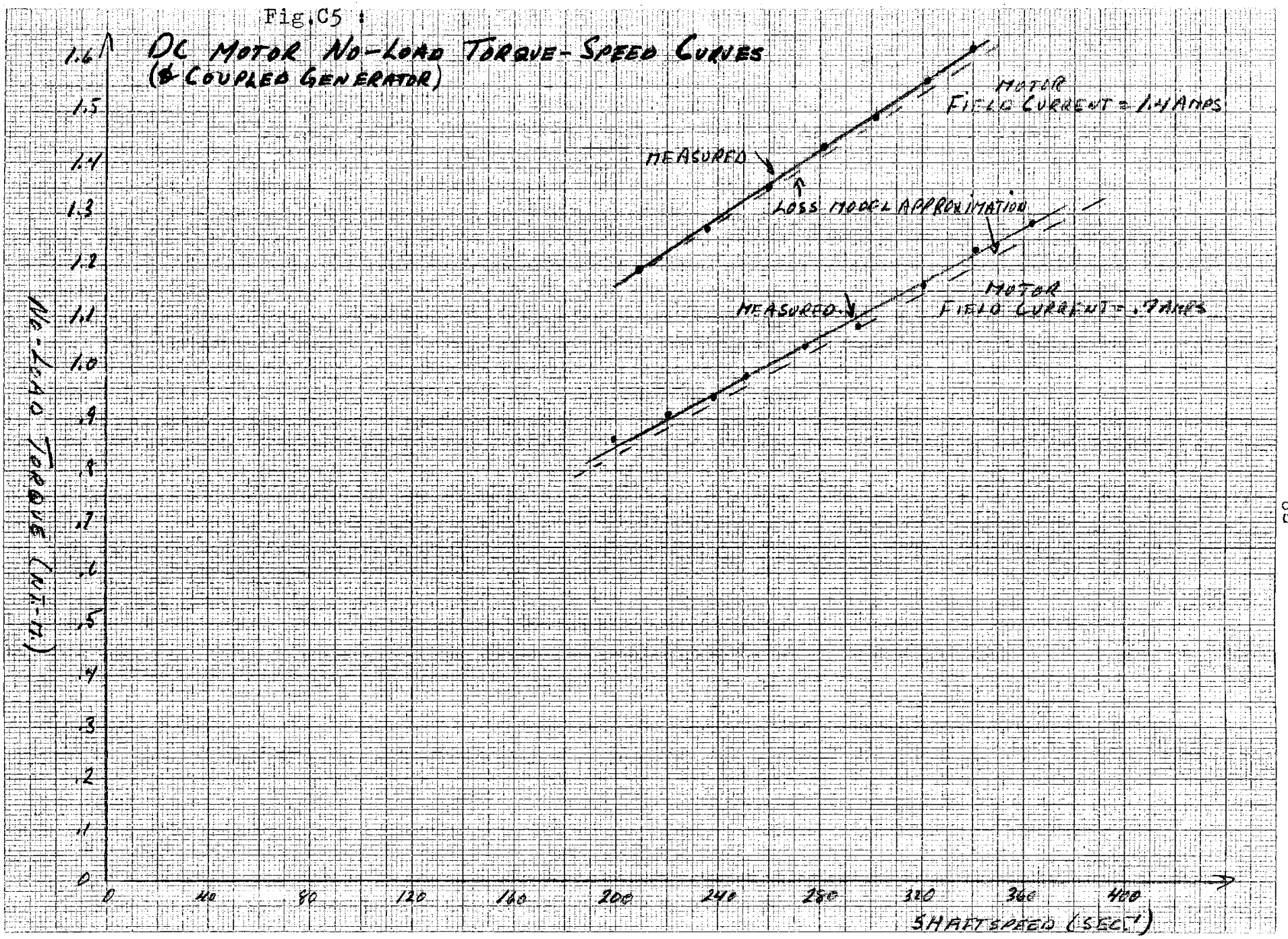
DC MOTOR NO-LOAD TORQUE-SPEED CURVES
(& COUPLED GENERATOR)
MOTOR FIELD CURRENT = 1.4 AMPS
MEASURED
LOSS MODEL APPROXIMATION
MOTOR FIELD CURRENT = .7 AMPS
MEASURED
NO-LOAD TORQUE (IN-LB)
SHAFT SPEED (SEC⁻¹)
1.6
1.5
1.4
1.3
1.2
1.1
1.0
.9
.8
.7
.6
.5
.4
.3
.2
.1
0
0
40
80
120
160
200
240
280
320
360
400

Fig.C5

square dependence on shaftspeed.

The quantity to express flux, from here on, will be $k\phi$, as defined in Eq.C.7. $k\phi$, as a function of field current, can be obtained directly from the dc motor's magnitization curve, Fig.C4, by dividing the open-circuit voltage by the operating shaftspeed. The units of $k\phi$ are thus volts-sec.

Fig.C6 shows a linear relationship between no-load power losses and the square of the field flux intensity, i.e.$(k\phi^2)$. the two curves represent measurements made at two values of shaftspeed. The loss measurements were plotted in this manner so that the readings can be encorporated into a power-loss model to be described in the following section.

C.6 Motor Power-Loss Model

To simplify the analysis stray losses and armature I^2R losses will be considered negligible and thus ignored.

From the discussion in section C.5 the power losses in the dc machine can be modeled as the sum of three components.

Power Losses = (Eddy Current Loss)+(Hysterisis Loss)
+(Mechanical Loss)

$$P_l = (k_e\phi^2 w_s^2)+(k_h\phi^2 w_s)+(k_{t1}w_s+k_{t2}w_s^2)$$

where k_{t1} ard k_{t2} are mechanical loss constants.

P_l can also be represented as

Fig, C6 :

NO-LOAD POWER AS A FUNCTION OF (MOTOR FIELD FLUX)^2
(COUPLED MOTOR & GENERATOR)

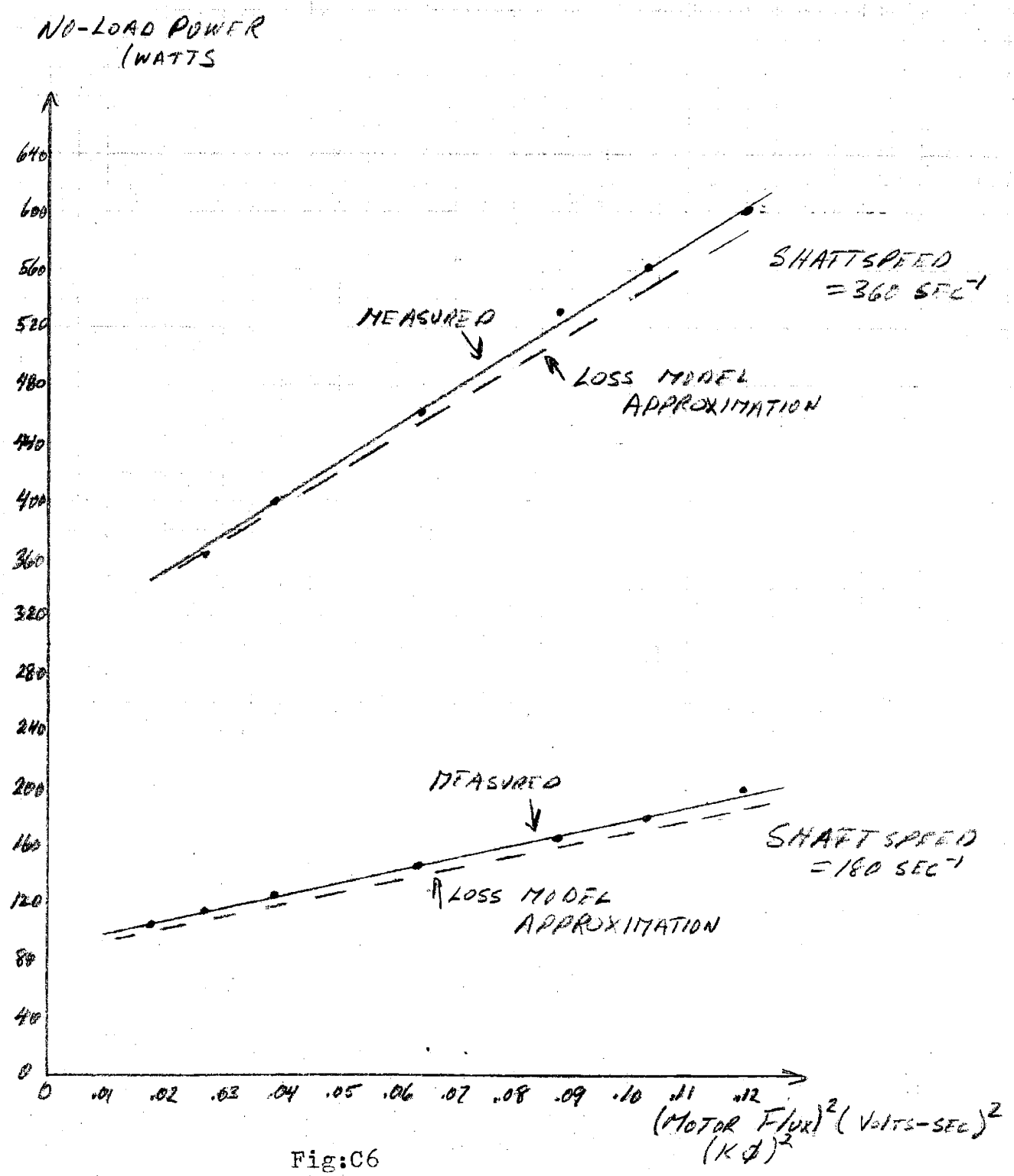

Fig:C6

$$P_l = C_1(k\phi)^2 w_s^2 + C_2(k\phi)^2 w_s + C_3 w_s + C_4 w_s^2 \qquad (C.14)$$

where C_1, C_2, C_3, and C_4 are constants of the machine and $k\phi$ has been used as the measure of flux.

The task now is to estimate C_1 through C_4 from the measured losses depict in Fig.C.5 & C.6. This will be done in three ways auch that an average value can be picked for each of the four constants.

Method 1) Relating loss model to no-load torque-speed curve

From Fig.C.5:

for $k\phi$=.36V-sec $\quad P_l = T_l w_s = 0.0033 w_s^2 + 0.49 w_s$ watts

for $k\phi$=.25V-sec $\quad P_l = 0.0027 w_s^2 + 0.30 w_s$ watts

From the model, Eq.C.14

for $k\phi$=.36V-sec $\quad P_l = (0.13C_1 + C_4) w_s^2 + (0.13C_2 + C_3) w_s$ watts

for $k\phi$=.25V-sec $\quad P_l = (0.064C_1 + C_4) w_s^2 + (0.064C_2 + C_3) w_s$ watts

Equating coefficients, C_1 through C_4 can be determined.

Method 2) Relating loss model to power-vs-$(\text{flux})^2$ curve.

From Fig.C.6

for $w_s = 360 \text{sec}^{-1}$ $\quad P_l = 2500(k\phi)^2 + 300$ watts

for $w_s = 180 \text{sec}^{-1}$ $\quad P_l = 900(k\phi)^2 + 90$ watts

From the loss model,

for $w_s = 360 \text{sec}^{-1}$ $\quad P_l = ((360)^2 C_1 + 360C_2)(k\phi)^2 + ((360)^2 C_4 + 360C_3)$ watts

for $w_s = 180 \text{sec}^{-1}$ $\quad P_l = ((180)^2 C_1 + 180C_2)(k\phi)^2 + ((180)^2 C_4 + 180C_3)$ watts

Again C_1 through C_4 can be determined.

Method 3) w_s=360,180sec^{-1} and kϕ=0.36,0.25V-sec are common points to both Fig.C5 and C6. From the curves the power loss corresponding to these points can be read. The results are summarized below.

w_s(sec^{-1})	kϕ(V-sec)	P_1,Fig.C5(watts)	P_1,Fig.C6(watts)
360	0.37	610	600
360	0.25	455	465
180	0.37	200	190
180	0.25	145	145

These readings can be encorporated into the power-loss model, Eq.C.14, and when the average of the readings, from Fig.C5 and C6 are used, the following equations result:

$$P_L[K\phi=0.37,\ w_s=360] = (360)^2(0.13)C_1 + (360)(0.13)C_2 + 360C_3 + (360)C_4 = 605 \text{ WATTS}$$

$$P_L[K\phi=0.37,\ w_s=180] = (180)^2(0.13)C_1 + (180)(0.13)C_2 + 180C_3 + (180)^2C_4 = 195 \text{ WATTS}$$

$$P_L[K\phi=0.25,\ w_s=360] = (360)^2(0.064)C_1 + (360)(0.064)C_2 + 360C_3 + (360)^2C_4 = 460 \text{ WATTS}$$

$$P_L[K\phi=0.25,\ w_s=180] = (180)^2(0.064)C_1 + (360)(0.064)C_2 + 360C_3 + (360)^2C_4 = 145 \text{ WATTS}$$

Through row reduction C_1 through C_4 can easily be determined.

The results of Solving for C_1 through C_4, in the three methods above, are summarized in Table.C3.

Table.C3 : Determination of Power-Loss Constants C_1 through C_4

Method	C_1	C_2	C_3	C_4
1	0.0095	3.0	0.11	0.0021
2	0.011	3.0	0.17	0.0019
3	0.010	3.4	0.09	0.0020

When the values $C_1=0.01$, $C_2=3.0$, $C_3=0.1$ and $C_4=0.002$ are replaced into Eq.C.14 then the dashed curves in Fig. C5 & C6 can be plotted. These calculated curves correlate well with the measured losses.

Again substituting C_1 through C_4 into Eq.C.14 and then substituting Eq.C.14 and C.8 into Eq.C.13 results in an equation that relates the shaft power of the machine to the armature terminal voltage, v_t, the series resistance, R_a, the field flux, $k\phi$, and the shaftspeed, w_s, i.e.

$$P_m^* = \frac{(k\phi)^2}{R_a}\left(\frac{v_t}{k\phi} w_s - w_s^2\right) - \left(0.01(k\phi)^2 w_s^2 + 3(k\phi)^2 w_s + 0.1 w_s + 0.002 w_s^2\right) \quad (C.15)$$

Maximum shaft power occurs at the shaftspeed where the derrivative $\frac{dP_m^*}{dw_s} = 0$, or

$$w_s(\text{maximum power}) \equiv w_{so}^{*} = \frac{\frac{v_t k\phi}{R_a} - 3(k\phi)^2 - 0.1}{(\frac{2}{R_a} + 0.02)(k\phi)^2 + 0.004} \quad (C.16)$$

For the measured ranges of shaftspeed and field flux Eq.C.16 may be considered a good approximation of the maximum power shaftspeed. These measured ranges are, as seen from Fig.C5 & C6, $180\text{sec}^{-1} \leq w_s \leq 360\text{sec}^{-1}$ and $0.25\text{V-sec} \leq k\phi \leq 0.36\text{V-sec}$. The flux ranges correspond to a field current range of $0.7\text{amp} \leq i_f \leq 1.4\text{amp}$.(from Fig.C4).

To find the value of the peak shaft power, as a function of the parameters in Eq.C.16, would entitle replacing Eq.C.16 into C.15, a sizeable task for any sane person.

C.7 Windmill Simulation Objectives(revisited)

At this point of the discussion it may be a good idea to step back and see what we have, and refresh our minds on where we want to go.

A model has been developed for a nonideal, or lossy, dc machine. This model relates the peak shaft power of the machine, and the corresponding shaftspeed, to the machine's terminal variables. Eq.C.15 & C.17 are the results of this model.

Our objectives are two fold. Firstly, it is desired to simulate, on a proposed dc machine, the steady-state behavior of a windmill. To simulate an ideal windmill would be impractical for, due to losses, no windmill is ideal. Thus the objective is to find the shaftspeed

where shaftpower is at a maximum, and not where power extraction from the wind is at a maximum. Therefore we must solve for values of w^*_{so}, in Eq.C.3 & 31, over the desired range of wind velocities.

Secondly, it was previously shown (section C.4) that 1800 watts of shaft power is necessary to supply 1500 watts of electrical power to the generator load. Eq.C.3 & 31 show that, in a windmill system, a particular value of power can only be achieved at a particular wind velocity. Thus 1800 watts of shaft power can only be achieved at the wind velocity, v_{wm}, where the maximum power, for a lossy windmill, is given by Eq.C.3, i.e.

$$P^*_{mo}[v_{wm}] = 1800\text{watts} = P_m[v_{wm}, w^*_{som}] - P_l[w^*_{som}]$$

where, from Eq.31

$$w^*_{som} = a[w^*_{som}]v_{wm} \text{ , or } a[v_{wm}]v_{wm}$$

The task now is to find values of 'a', b, and v_{wm} and relate them to the motor terminal variables to accomplish the simulation. The equations that relate ideal windmill behavior to the dc motor terminal variables were derived previously (section C.2) and are reproduced here as a reminder of what has been accomplished:

$$v_t = 2(bR_a)^{\frac{1}{2}} v_w^{3/2} \qquad (C.11)$$

and $$k\phi = \frac{(bR_a)^{\frac{1}{2}}}{a} v_w^{\frac{1}{2}} \qquad (C.12)$$

where 'a' and b are constant of the windmill to be simulated and R_a is the series resistance in the armature circuit of the dc machine.

C.8 Procedure for Windmill Simulation

As a starting point the assumption is made that 1800 watts of power is in the shaft of the coupled motor-generator when the dc motor is running at its rated voltage and speed. It was stated (section C.4) that 1800 watts of shaft power was necessary, at rated generator speed and maximum generator flux, to supply 1500 watts to the batteries. The difference of the two powers is consumed by losses in the generator.

The dc motor's voltage and speed ratings are, from Table C2 (section C.3), a speed voltage of 115V and shaftspeed of $360sec^{-1}$. At this shaftspeed the field flux level necessary to attain this speed voltage of 115V is, from Eq.C.5,

$$k\phi = \frac{e_a}{w_s} = \frac{115V}{360sec^{-1}} = 0.32V\text{-}sec \qquad (C.17)$$

The dc motor power losses, at this speed and flux level are, from Eq.C.14 and Table C3, approximately 550 watts. Thus to put 1800 watts into the motor shaft requires, from Eq.C.5 & C.7, the product of speed voltage and armature current to be 2350 watts. Since the speed

voltage has been stated to be 115V then an armature current of 20.5 amps is necessary to supply this power.

The relation between armature terminal voltage, v_t, terminal current, i_a, series resistance, R_a, and speed voltage, e_a, is shown in Fig.C1. This relation is

$$v_t = e_a + i_a R_a$$

Usung the values for e_a and i_a calculated above and defining v_t as v_{tm}, the armature voltage necessary to put 1800 watts onto the motor's shaft, results in a relationship between v_{tm} and armature resistance, R_a,

$$v_{tm} = 115 + 20.5R_a \quad \text{volts} \qquad (C.18)$$

For the windmill simulation it is necessary that the shaft power of 1800 watts be at the peak of a shaft-power versus shaftspeed characteristic. Therefore the rated shaftspeed of 360 sec^{-1} must be a maximum-power shaftspeed and thus satisfies Eq.C.16, where $k\phi$ is given by Eq.C.17 and v_t is now v_{tm}, the terminal voltage necessary to put 1800 watts into the shaft. Then, from Eq.C.16

$$360\text{sec}^{-1} = \frac{\frac{0.32v_{tm}}{R_a} - 3(0.32)^2 - 0.1}{(\frac{2}{R_a} + 0.02)(0.32)^2 + 0.004}$$

or $$0.32v_{tm} = 2.6R_a + 73 \qquad (C.19)$$

Solving Eq.C.18 & C.19 results in

$$v_{tm} = 305V$$

$$R_a = 9.25 \text{ ohm}$$

Now that R_a is known, the maximum-power shaftspeed, w^*_{so} in Eq.C.16, is only a function of armature terminal voltage and field flux level.

$$w^*_{so} = \frac{0.11v_t(k\phi) - 3(k\phi)^2 - 0.11}{0.34(k\phi)^2 + 0.004} \qquad (C.20)$$

Since the field current is directly related to field flux, w^*_{so} can be plotted as a function of terminal voltage and field current. This is done in Fig.C7 where the vertical axis is the nonideal, or lossy system's, maximum-power shaftspeed, w^*_{so}, normalized to the ideal maximum-power shaftspeed, w_{so}, given by Eq.C.9. The family of curves is w^*_{so}/w_{so} plotted for different values of terminal voltage, v_t. The dashed curve will be referred to later.

--Finding 'a', b and v_{wm}--

The ideal windmill simulation equations, C.11 & C.12, can now be used to relate 'a', b and v_{wm}. When $v_t=v_{tm}=305V$, $k\phi=.32V\text{-sec}$, $R_a=9.25\text{ohm}$ and $w_s=360\text{sec}^{-1}$ then 2350 watts is expected to be supplied to the dc motor. If v_{wm} is the wind velocity, in miles per hour*, at which this amount of power is extracted from the wind, then from Eq.C.11 & C.12,

$$0.32 = \frac{(9.25b)^{\frac{1}{2}}v_{wm}^{3/2}}{a}$$

*these units are used for convenience

Fig.C7 :

NORMALIZED NON-IDEAL PEAK-POWER SHAFTSPEED

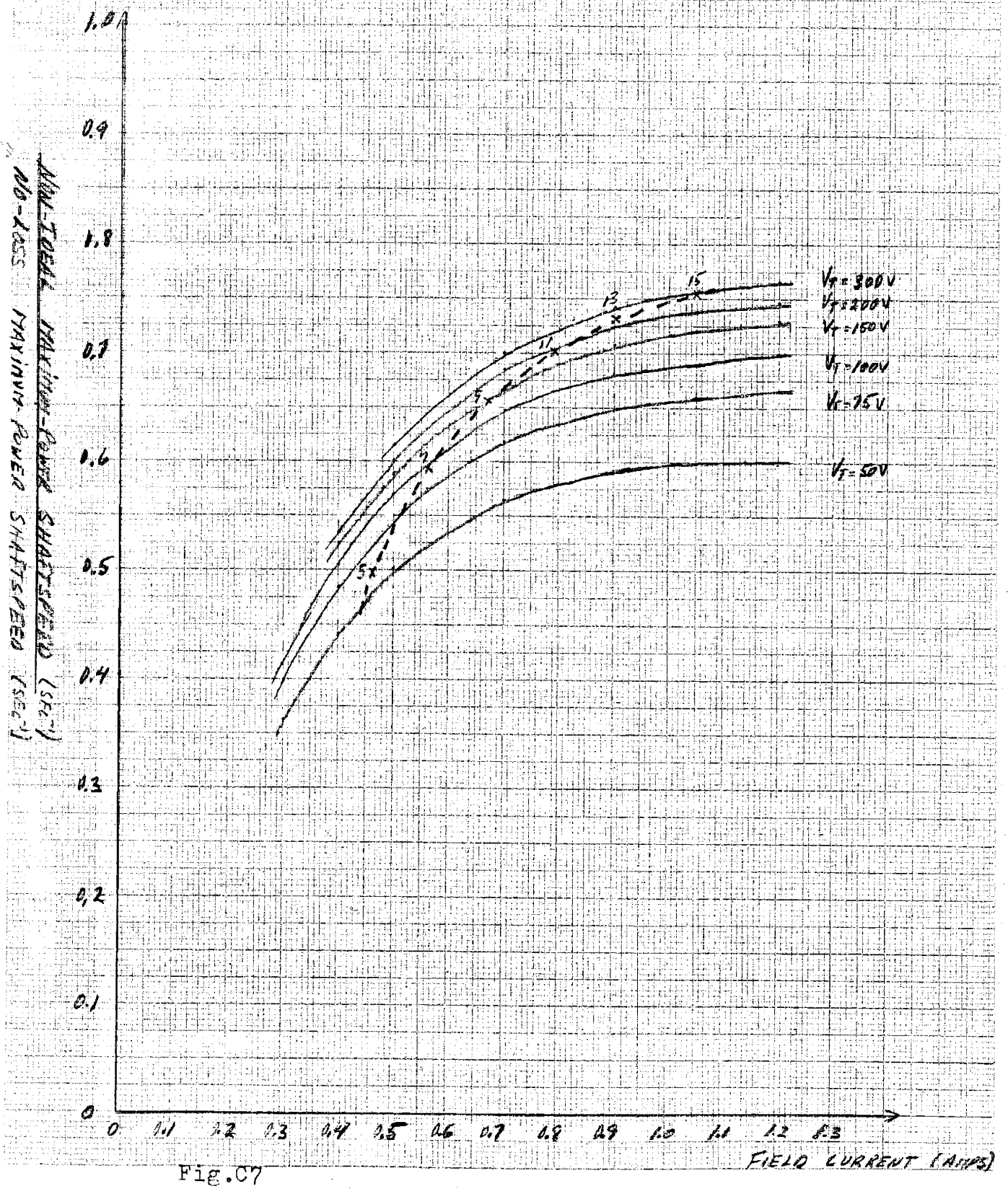

Fig.C7

and $305 = 2(9.25b)^{\frac{1}{2}} v_{wm}^{\frac{1}{2}}$

or

$$475 = a v_{wm} = w_{som} \qquad (C.21)$$

and $$2500 = b v_{wm}^{3} = P_{mom} \qquad (C.22)$$

where P_{mom} and w_{som} are, respectively, the peak power and corresponding shaftspeed for an ideal, no-loss, windmill at the wind velocity v_{wm}. These results prove interesting. If the dc motor was simulating an ideal windmill then Eq.C.21 & C.22 show that 2500 watts would be extracted from the wind at a shaftspeed of $475 sec^{-1}$. In the presence of losses, the shaftspeed for which maximum power is transferred to the shaft is somewhat less than $475 sec^{-1}$, i.e. $360 sec^{-1}$. At this reduced speed only 2350 watts is extracted from the wind, in the windmill case, or from the electrical system suppling the motor, in the simulated windmill case. Reduced power losses at this lower shaftspeed results in a net higher shaft power.

If any one of 'a', b or v_{wm} are specified then this will result, through Eq.C.21 & C.22, in values for the other two constants. Assuming a windmill that can extract 2500 watts from the wind, at a conservative wind velocity of 15 mph, results in the following values for 'a' and b

$$a = 32 \quad ; \quad b = 0.74$$

From Eq.C.11 & C.12 the terminal excitations for the dc motor can now be directly related to desired operating wind velocity.

$$v_t = 2(bR_a)^{\frac{1}{2}} v_w^{3/2} = 5.3 v_w^{3/2} \qquad (C.23)$$

and

$$k\phi = \frac{(bR_a)^{\frac{1}{2}}}{a} v_w^{\frac{1}{2}} = 0.83 v_w^{\frac{1}{2}} \qquad (C.24)$$

where R_a=9.25ohm has been used.

Thus for specified simulated wind velocities an armature terminal voltage and a field flux excitation, given by Eq.C.23 & C.24, must be impressed on the dc motor. The dashed line superimposed on Fig,C7 was plotted by using Eq.C.23 & C.24 and the relationship between field flux and field current, given by the magnitization curve of the dc machine, Fig.C4. The numbered points along the curve represent steady state operating points for specific wind velocities. This locus of points thus relates wind velocity to the normalized nonideal peak-power shaftspeed. The locus has been replotted in Fig.C8 with wind velocity as the horizontal axis. This plot tells us at what shaftspeed to operate the coupled motor-generator to maximize the power in the shaft. In other words we have found the nonlinear function $a[v_w]$ in Eq.31. The actual plot in Fig.C8 is $w^*_{so}[v_w]/w_{so}$ or, from Eq.C.2 and 31, $a[v_w]/a$.

Replacing w^*_{so}, Eq.C.20, for w_s in Eq.C.15 gives the

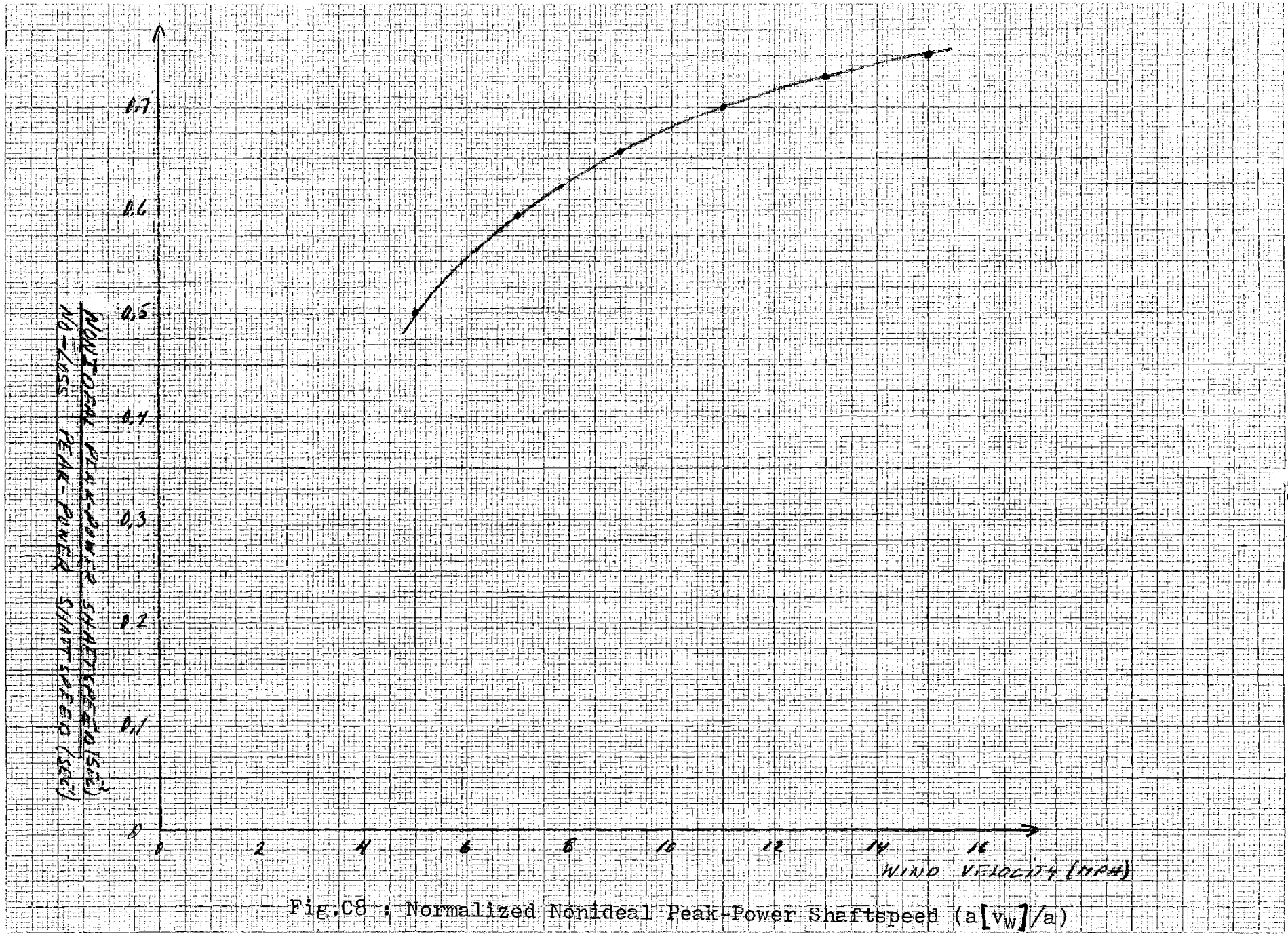

Fig.C8 : Normalized Nonideal Peak-Power Shaftspeed ($a[v_w]/a$)

peak shaft power in terms of v_t and $k\phi$. From the resulting equations and Eq.C.23 & C.24 a plot can be made relating peak shaft power to wind velocity. The family of curves in Fig.C9 shows the relation between v_t, $k\phi$, and what has been termed "peak power efficiency". The peak power efficiency is the ratio of P^*_{mo}, the nonideal, or lossy, peak shaft power, to P_{mo}, the ideal peak shaft power. Eq.C.23 & C.24 are represented by the dashed curve, in Fig.C9, with marked points being specific wind velocities, in mph. This locus of points gives the calculated steady-state peak shaft power operating-points of the system, with the shaftspeed controlled such that $w^*_{so}=a\lfloor v_w \rfloor v_w$.

Using Fig.C7 &C9, Fig.C10 is plotted showing ideal and nonideal peak shaft power versus shaftspeed for the marked wind velocities. For the ideal case

$$P_{mo} = bv_w^3 = \frac{b}{a^3} w_{so}^3$$

is the curve plotted with a=32 and b=0.74. For the non-ideal case the plotted function is Eq.C.15 with $w_s=w^*_{so}=a\lfloor v_w \rfloor v_w$ (from Fig.C8)

An interesting, yet not unexpected, plot is the one in Fig.C.11. It shows the ratio of how much shaft power we would have gotten, had the simulator been controlled as an ideal windmill (i.e. $w_s=av_w$), to the power we could have have gotten if the simulator was controlled as an nonideal windmill (i.e. $w_s=a\lfloor v_w \rfloor v_w$).

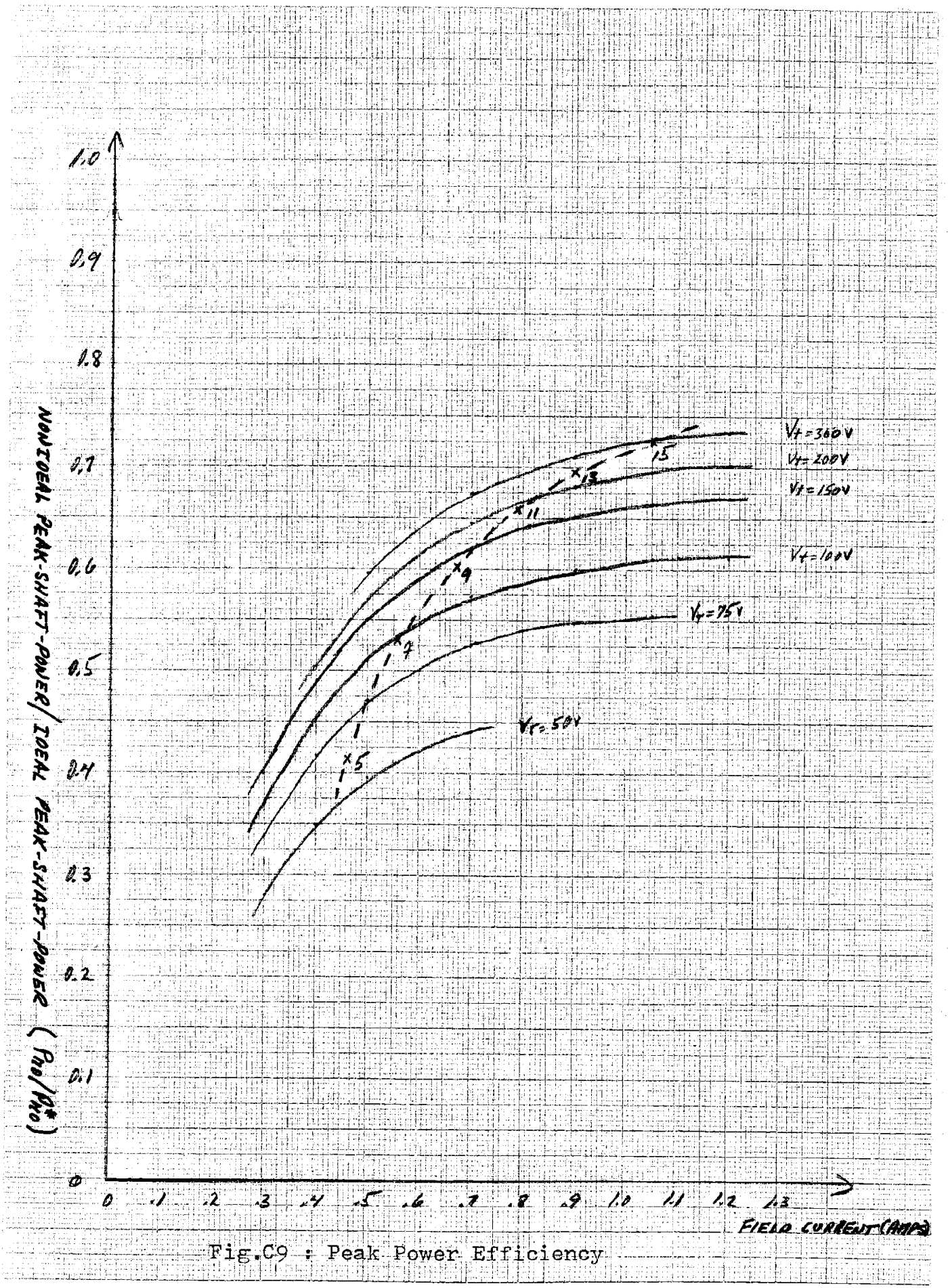

Fig.C9 : Peak Power Efficiency

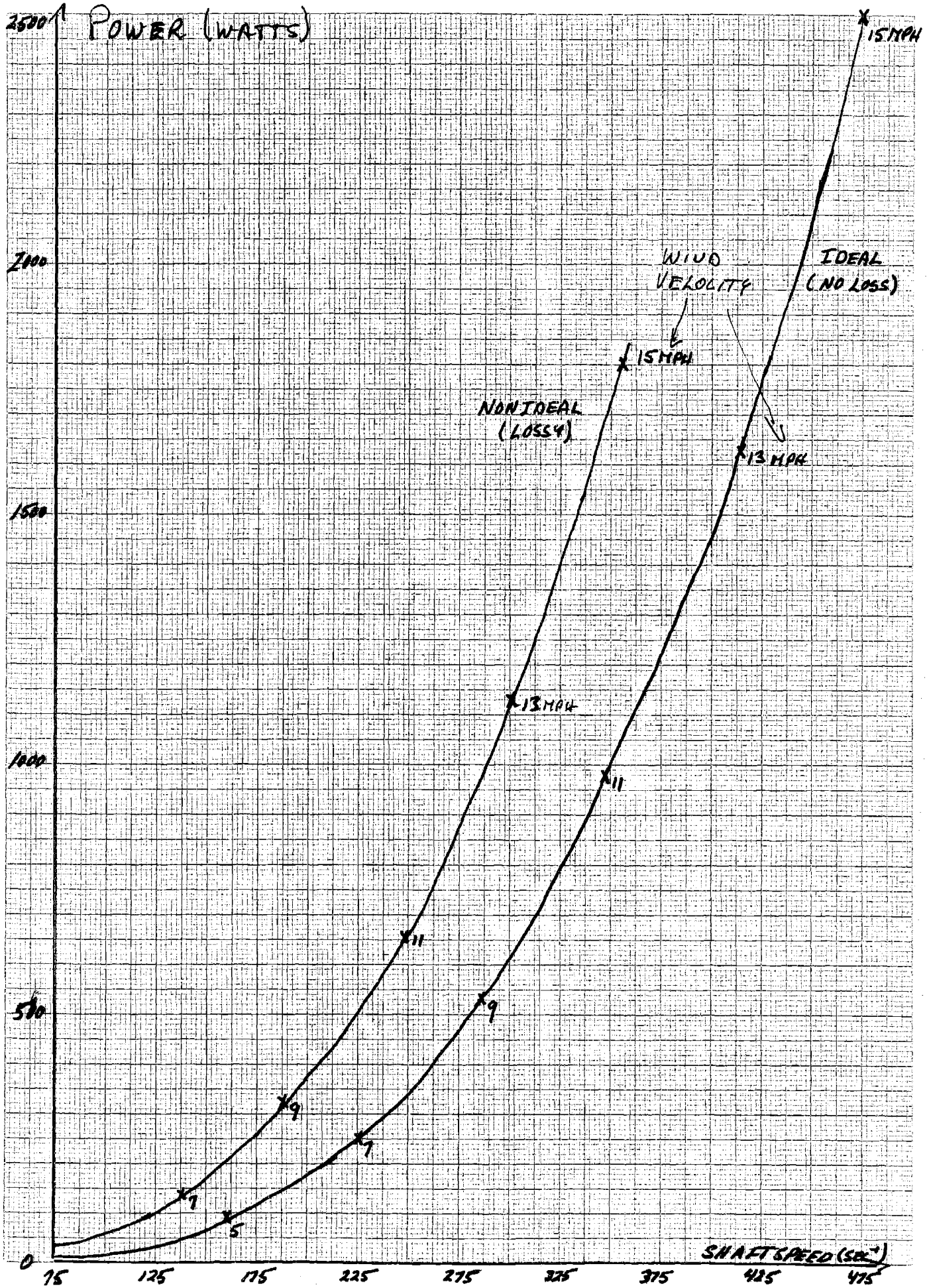

Fig.C10 : Ideal vs. Nonideal Peak Shaft Power

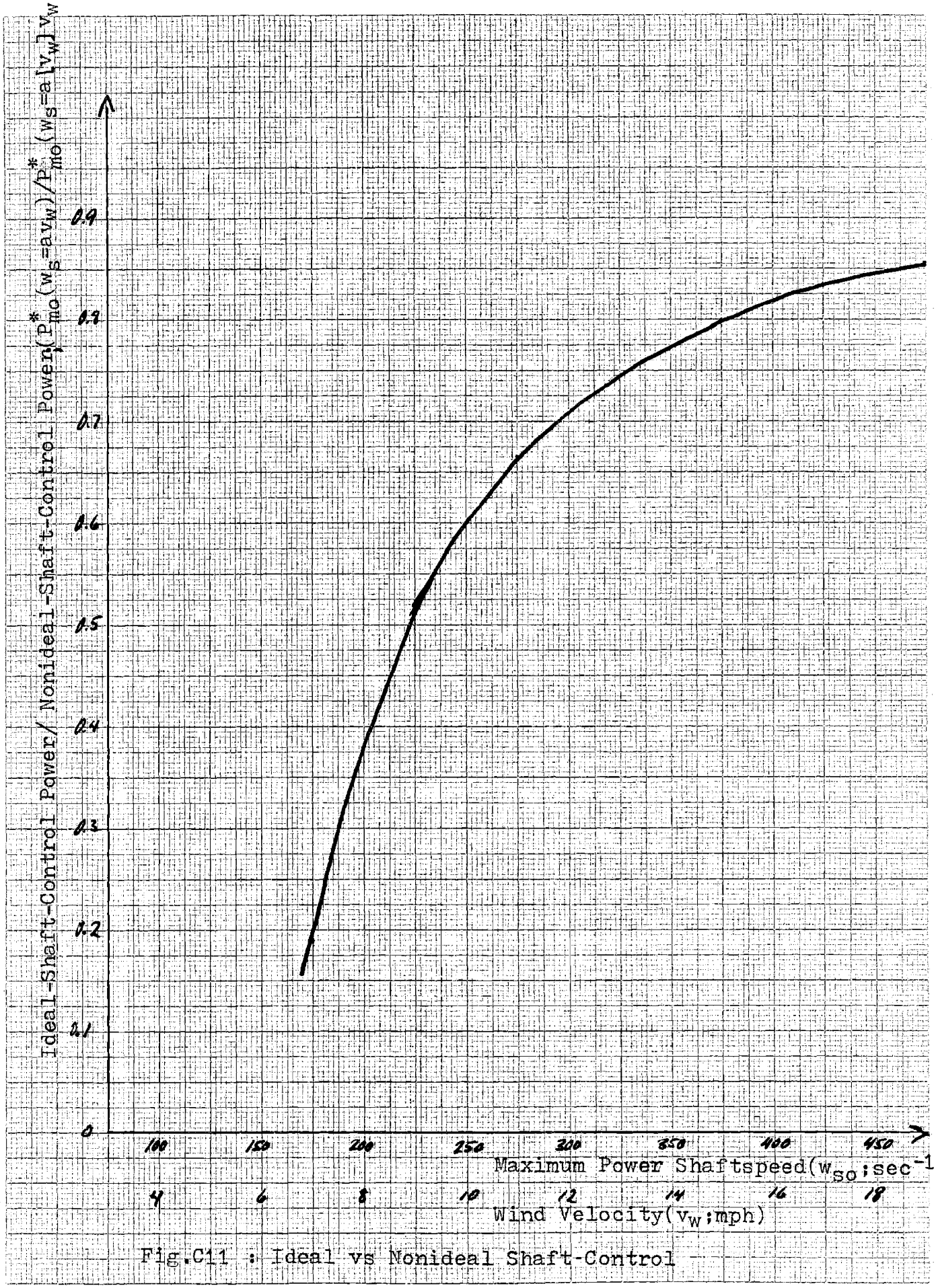

Fig.C11 : Ideal vs Nonideal Shaft-Control

C.9 Implementation of Windmill Controls

The equations to be simulated on the dc machine are Eq.C.23 & C.24. The input to the simulation circuitry will be a voltage reresenting wind velocity. This voltage will be processed so as to impress the proper source voltage on the armature circuit and the proper field flux excitation in the field windings of the machine. The electronic control of the field flux is via a current source impressed on the field windings of the machine. However, the relationship between field current and field flux is nonlinear and is given by the dc magnitization of the machine. The solid line in Fig.C.12 shows this relationship. The curve was generated by measuring the open-circuit voltage of the machine (at rated shaft-speed) as a function of field current, and dividing the result by the shaftspeed. This gives a direct measure of the flux level in the machine. To obtain a certain flux level would require exciting the motor field winding with the corresponding field current given by Fig.C.12. For a given flux level the corresponding wind velocity, given by Eq.C.24, is also plotted in the figure.

For simplicity the relationship between field current and field flux was electronically implemented via a piecewise linear function with only one break point. The broken line in Fig.C 12 represents this function. The broken line can be considered a reasonable approximation

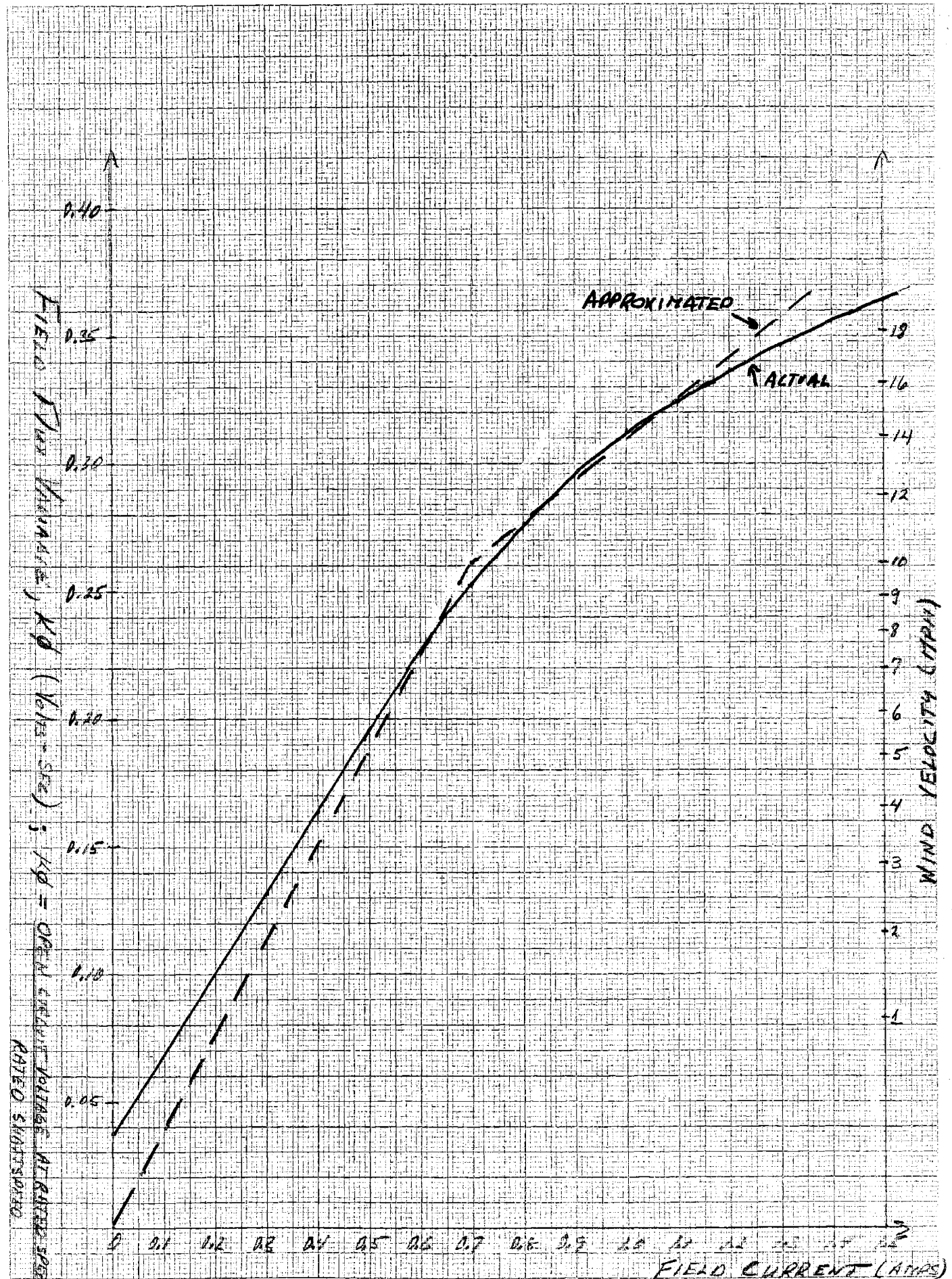

Fig.C12 ; Actual and Approximated Magnitization Curve

to the solid curve for several reasons. Firstly the large deviation in the two curves at low simulated wind velocities is of little importance. Measurements on the machine showed that at least a $3\frac{1}{2}$ mph simulated wind velocity was required to overcome coulomb friction in the shaft and bearings of the machine. Since power cannot be generated until the generator shaft, coupled to the motor, is turning then accurate windmill simulation is of little importance at these very low simulated wind velocities. Secondly it was decided (in section C.8) that a 15 mph wind velocity would supply enough power to match the largest battery load on the generator. Thus accurate windmill simulation above a 15 mph simulated wind velocity is less important since the load cannot absorb any more power. Lastly, hysterisis effects in the machine iron cause a few percent variation in the dc magnitization curve. Thus a more accurate approximation to the solid curve in Fig.C.12 would be of little value.

C.9.1 Armature Voltage Control Circuitry

From Eq.C.23 it can be seen seen that a source voltage proportional to the 3/2 power of a simulated wind velocity is necessary. Also the source must supply enough power to drive the dc motor.

The circuit diagram for the motor armature drive is shown in Fig.C 13. Two Intronics M530J analog multipliers were used to produce the 3/2 power function (one to perform a square-root an the other to perform a multiplication). A phase-controlled three-phase full-wave

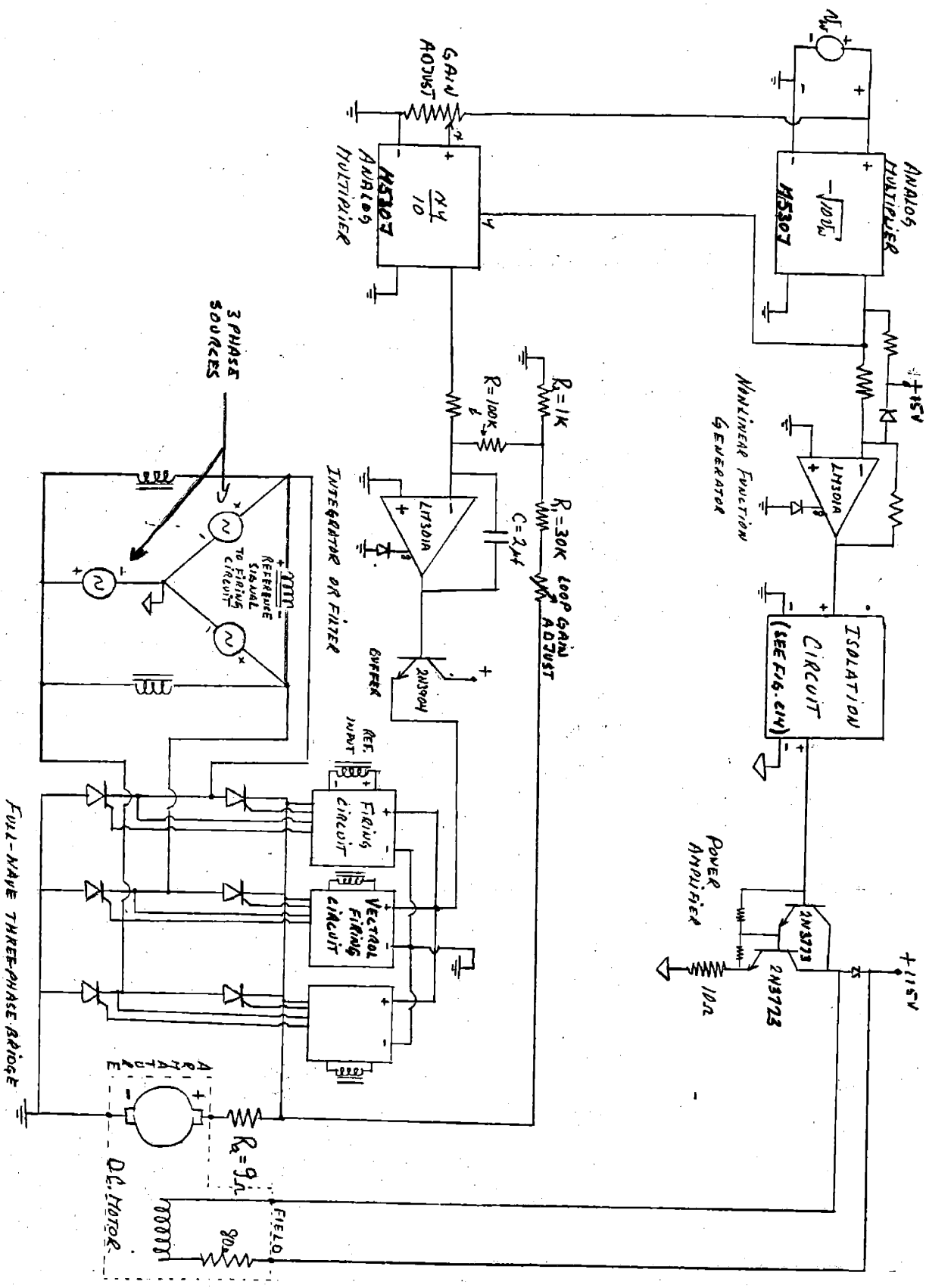

Fig.C13 : Windmill Simulator Circuitry

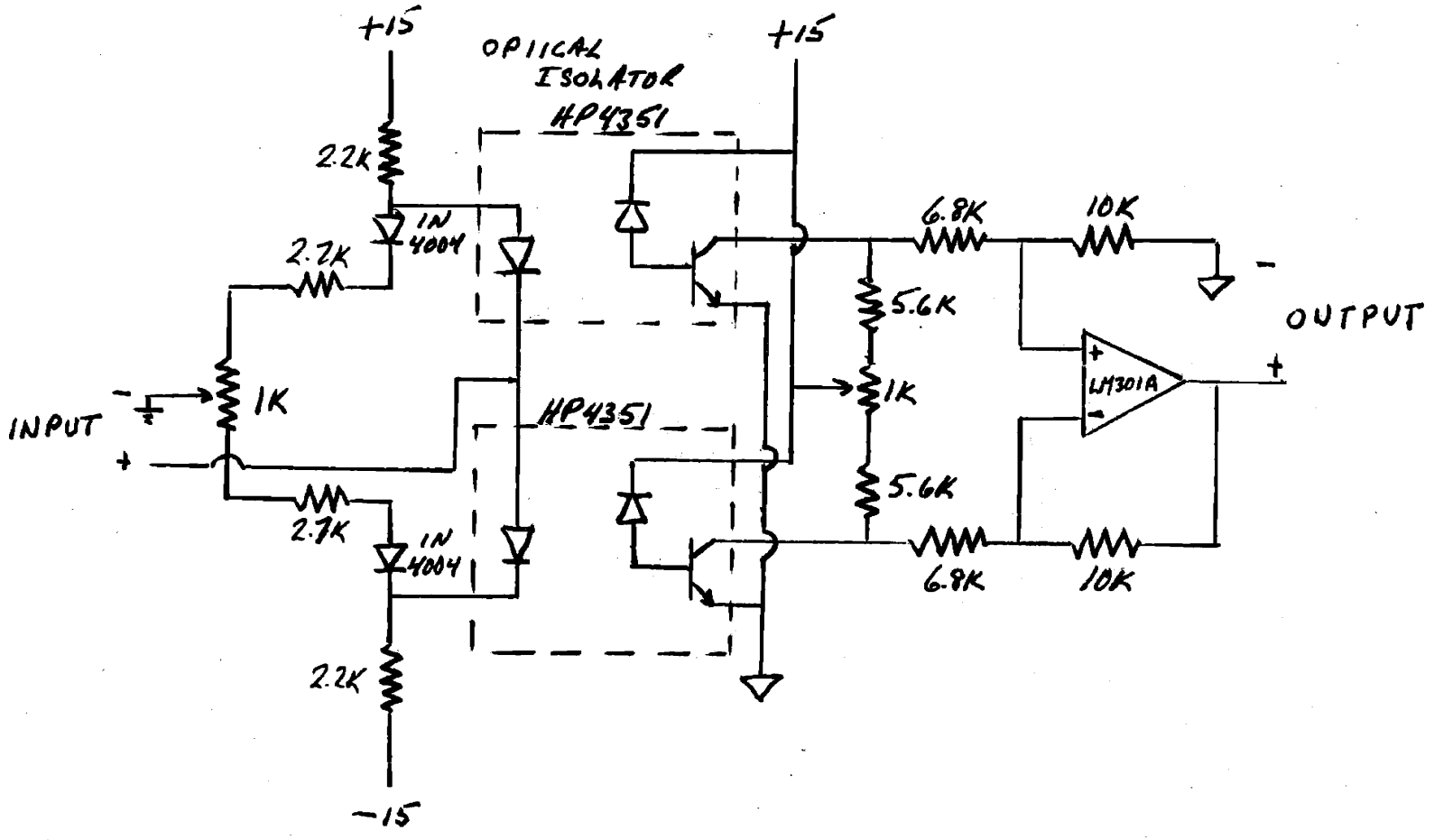

Fig.C14 Basic Optical Isolator Circuit

bridge was used to supply the drive to the motor. A full-wave bridge was used over a half-wave bridge since it offers a greater average-to-peak voltage ratio. Three Vectrol firing circuits were also used to provide the synchronous gate signals to the SCR's in the full-wave bridge.

For a voltage input varying from 0 to 5V the Vectrol circuits produce a gate signal that varies from 180^{o} to 0^{o} from the zero crossing of a reference sine wave input. The reference signal is derived from across the phases of the three-phase source. The firing angle, for a single Vectrol firing circuit, is thus measured from the point where the voltage across the corresponding pair of phases is zero. The Vectrol circuit also puts out two separate gate signals, 180^{o} apart, one for the positive half-cycle and the other for the negative half-cycle of the reference signal. These two outputs are used to control the firing of a pair of SCR's in the bridge.

The relationship between the voltage to the input of the firing circuit and the voltage appearing at the output of the three-phase bridge is very nonlinear. This nonlinearity was linearized through the use of feedback. The voltage from the output of the bridge is compared with the voltage out of the analog multipliers. The difference voltage is fed to the operational amplifier and drives the input voltage of the firing circuits

until the desired output is reached. Since the voltage output of the analog multiplier varies from 0 to 13V, a resistor devider R_1, R_2 provided the loop gain necessary to drive the bridge output voltage to that required for the windmill simulation.

The choice of capacitor C is also of interest and essential to loop stability. The phase control circuits can be modeled as a pure time delay. Each circuit fires twice for every cycle of the reference signal input, once for every positive and once for every negative half-cycle.Thus the fastest the firing controls can react to a changing input is within one half cycle of the reference signal. This means that for an input voltage changing at the rate of the reference frequency the firing circuits would cause a 180^{o} phase shift. It is the function of the integrator, which is also acting as a low-pass filter, to bring the gain of the loop down below a magnitude of 1 before the reference frequency is reached.

The dc loop gain of the circuit was chosen to be approximately 30. This value was chosen because a simulated wind velocity of 15 mph brought the output of the analog multiplier to 10V. Since, from Eq.C.23, approximately 300V is needed at the input of the motor armature circuit when the simulated wind velocity is 15 mph, a gain of 30 is necessary through the phase control stage.

Considering the dc gain of the loop, the reference frequency, which is 60 hz or 377 sec^{-1}, and the fact

that a single pole rolloff is at 6db/octave, the value of RC necessary for the single pole filter must be greater than approximately 0.1 seconds.

The response time of the loop to varing inputs would be of this same order. A fast response time for this circuit is not important as long as it is faster than the mechanical time constant of the motor. This is because the motor cannot react to a changing armature voltage faster than its mechanical time constant. For the proposed motor the mechanical time constant is on the order of a few seconds. The RC product, for the filter, was chosen to be about 0.2 seconds. This time is about an order of magnitude faster than the response time of the motor and also large enough to keep the loop stable.

C.9.2 Field Current Control Circuitry

The output of the analog multiplier performing the square-root operation is used as the input to the field current drive. The nonlinear operational amplifier circuit of Fig.C13 is used to give the correct field current for a simulated wind velocity input, as discussed previously.

The optical isolator stage, shown in more detail in Fig.C14, provided isolation between the armature voltage and field current controls. This circuit configuration was used due to its low dc drift. It is an adapt-

ation of a circuit introduced by Hewlett Packard Corp.[6]

The output of the isloator stage can be adjusted to give a dc bias. This bias compensates for the base-emitter diode drops in the Darlington power amplifier stage that drives the field current.

The Darlington power amplifier produces a current through the field winding of the motor that is linearly related to the voltage applied to the base of the amplifier.

The gains of each stage were chosen such that a 0 to 15V input to the square-root function device produces a 0 to 10.7 amp corrent in the field winding of the motor. This is precisely the required limits on the transfer function given by Eq.C.24 and Fig.C12.

C.10 System Testing and Evaluation

Measurements were made to see how well the system performs its functions. Fig.C15 & C16 show calculated versus measured values of armature circuit voltage, v_t defined in Fig.C1, and field flux level, $k\phi$. The calculated values are from Eq.C.23 & C,24. The field flux was determined by measuring the field current and using the solid line in Fig.C12 to relate the field current to the field flux level. The correlation between measured simulation values and calculated values is quite good except for the case of field flux at low wind velocities. This may be attributed to nonlinearities in the isolation

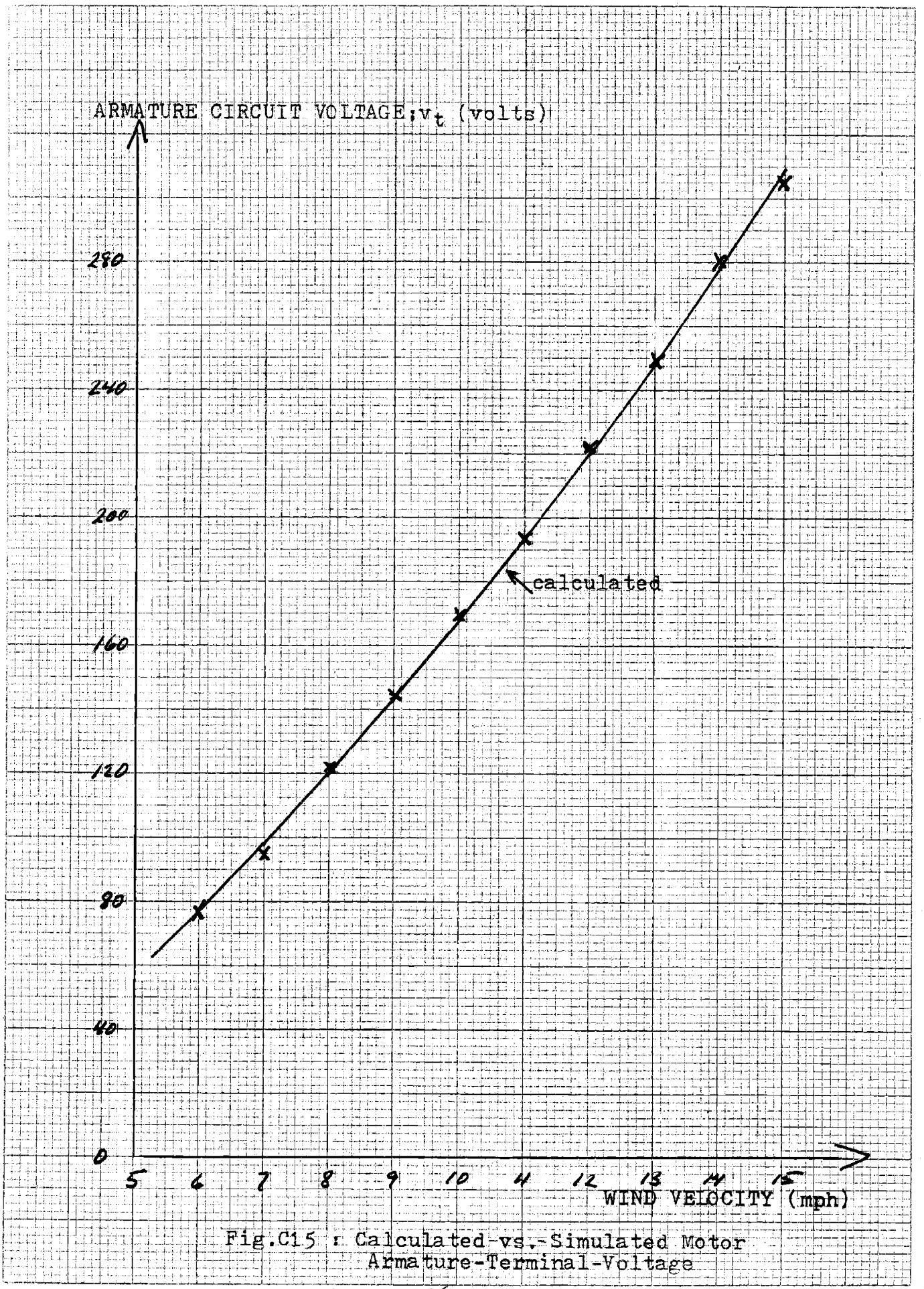

Fig.C15 : Calculated-vs.-Simulated Motor Armature-Terminal-Voltage

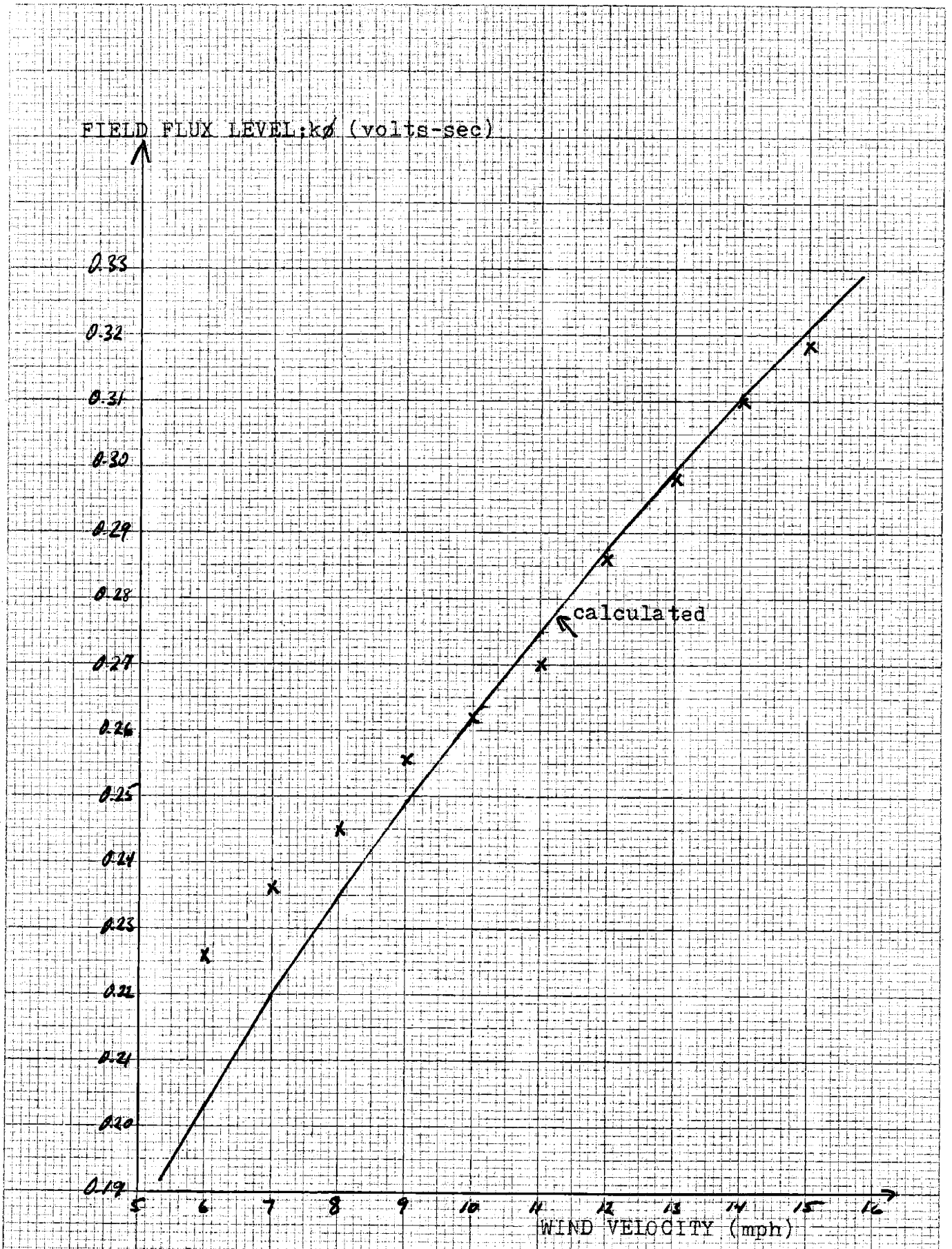

Fig.C16 : Calculated vs. Simulated Motor Field Flux

stage which occur if the two optical isolators are not matched or the input bias currents to the isolators are not identical. However, as stated in the previous section, accurate simulation at low wind velocities is unimportant.

Fig.C17 & C18 show the production of the square-root and 3/2 power functions by the analog multipliers. Each device performed to specs, within 2%, for inputs up to 15V and outputs up to about 13V. Fig.C19 shows the production of the nonlinear function and Fig.C20 shows the input-output relationship for the square-root, nonlinear and isolation circuits. The bias for zero input, for the combined circuits, is necessary to compensate for the base-emitter diode drops in the Darlington power amplifier stage. Potentiometers were used in the nonlinear circuit to adjust the break point and gains until desired characteristics, within several percent, were attained. Performance of the overall transfer function, square-root function to Darlington amplifier, was surprisingly accurate, within one or two percent over most of the simulated wind velocity range (see Fig.C16). However, notice the almost linear nature of the transfer function in Fig.C20, except for low simulated wind velocities. Since simulation at low wind velocities is unimportant (see section C.9) then a linear approximation to the the function in Fig.C20 may have resulted in accurate enough windmill simulation.

Plots were made of machine power as a function of

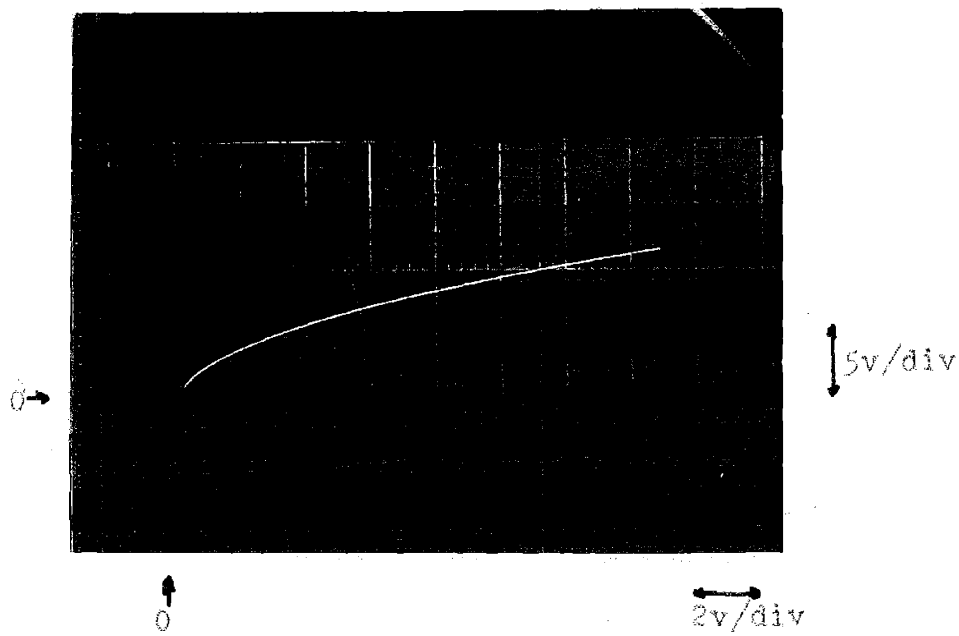

Fig C17 Square-Root Function

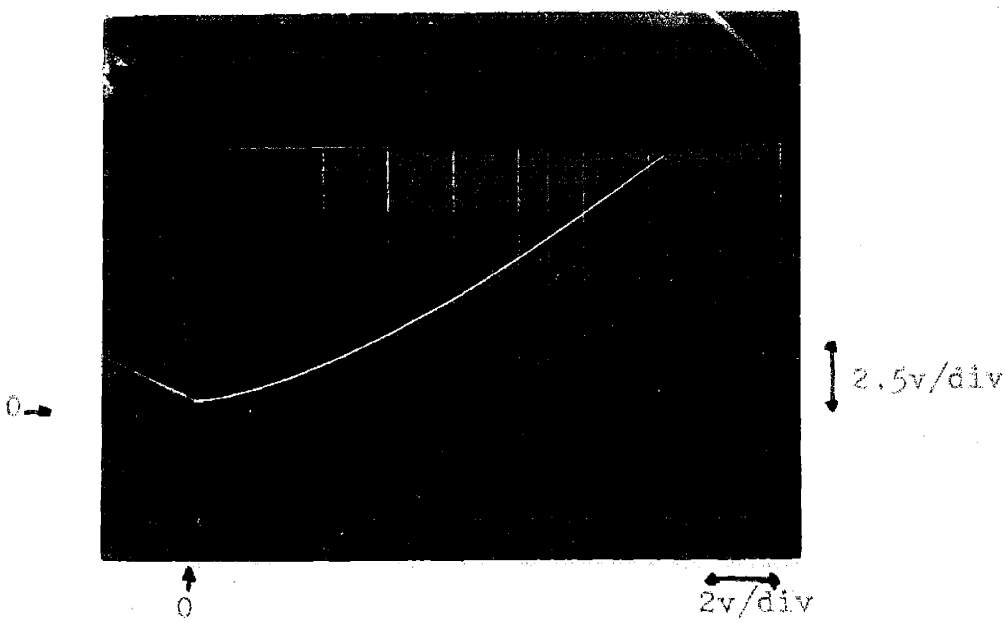

Fig C18 Three-Halves Power Function

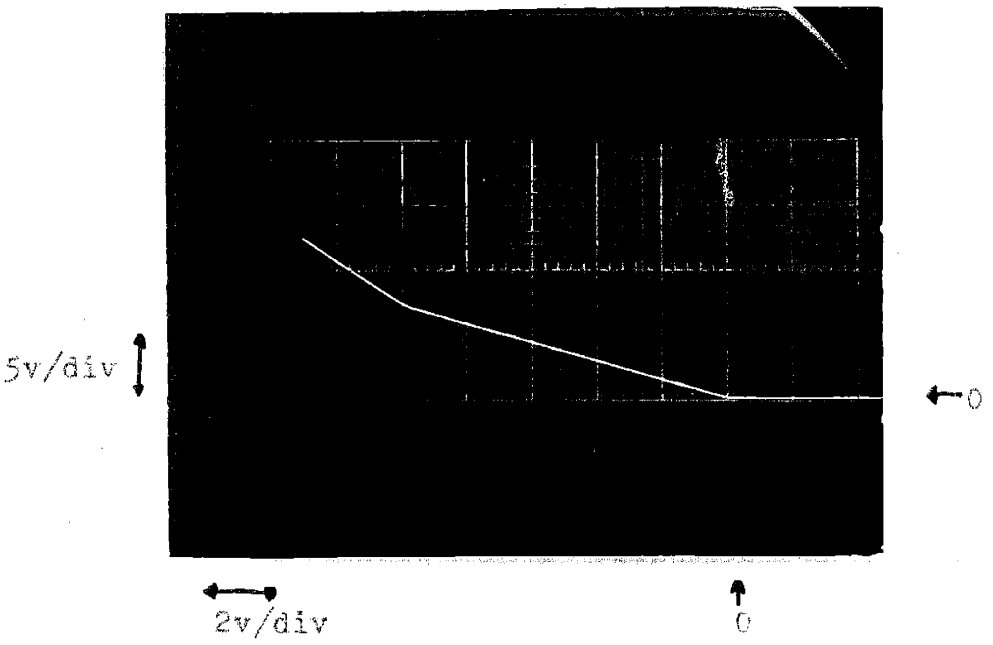

Fig C19. Nonlinear Function-Generator Characteristic

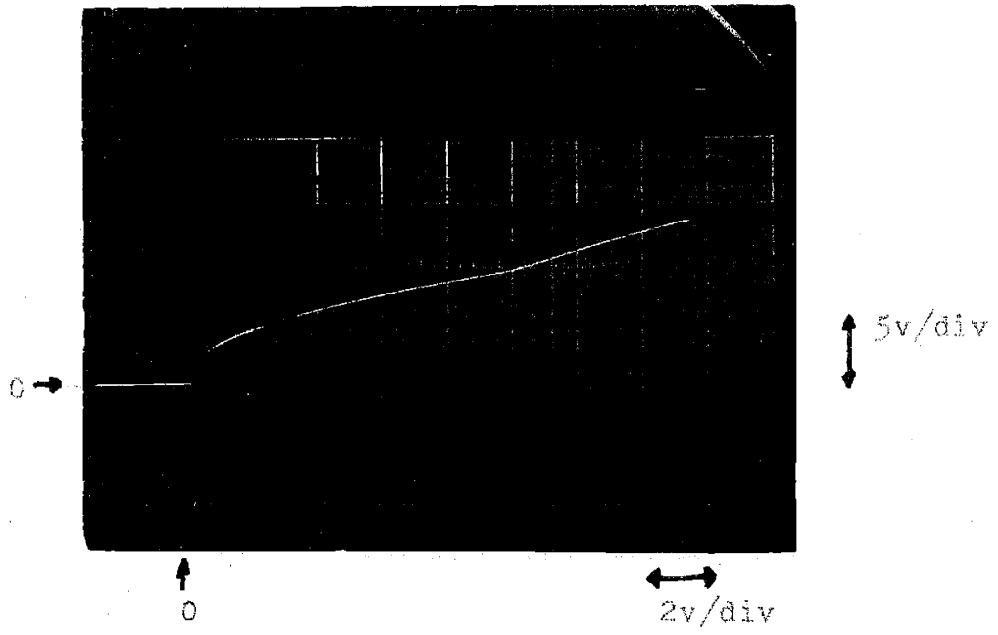

Fig C20. Input-Output Characteristic for Square-Root, Nonlinear & Isolation Circuits

shaftspeed for different values of wind velocities and for different numbers of battery sections on charge. The varying parameter was generator flux which was used to change generator load such the power curves could be plotted.

The plots to be presented show

(1) the measured versus calculated power into the windmill simulator, i.e. dc motor,

(2) the calculated power in the shaft of the coupled motor-generator,

(3) the measured power output of the generator,

(4) the estimated power being stored in the barreries.

Fig.C21 & C22 show these plots.

The power entering the motor is given by Eq.C.8. From Fig.C15 & C16 the deviation between measured and calculated values of armature voltage, v_t, and field flux, $k\phi$, is less than 2% for most wind velocities. The only other source of error between measured power into the motor (solid line in Fig.C21 & C22) and calculated power onto the motor (dashed line in figures) is in fluctuations of armature resistance due to I^2R heating. Air-cooled high-power resistors were used to keep these fluctuations to a minimum. As one can see the deviation between calculated and measured power into the motor is almost negligable.

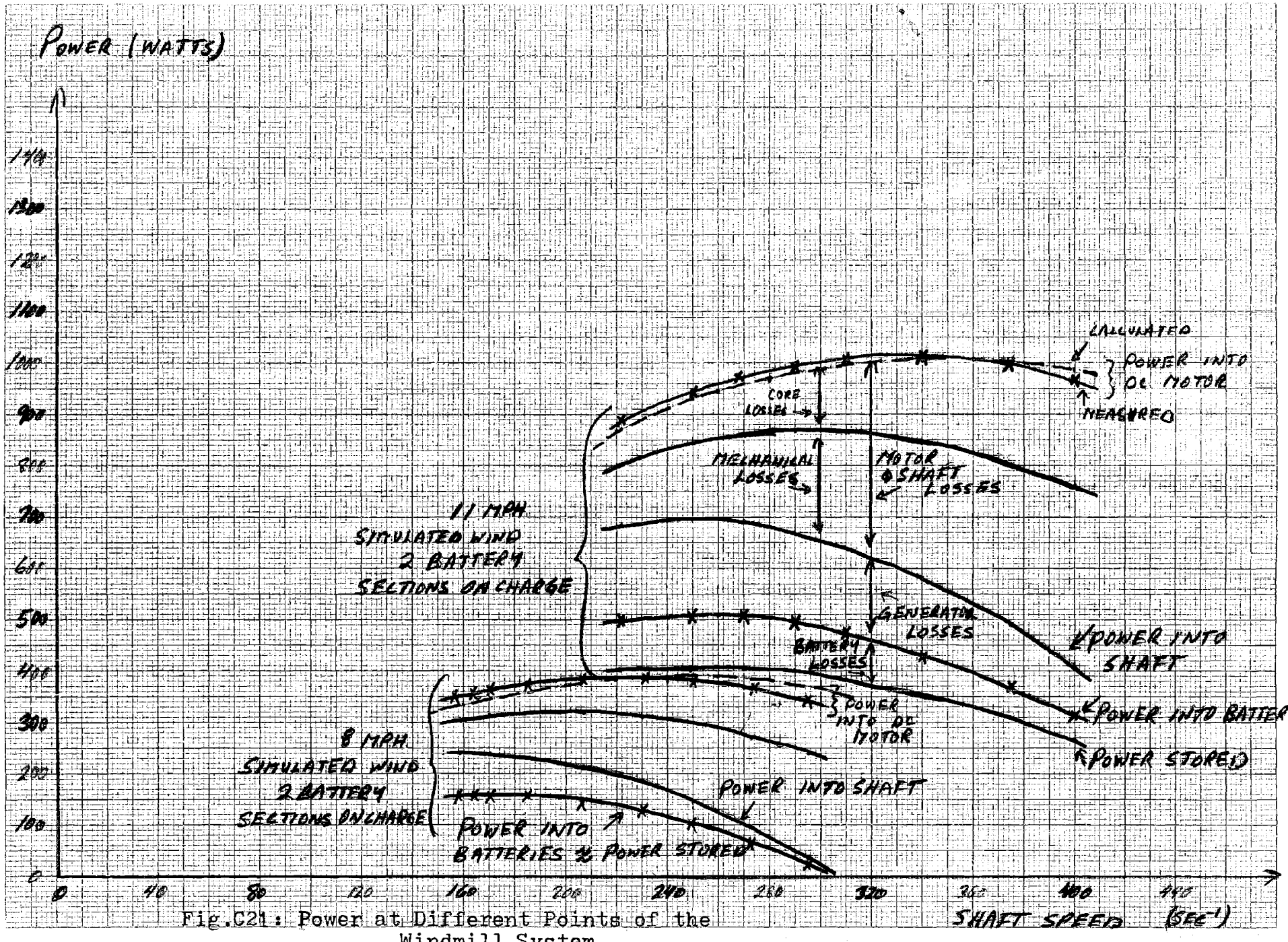

Fig.C21: Power at Different Points of the Windmill System

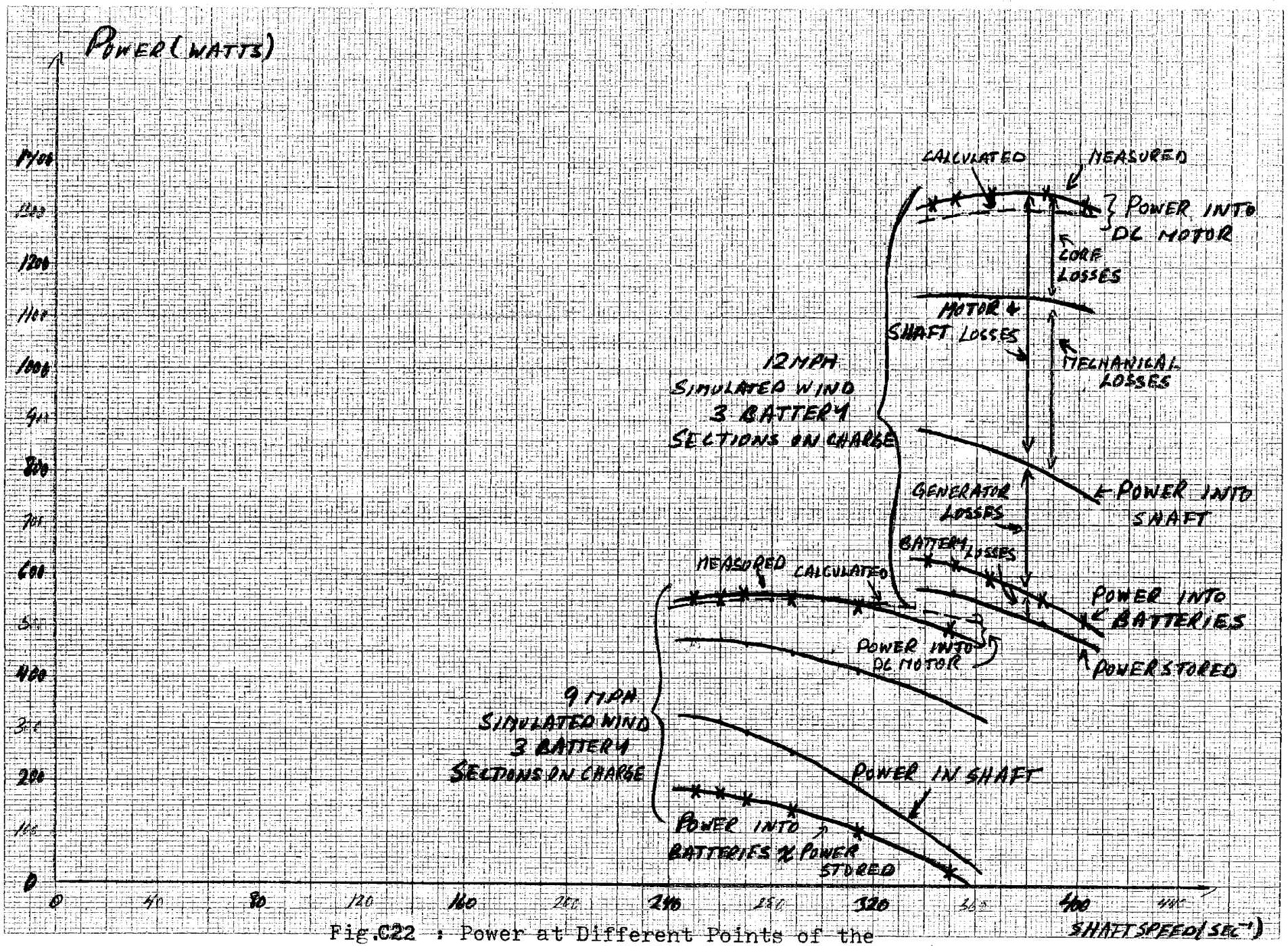

Fig.C22 : Power at Different Points of the Windmill System

Due to flux saturation in the generator, and thus a limit on generator load when feeding power into a battery load, the power curves could not be extended to lower shaftspeeds as shown. Also due to limitations on generator shaftspeed, the curves could not be extended to higher shaftspeeds. However,only the peaks of the windmill power-speed curves, as shown, are of interest since desired operation, in a controlled system, will occur there.

The curve showing the power in the shaft was calculated from the derived loss-model equation for the dc machine, Eq.C.15. The difference between the power entering the motor and the power in the shaft is due to mechanical power losses in the shaft and core losses in the motor. These losses are shown separately in both Fig.C21 & C22.

The power output of the generator was measured and is identical to the power entering the batteries, i.e. the product of average charging current and battery terminal voltage. The difference between the power in the shaft and the power entering the batteries is due to core, stray, and I^2R power losses in the generator, shown in the figures.

The battery losses were estimated by calculating I^2R where I is the average charging current and R, the battery resistance, was measured to be about 1 ohm per battery section.

Notice from Fig.C21 & C22 that the peaks of both

MIS TYPE:
NO PG. 115

maximum SHAFT and battery powers occur at much lower shaftspeeds than the peak in power into the motor. The effect of motor, or simulated windmill, losses being much less at lower shaftspeeds readily explains this effect.

The only question remaining is how well has the dc machine simulated an actual windmill power-speed characteristic like the ones shown in Fig.3. The criteria for simulation was the production of a power-speed characteristic where 1) the peak power is proportional to the cube of a wind velocity parameter and 2) the shaftspeed at which this power peak occurs is directly proportional to the same parameter. This has been done to a fairly good extent. The shape of the simulated wind-power-extraction curve has been calculated, Eq.C.8, and is in the form of a parabola, Fig.C3. Whether the rest of the power-speed curve, other than the peak, follows that of a typical windmill is, however, unimportant, since desired steady-state operation is only at the peak of the curve.

Lastly a major difference between an actual windmill and the motor simulation is in the source of power losses. In a windmill the loss mechanisms are of mechanical origin. In a motor, however, magnetic core losses consume a substantial amount of power (see Fig.C21 & C22). One question that needs answering is : Are mechanical losses in a windmill comparable to mechanical and core losses in a dc machine? Unfortunately the author does not have

the answer to this question. Yet this question must be answered before one can consider a dc machine as an adequate windmill simulator.

APPENDIX D

SOURCES OF POWER LOSS IN A WINDMILL POWER SYSTEM

There are four major sources of power loss in the considered electromechanical conversion system.

1) Mechanical losses consist of bearing friction, windage and losses incured if a gearing system is needed to increase the windmill's shaftspeed to a range that is suitable for a desired generator. These losses, in a suitable model, vary linearly as well as with the square of shaftspeed.

2) Generator Iron-Core losses consist of hysterisis and eddy current losses incurred in the generator due to the changing flux densities in the iron of the machine. Eddy current current loss varies with the products of the squares of both flux density and shaft speed. Hysterisis loss vary with the product of shaftspeed and the approximate square of flux density.

3) Stray losses arise from a) nonuniform current distributions in the copper windings, and b) core losses produced by the distortion of the magnetic flux when the machine is running a load. These losses are related to flux density and shaftspeed yet they are difficult to determine.

4) Copper losses, or I^2R losses, are present

in both the armature winding of the machine and the charging batteries.

For the proposed generator, mechanical, iron-core, stray and I^2R losses were measured under certain conditions and are shown in Fig. D.1, D.2 & D.3.

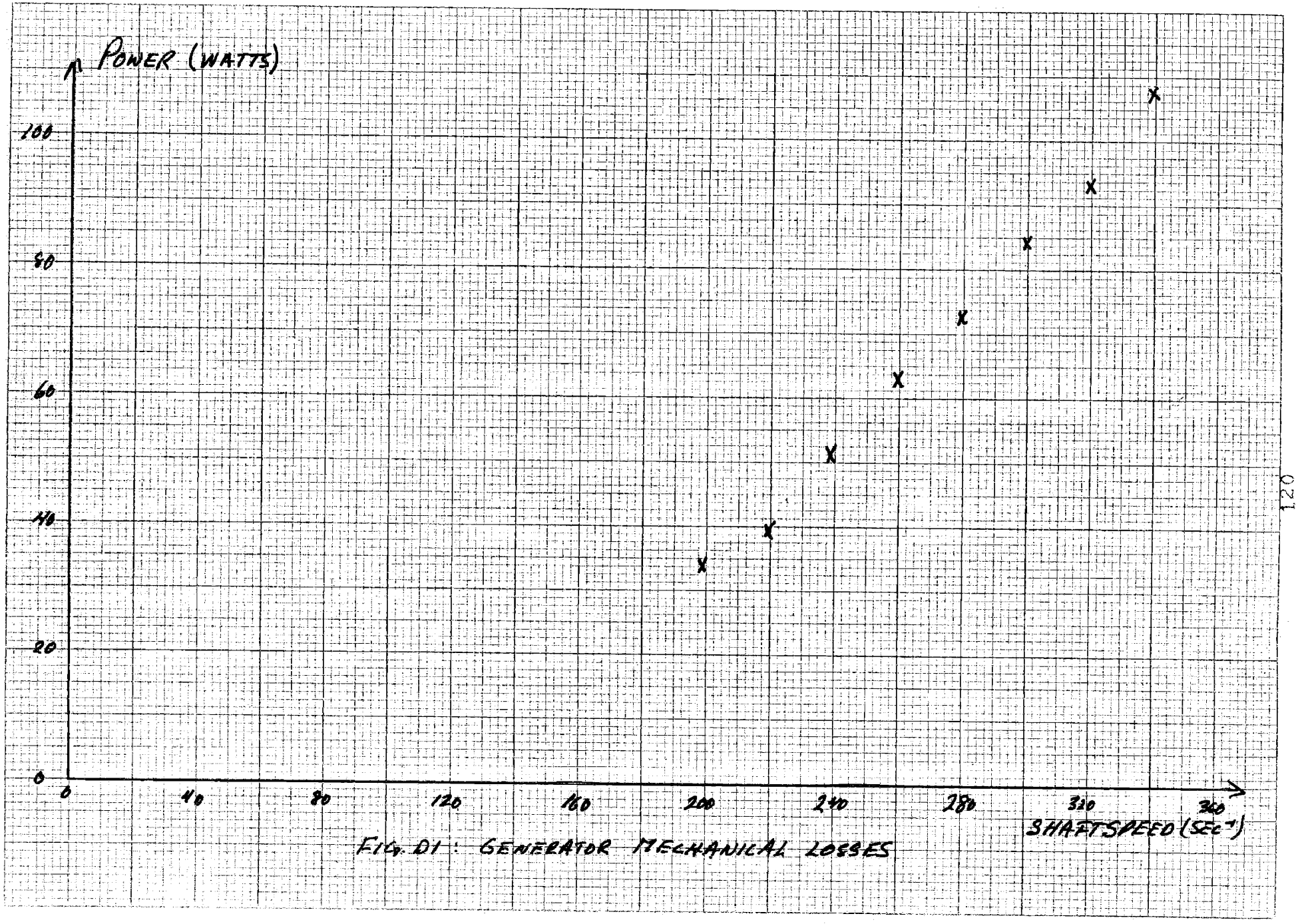

FIG. D1 : GENERATOR MECHANICAL LOSSES

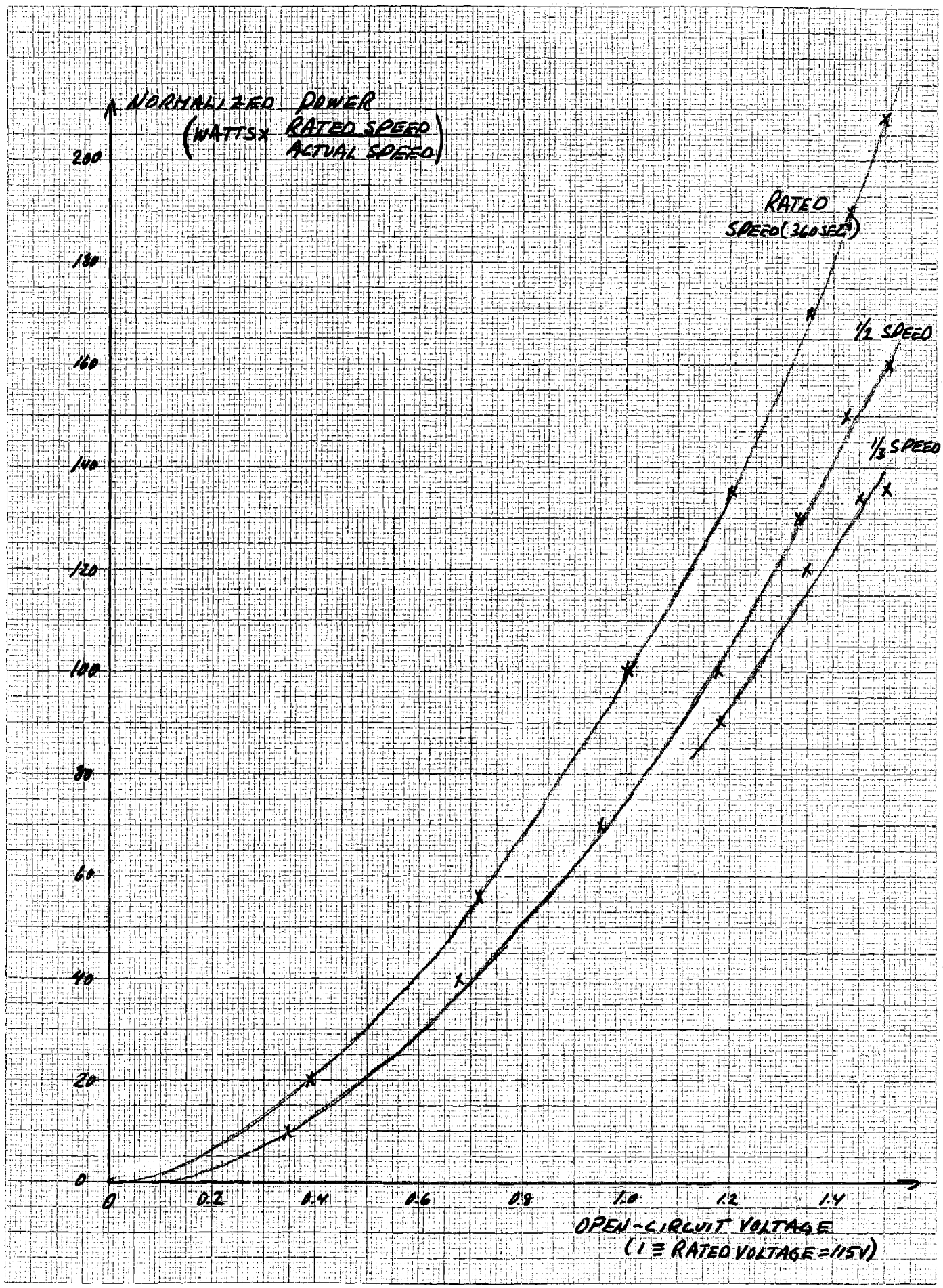

FIG. D2: GENERATOR CORE LOSSES

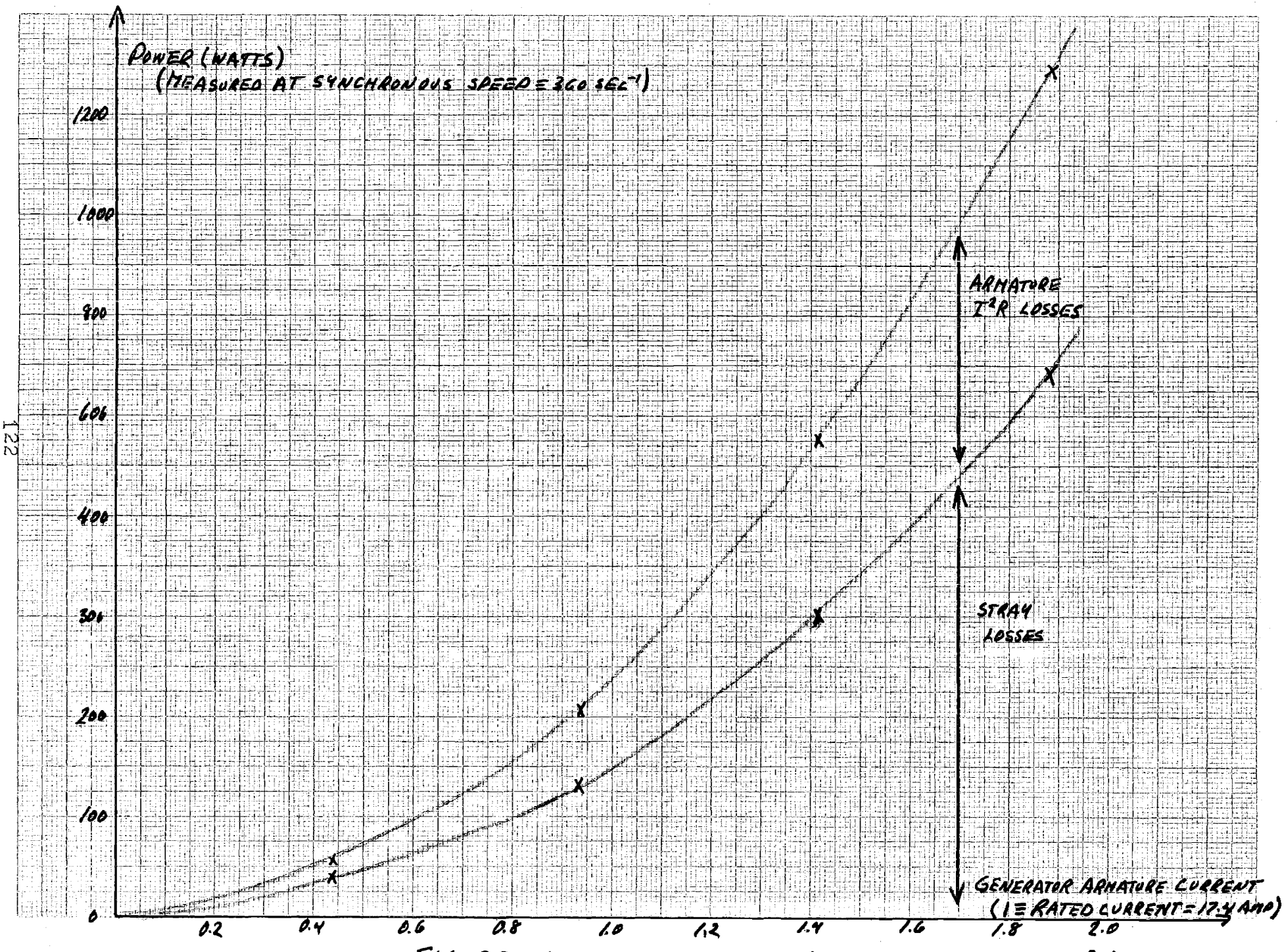

FIG. D.3 GENERATOR SHORT-CIRCUIT LOAD LOSSES (STRAY & I^2R)

REFERENCES

1. Fitzerald, Kingsley and Kusko, Electric Machinery , McGraw-Hill, Inc. 1971

2. S. B. Dewan and A. Straughen, Power Semiconductor Circuits, John Wiley and Sons, Inc. 1975

3. Trevor A. Creary, "An Improved Design of a Variable Voltage Variable Frequency Converter for Power Systems", S. M. Thesis, Mass. Inst. of Tech. June 1976.

4. Hewlett Packard Corp. Solid State Display and Optoelectronics Designer's Catalog, July 1973, pp. 28.